Response to Referee number 3

The authors thank Referee #3 for his/her work. We have considered all comments thoroughly and profoundly. Unfortunately, many of them cannot be accepted at all or fully. Our specific responses are as follows, while the textual modifications are highlighted in red or by crossing out in the revised MS.

The paper summarizes a large body of data and tries to extract information on the underlying processes of new particle formation. This is rather difficult as the lowest particle size they measure is 6 nm and growth rates can only be determined around 10 nm.

1. The lower measurable particle diameter limit of DMPS/SMPS systems is important for identification of NPF and growth events and further data treatment. Evaluations of this type of atmospheric measurements are mostly based on particle diameter range <20 nm (e.g. Kulmala et al., Nat. Protoc., 7, 1651–1667, 2012). In order to separate reliably the NPF and growth events from huge emission peaks which can occur in cities and which can temporarily influence the size intervals down to even smaller diameters, it is highly preferable to have the lower limit below 10 nm. Our limit value of 6 nm was proved to be already satisfactory since it allows to identify and separate different particle generation processes (see e.g. Fig. S1b of the present MS and Salma et al., Atmos. Chem. Phys. 16, 7837–7851, 2016). It is also worth mentioning that from 6 urban cites involved in a recent global analysis of NPF over long-term measurements (Nieminen et al., Atmos. Chem. Phys., 18, 14737–14756, 2018), the lower diameter limit was 3 nm at 2 sites, it was 6 nm at 3 locations, while it was 11 nm at 1 of the sites, and both the J_{nuc} and GR were determined for the diameter interval of 10–25 nm. All these indicate that in atmospheric studies, our experimental systems and evaluation protocols seem completely adequate for the time being.

The authors do not provide much more insight than in the paper of Niemienen et al., where they are coauthors of, except that the results are now based on a larger data set.

2. The goals of the paper mentioned in the comment were largely different from our aims. We can list several important insights explicitly as examples which are part of the present MS and which were not dealt with in the referred paper. They primarily include 1) the evaluation

and discussion of monthly distributions of J_6 an GR_{10} together with their relationships with nucleation occurrence frequency and relevant atmospheric parameters, 2) timing properties of NPF and growth events, 3) refinements of J and GR calculations dedicated to urban environments, 4) statistical distributions of J_6 an GR_{10}, 5) occurrence and properties of extreme events and events with broad onset. These items represent a considerable piece of novelty and new knowledge. Furthermore, the results and conclusions are based on 247 quantifiable NPF and growth events in an urban environment, which means a rather strong background. Finally, we can quote from the Summary and conclusions section of the Nieminen et al. paper (p. 14750): "For future studies, it would be very valuable to make detailed investigations on the interdependencies among J_{nuc}, GR, and NPF event frequency, at both single measurement sites and among sites of seemingly similar environmental characteristics." This is exactly what we did in our MS. In addition to our arguments, we can offer to all persons involved a recent and excellent review paper of Kerminen et al., Environ. Res. Lett. 13 (2018) 103003, 2018 dedicated to field observations, which also gives a scientific outlook and summarizes future research needs, and which can help putting our present results and conclusions more adequately into a scientific frame of international atmospheric NPF and particle growth studies.

Also the fact that the sulphuric acid proxy does not correlate with J6 and GR10 has already been reported in an earlier paper. Although sulphuric acid does only contribute 12.3% to GR10 it does not mean that it is not relevant for NPF (line 608).

3. This conclusion was mentioned in the MS as a minor outcome of the study with the purpose of confirming earlier results (as explicitly stated in the line specified in the comment). The related sentence was modified now to emphasize the key role of H_2SO_4 in the nucleation process and early particle growth.

Many studies have shown a relation between NPF rates measured at small sizes and sulphuric acid, while the growth is dominated by organics. In Figure 4 the authors relate basically reciprocal (sulfuric acid proxy) versus reciprocal (sulfuric acid proxy) modulated by the GR. The linear relation is not surprising and does not lead to any conclusions. As the authors repeat several times in the paper NPF and growth is a complex process. Nevertheless, they test only relations of one single parameter with J6 or GR10. Why do the authors not make an attempt to combine parameters?

4. Figure 4 and the related discussion were removed from the MS to avoid any misunderstanding or incompleteness. The remaining part was also restructured, split into shorter pieces and clarified. Evaluation of the overall data set by multistatistical methods is indeed planned. This comprehensive evaluation is, however, to be accomplished after some markers or proxies for biogenic emission sources (such as e.g. photosynthetical activity) are also included. The extension of the present MS by this comprehensive statistical analysis would not fit among the present objectives and would not be advantageous or feasible considering both the length and timing of this MS as well. See also response no. 5.

It is known that low temperature stabilizes nucleating clusters and that organics promote growth and thus the survival probability. It might thus be worthwhile to look for a proxy representing condensing organics.

5. Chemical species including organics participating in the urban atmospheric NPF and growth were investigated in an intensive international measurement campaign in Budapest over March-May 2018 by deploying API TOF-MS with/without CI, PSM, AIS and DMPS systems. Some potential proxy values for condensing organics are under evaluation. This was mentioned in the Conclusions section, and it is further emphasized and explained in the revised version.

I also question if daily averages are the appropriate parameter to inquire NPF mechanisms. Although it is worth to report on this large data set, I find the paper does not provide much new information and I do not see what the authors' "consequences of dynamic and timing properties" are as announced in the title.

6. Daily averages were calculated for those variables which change slowly over a day (e.g. [SO_2]). For some other variables such as CS, we constrained the averaging for the time intervals from t_1 to t_2, thus over the nucleation process itself. Some other variables, such as the gas-phase H_2SO_4 proxy, were characterized by their daily maximum. They are accurate

specified in Section 4.1 Ranges and averages. As far as the novelty of the MS is concerned, we must refer again to the list in response no. 2. The main conclusions drawn from the dynamic and timing properties are readily collected in the Abstract.

Line 151 and 494: What is the detection limit of the SO2 detector? Are the low SO2 concentrations measured significantly above DL?

7. The limit of determination (LOD) of the SO_2 analyzer system applied is approximately 0.2 µg m^{-3}. More than 98% of the hourly-mean concentrations were above the LOD. The information is also included into the text now.

Line 318-319: I do not see a trend in particle concentrations.

8. The annual medians for the city centre in the measurement years 2008–2009, 2013–2014, 2014–2015, 2015–2016 and 2017–2018 are as follows: 11.5×10^3, 9.7×10^3, 9.3×10^3, 7.5×10^3 and 10.6×10^3 cm^{-3}, respectively. The first 4 data indicate unambiguously a decreasing tendency, while the last data point may look somewhat different. Rigorous statistical evaluation of the joint data set of particle number concentrations in various size fractions over a decennial time interval from 03–11–2008 to 02–11–2018 is in progress, and its preliminary results in the one hand, confirm the decreasing tendency, and in the other hand, reveal some fine structure to this dependency. This information was added to the revised MS.

Table 2: the authors use local time as time base. We know that photolysis is an important driver of sulfuric acid and oxidant production. Would it not be more appropriate to use time after sunrise for starting time?

9. The suggestion represents an option, which can be consider for specific studies. In the present MS, we selected the local time as the time base of most data on purpose and as a compromise because we had experienced in several earlier investigations (e.g. Salma et al., Atmos. Environ., 92, 154–161, 2014) that it is the daily activity time pattern of inhabitants that substantially influences or determines many atmospheric sources and important processes in Budapest. It was explained in lines 123–125 of the original MS, and a reference

for the statement was included as well. The timing parameters of the NPF were given in UTC+1.

Line 441: how can you conclude that NPF is not sensitive to temperature? Indeed the yearly average does not vary much, but is the yearly average really important? What matters more is the temperature during an event in combination with formation rates of nucleating and condensing vapors.

10. The sentence mentioned was replaced from its original location to section 4.2 Monthly distributions. It was largely corrected and extended to a discussion by involving the temperature profiles on nucleation and non-nucleation days, biogenic emissions, photochemistry and results from other international studies.

Line 498: What do you mean by "CO is less certain"?

11. The related sentence was modified to express our intention better that the variability of CO was without obvious tendentious temporal structure or feature.

Figure 2: Is the low value of H2SO4-proxy in May real or an artefact? What is the reason for that?

12. It is the monthly distribution of daily maximum gas-phase H_2SO_4 proxy that is shown in Fig. 2. The mean value for May represents 23 days. Its low value seems to be influenced by enhanced effect of multiplying relatively low GRad with relatively small $[SO_2]$ for a few days particularly in 2015 (which was a strange year as far as the monthly distribution of nucleation frequency as well is concerned; see Fig. 1 of this response). The reliability of the monthly data is to be increased with the length of the overall data sets in the future. This additional information is added now in a synthetized manner to the text.
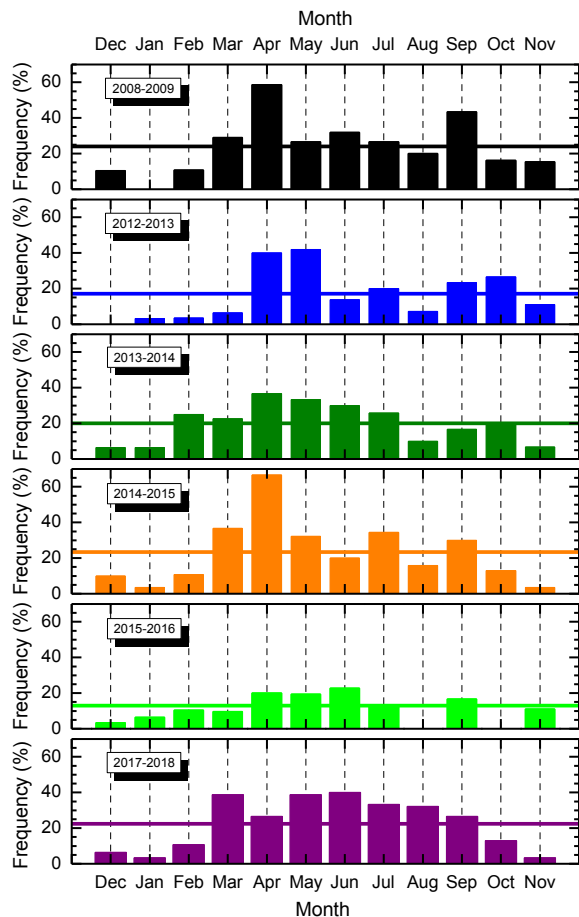
Figure 1. Monthly distribution of relative nucleation frequency in Budapest for measurement years of 2008–2009, 2012–2013, 2013–2014, 2014–2015, 2015–2016 and 2017–2018. The horizontal lines indicate the annual mean frequency. More information is given in the MS.

Line 545: This is not the line of equality. The units of each axis is different. There is also no discussion of this relation with respect to literature, e.g. Nieminen et al.

13. We used the expression "line of equality" in its broader sense, hence when the abscissa and ordinate are on the same scale even they do not have the same units. To the explicit request of Referee #3, however, we can change it to another expression, e.g. "line with a slope of 1". We also amended the discussion of the relationship between *J* and GR at several places by considering the international results available in the literature.

Line 547: The difference between slopes for centre and near–city station is not very convincing. If the authors would also restrict the city centre plots to GR<10 nm/h I expect a large scatter of the slopes. The near-city data do not seem to be different from the other data.

14. We were aware of this inherent limitation mainly caused by smaller dynamic properties (and partly by shorter measurement time interval) in the near-city background than in the city centre, and expressed it by ourselves in lines 554–556 of the original MS. Now, we reformulated the statement completely and turned it from a conclusion into a working hypothesis because a rigorous statistical treatment would indeed require stronger/larger variability in the near-city background data.

Line 559: It should say "that leads to J6>0". J=0 cannot be measured and is meaningless.

15. The suggestion was accepted and adopted.

Line 565: what do you mean by "weak phenomena"?

16. The related sentence was modified to express that we mean the NPF events with relatively small particle formation rate (weak events).

Line 611ff: This explanation is unclear. Surely, GR need to be faster in urban areas but that does not mean that there could be no correlation. Simply speaking higher CS should lead to lower GR. Apparently, a positive correlation is found, isn't it? This would be counterintuitive.

17. The GR of newly formed particles to larger sizes is primarily coupled to 1) CS, which is further linked to the entire aerosol particle population (including the newly formed particles, thus the NPF itself), 2) to the total concentration and some physicochemical properties of non-volatile gaseous compounds and 3) to their production rate in the gas phase from aerosol precursor compounds (e.g. Kerminen et al., Environ. Res. Lett. 13 (2018) 103003, 2018). Understanding these couplings is essential when analyzing atmospheric observations. It is not fully plausible to make intuitive expectations on simplified paired relationships, for instance between CS and GR, under such complexity. Therefore, we stuck to the experimental data and are to contribute to the phenomenological picture on the system of relationships in this part of the MS, which will be eventually leading to a comprehensive and

qualitative explanation of the connections in the future. We extended the sentence briefly with these additional arguments and explanation.

Section 4.4 needs much improvement.

18. We split the section into shorter parts and clarified it by clearer formulations.

Line 739: Where does this number of contribution of NPF to total particle concentration come from? How was the analysis done?

19. Typical number of particles generated by an NPF and growth event on a nucleation day was roughly estimated by considering the median J_6 and median duration of nucleation, Δt (their distribution function is lognormal; see Table 2) and mean relative coagulation loss, F_{coag} (see Table S1) as: $J_6 \times \Delta t \times (1-F_{coag}) = 4.6 \times 180 \times 60 \times 0.83 = 41 \times 10^3$ cm$^{-3} \approx 10^4$ cm^{-3}. This concentration is in line with other results achieved by nucleation strength factor according to which the particle number concentration due to NPF and growth process on a general nucleation day is increased by a factor of approximately 2 (Salma et al., Atmos. Chem. Phys., 17, 15007–15017, 2017). A more detailed description of the estimation process and the mathematical expression utilized are added now together with the last reference mentioned.

In addition to the issues above, we also adopted some smaller changes and added a few recent papers as references to further improve the MS.

Finally, we think that the comments of Referee #3 eventually helped us to formulate our thoughts and ideas better. We appreciate this. We wish, however, to emphasize that the major message of the MS lies in a considerable variety of contributions to the emerging research field of urban atmospheric NPF and growth, which have been becoming possible and increasingly recognized thank to gradually generating, several-year long, semi-continuous, critically evaluated, complex and coherent data sets. We further stressed this aspect of the MS now in the Conclusion section and added a new opening sentence to the Abstract as well.

Imre Salma

Response to Referee number 4

The authors thank Referee #4 for his/her detailed, expertise and valuable comments to further improve and clarify the MS. We have considered all recommendations and made appropriate alterations. Our specific responses to the comments are as follows, while the detailed textual modifications are highlighted in red or by crossing out in the revised MS.

Page8, line 256: the mean new-to-old rate ratios of J6 were 1.23 for city center and 1.20 for near-city background. I would expect that traffic emission causes overestimation of formation rates because it is a source of nanoparticles. Please specify why correcting traffic emission in formation rates calculation gives higher J6.

1. Several modifications were simultaneously adopted in the revisited and refined calculations protocol of the new set of J_6 for the measurement years of 2008–2009 (city centre) and 2012–2013 (near-city background). They include the subtraction of particle number concentrations emitted by road traffic from N_{6-25}, which usually leads to a decrease in the coagulation loss and loss due to growth out from the diameter range of 6–25 nm, and which can sensitively influence the slope of the concentration change in time (dN_{6-25}/dt) in a positive or negative manner depending on the actual time evolution of perturbing emission source. In addition to that, the time interval in which this slope is considered to be constant was determined within a completely new treatment. We would also like to mention the mean relative contribution of the concentration increment, coagulation loss and growth out from the diameter interval to J_6 have different weights of 71%, 17% and 12%, respectively (lines 246–249 of the original MS, and Table S1). Furthermore, J_6 itself also depends on GR_{10}, which makes the relationships even more complex. These explain why the overall effect of urban influence generally resulted in increased dynamic properties. The mean new-to-old ratio for J_6 was larger for the city centre (1.23) than for the near-city background (1.20). It should also be emphasized that the re-calculation mainly affected the individual dynamic properties with relatively small absolute values. The whole process is considered as a methodological improvement over the years of research. The MS was amended by a more detailed description of Equation (1) and by a brief explanation of the issues above.

Section 4.2: Discussion on NPF events frequency should include conditions of NPF days as well as non-NPF days. Properties discussed in the section are only based on events days. This could be misleading because non-events day conditions are not discussed.

2. Information on the average CS (calculated for whole days), gas-phase H_2SO_4 proxy, GRad, air T and concentration of some criteria pollutants on non-nucleation days were partly included now. Many properties are, however, biased by the seasonal cycle of solar electromagnetic radiation via the seasonal variation of new particle formation frequency, and therefore, they interpretation needs special attention. They are to be fully utilized and explained for investigating the changes in annual patter of relative nucleation frequency over the years, and a more comprehensive evaluation and discussion is to be realized in a future study outlined in response no. 5.

Line 484 conclude gas-phase H2SO4 are unlikely to be the limiting factor of NPF occurrence in Carpathian Basin including Budapest from the misalignment between the monthly occurrence frequency and the other properties. To make this statement solid, H2SO4 proxy for events days and non-events days is needed.

3. Averages of several atmospheric properties involved in the H_2SO_4 proxy were derived separately for the event days and non-event days, their effects were briefly discussed, and as a result of it, the statement mentioned was removed.

Page18, line548: Direct compare the numbers of J and GR or saying something contribute equally to the formation of particle and to their growth don't make sense because they are different physical variables. Correlation between J and GR are expected but comparison of the regression line with J6=GR10 doesn't give any useful information.

4. The sentence was modified to express clearly that we mean that the chemical species available in the air affect the formation rate and growth rate differently at the 2 urban sites. This could partially be caused by differences in chemical composition. We reformulated the whole statement completely and turned it from a conclusion into a working hypothesis because a rigorous statistical treatment would indeed require larger variability in the near-city background data.

Page20: Lacking correlation with single parameters to J/GR doesn't tell too much as NPF is controlled by multiple parameters. With the size of the data set, authors could perform analysis on subsets of the data with certain constrains like temperature or H2SO4 proxy.

5. Evaluation of the overall data set by multistatistical methods is indeed planned. This comprehensive evaluation is, however, to be accomplished after some markers or proxies for biogenic emission sources (such as e.g. photosynthetical activity) are also included. The extension of the present MS by this comprehensive statistical analysis would not fit among the present objectives and would not be advantageous or feasible considering both the length and timing of this MS as well. The present study can be considered as the first step in a larger statistical evaluation process and which supplied orienting ideas on the specific directions to proceed in. This perspective further study is very briefly mentioned in the Conclusions section now.

Page 20, line 625 to 636 and figure 4: GR/H2SO4 proxy =b*(1/H2SO4 proxy)+a is equivalent to a*H2SO4 proxy+b=GR. A negative 'a' means the higher H2SO4, the lower the GR. This is contradictory to the interpretation of increasing gas-phase H2SO4 related to larger contribution of other vapors to particle growth. Another concern would be special care should be taken when combine H2SO4 proxy at sub-urban site and urban site as the VOCs and NOx condition could be totally different but not taken into consideration.

6. Figure 4 and the related discussion were removed from the MS to avoid any misunderstanding or incompleteness. The remaining part of the section was restructured, split into shorter pieces and clarified.

Page 24, line 739: To make the full potential of the data set, more detailed studies on the contribution of NPF to regional particle concentration could be performed.

7. We fully agree on this item and will proceed in that direction in the future.

Spelling

Line 113: mean see level-> mean sea level
Line 751: cloud -> CLOUD

8. The typing errors were corrected.

In addition to the issues above, we also adopted some smaller changes and added a few recent papers as references to further improve the MS.

Imre Salma

Consequences of dynamic and timing properties of new aerosol particle formation and consecutive growth events

Imre Salma and Zoltán Németh

Institute of Chemistry, Eötvös University, H-1518 Budapest, P.O. Box 32, Hungary

Correspondence to: Imre Salma (salma@chem.elte.hu)

Abstract. A variety of contributions to the emerging research field of urban atmospheric new particle formation (NPF) and consecutive particle diameter growth based on gradually generating, several-year long, semi-continuous, critically evaluated, complex and coherent data sets are presented here. Dynamic properties, i.e. particle formation rate J_6 and particle diameter growth rate GR_{10}, and timing properties, i.e. starting time (t_1) and duration time interval (Δt) of 247 quantifiable atmospheric NPF and growth events identified in the city centre and near-city background of Budapest over 6 full measurement years together with related gas-phase H_2SO_4 proxy, condensation sink (CS) of vapours, basic meteorological data and concentrations of criteria pollutant gases were derived, evaluated, discussed and interpreted. In the city centre, nucleation ordinarily starts at 09:15 UTC+1, and it is maintained for approximately 3 h. The NPF and growth events produce 4.6 aerosol particles with a diameter of 6 nm in 1 cm^3 of air in 1 s, and cause the particles with a diameter of 10 nm to grow with a typical rate of 7.3 nm h^{-1}. Nucleation starts approximately 1 h earlier in the near-city background, it shows substantially smaller J_6 (with a median of 2.0 cm^{-3} s^{-1}) and GR_{10} values (with a median of 5.0 nm h^{-1}), while the duration of nucleation is similar to that in the centre. Monthly distributions of the dynamic properties and daily maximum H_2SO_4 proxy do not follow the mean monthly pattern of the event occurrence frequency. The factors that control the event occurrence and that govern the intensity of particle formation and growth are not directly linked. ~~Condensing atmospheric chemical species and/or their processes in the city centre seem to contribute equally to new particle formation and particle growth. In the near-city background, however, chemical compounds available and their processes power particle growth more than particle formation.~~ New particle formation and growth processes advance in a different manner in the city and its close environment. This could mainly be related to diversities in atmospheric composition, chemistry and physics. We showed that there is a minimum growth rate (1.8 nm h^{-1} is our case) that is required for nucleated particles to reach the lower end of the diameter interval measured (in our case 6 nm). Monthly distributions and relationships among the properties mentioned

32 provided indirect evidence that chemical species other than H_2SO_4 largely influence the particle

33 growth and possibly atmospheric NPF process as well. The J_6, GR_{10} and Δt can be described

34 by log-normal distribution function. Most of the extreme dynamic properties could not be

35 explained by H_2SO_4 proxy, CS, meteorological data or pollutant gas concentrations.

36 Approximately 40% of the NPF and growth events exhibited broad beginning, which can be an

37 urban feature. For 9% of all quantifiable days, it was feasible to calculate 2 separate sets of

38 dynamic properties. The later onset frequently shows more intensive particle formation and

39 growth than the first onset by a typical factor of approximately 1.4. The first event is attributed

40 to regional type, while the second event, superimposed on the first, is often associated with sub-

41 regional, thus urban NPF and growth process.

42

43 **1 Introduction**

44

45 Molecules and molecular fragments in the air collide randomly and can form electrically neutral

46 or charged clusters. Most clusters decompose shortly. Chemical stabilising interactions among

47 certain components within a cluster can enhance its lifetime, during which it can grow further

48 by additional molecular collisions through some distinguishable size regimes (Kulmala et al.,

49 2014). If the diameter of these clusters reaches a critical value of 1.5±0.3 nm (Kulmala et al.,

50 2013), they become thermodynamically stable, and their further growth turns into a spontaneous

51 process. Supersaturation is a necessary atmospheric condition for this principal transformation.

52 It is essentially a phase transition, which takes place in a dispersed manner in the atmosphere,

53 so it generates an aerosol system. The newly formed particles grow further by condensation to

54 larger sizes in most cases due to the existing supersaturation. Photochemical oxidation products

55 such as H_2SO_4 (Sipilä et al., 2010), extremely low-volatile organic compounds (ELVOCs, Ehn

56 et al., 2014; Jokinen et al., 2015) and highly oxygenated molecules (HOMs, Bianchi et al., 2016;

57 Kirkby et al., 2016; Tröstl et al., 2016) together with H_2O vapour, NH_3 (Kirkby et al., 2011),

58 amines (Almeida et al., 2013), other oxidation products of volatile organic compounds (VOCs;

59 Metzger et al., 2010; Schobesberger et al., 2013; Riccobono et al., 2014) and NO_2 can play an

60 important role in both the particle formation and growth. The VOCs include compounds of both

61 anthropogenic and biogenic origin, mainly isoprenoids such as α-pinene (Kirkby et al., 2016).

62 In some specific coastal regions, iodine oxides produced from marine biota are involved

63 (O'Dowd et al., 2002). Atmospheric concentration of these key compounds at a level that is

64 smaller by 12–14 orders of magnitude than the concentration of air molecules is already

65 sufficient for the phenomenon (Kulmala et al., 2014). Relative importance of the organics

increases with particle size (Riipinen et al., 2011; Ehn et al., 2014), and their supersaturation is maintained by fast gas-phase autooxidation reactions of VOCs (Crounse et al., 2013). The overall phenomenon is ordinarily confined in time for 1 day or so, and, therefore, it can be regarded as an event in time, and is referred as new aerosol particle formation (NPF) and consecutive particle growth event.

Such events appear to take place almost everywhere in the world and anytime (Kulmala et al., 2004; Kerminen et al., 2018; Nieminen et al., 2018). Their occurrence frequency and, more importantly, their contribution to particle number concentrations were found to be substantial or determinant in the global troposphere (Spracklen et al., 2006; Kulmala et al., 2014). Moreover, their contribution to the number of cloud condensation nuclei (CCN) can be 50% or even more (Makkonen et al., 2009; Merikanto et al, 2009; Sihto et al., 2011), which links the events to climate system, and emphasizes their global relevance (Kerminen et al., 2012; Makkonen et al., 2012; Carslaw et al., 2013; Gordon et al., 2016). New particle formation and growth events were proved to be common in polluted air of large cities as well with a typical relative occurrence frequency between 10% and 30% (Woo et al., 2001; Baltensperger et al., 2002; Alam, et al., 2003; Wehner et al., 2004; Salma et al., 2011; Dall'Osto et al., 2013; Xiao et al., 2015; Zhang et al., 2015; Kulmala et al., 2017, Nieminen et al., 2018). The coupling and relationships between regional and urban (sub-regional) NPF were demonstrated at least under favourable orographic conditions (Salma et al., 2016b). New particle formation can increase the existing particle number concentrations in city centres by a factor of approximately 2 on nucleation days, while it can produce approximately 28% of ultrafine (UF) particles on a longer (e.g. annual) time scale (Salma et al., 2017). Particle concentrations from NPF are also important when compared to the (primary) particles emitted by their dominant source in cities, namely by road vehicles with internal combustion engines (Paasonen et al., 2016). These results jointly suggest that particles from NPF and growth events in cities can influence not only the urban climate but can contribute to the public's excess health risk from particle number exposures (Oberdörster et al., 2005; Braakhuis et al., 2014; Salma et al., 2015), and, furthermore, could be linked to the role of human actions in all these effects.

Despite these potentials, conclusive interpretation of the data obtained, and results derived specifically for cities remained hindered so far. Several-year long, semi-continuous, critically evaluated, complex and coherent data sets are required for this purpose, which have been generating gradually. As part of this international progress, investigations dedicated to urban

NPF and growth events in Budapest have been going on since November 2008. Measurements for 5 full years were realised in the city centre at a fixed location, 1 full year was devoted to measurements in a near-city background environment, and some other measurements were accomplished in different urban microenvironments for time intervals of a few months. The main objectives of this study are to determine, present and analyse the dynamic properties, i.e. particle formation rate and particle diameter growth rate, timing properties, i.e. starting time and duration time interval of nucleation process of NPF and growth events together with the major sources and sink of condensing vapours, basic meteorological data and criteria pollutant gases for 6 years, to investigate and interpret their relationships, to discuss their monthly distributions, to evaluate and detect some of their features specific for urban atmospheric environments, and to demonstrate some specific urban influence on the calculation of the properties. These quantities and relationships are of basic importance in many atmospheric processes for several reasons. Our goals are in line with the research needs for global atmospheric nucleation studies (Kerminen et al., 2018; Nieminen et al., 2018).

2 Experimental methods

The measurements took place at two urban locations in Budapest, Hungary. Most measurements were realised at the Budapest platform for Aerosol Research and Training (BpART) facility (N 47° 28' 29.9'', E 19° 3' 44.6'', 115 m above mean sea level (a.s.l.; Salma et al., 2016a). This site represents a well-mixed, average atmospheric environment for the city centre. The other location was situated at the NW border of Budapest in a wooded area of the Konkoly Astronomical Observatory of the Hungarian Academy of Sciences (N 47° 30' 00.0'', E 18° 57' 46.8'', 478 m a.s.l.). This site characterises the air masses entering the city since the prevailing wind direction in the area is NW. The measurements were accomplished for 6 full-year long time intervals, i.e. from 03–11–2008 to 02–11–2009, from 19–01–2012 to 18–01–2013, from 13–11–2013 to 12–11–2014, from 13–11–2014 to 12–11–2015, from 13–11–2015 to 12–11–2016 and from 28–01–2017 to 27–01–2018. In the measurement year 2012–2013, the instruments were set up in the near-city background, while in all other years, they were installed in the city centre. Local time (LT=UTC+1 or daylight-saving time, UTC+2) was chosen as the time base of the data unless otherwise indicated because it had been observed in earlier investigations that the daily activity time pattern of inhabitants substantially influences the atmospheric processes in cities (Salma et al., 2014).

The main measuring system was a flow-switching type differential mobility particle sizer (DMPS). It consists of a radioactive (^{60}Ni) bipolar charger, a Nafion semi-permeable membrane dryer, a 28-cm long Vienna-type differential mobility analyser and a butanol-based condensation particle counter (TSI, model CPC3775). The sample flow was 2.0 L min^{-1} in the high-flow mode, and 0.31 L min^{-1} in the low-flow mode with sheath air flow rates 10 times larger than for the sample flows. The DMPS measures particle number concentrations in an electrical mobility diameter range from 6 to 1000 nm in the dry state of particles (with a relative humidity of RH<30%) in 30 channels, which finally yields 27 channels after averaging 3 overlapping channels when joining the data for the 2 flow modes. The time resolution of the measurements was approximately 10 min till 18–01–2013, and 8 min from 13–11–2013 (after a planned update of the DMPS system). There was no upper size cut-off inlet applied to the sampling line, and a weather shield and insect net were only attached. The sampling inlet was installed at a height of 12.5 m above the street level in the city centre, and of approximately 1.7 m in the near-city background. The measurements were performed according to the international technical standard (Wiedensohler et al., 2012). The availability of the DMPS data over 1-year long time intervals are summarised in Table 1. Synoptic meteorological data for air temperature (*T*), RH, wind speed (WS) and wind direction (WD) were obtained from a measurement station of the Hungarian Meteorological Service (HMS, no. 12843) by standardised methods with a time resolution of 1 h. Global solar radiation (GRad) data were measured by the HMS at a distance of 10 km in E direction with a time resolution of 1 h. Meteorological data were available in >90% of the possible cases in each year. Concentrations of SO_2, O_3, NO_x and CO were obtained from measurement stations of the National Air Quality Network in Budapest (in a distance of 4.5 km from the urban site, and of 6.9 km from the near-city background site) located in the upwind prevailing direction from the measurement sites. They are measured by UV fluorescence (Ysselbach 43C), UV absorption (Ysselbach 49C), chemiluminescence (Thermo 42C) and IR absorption methods (Thermo 48i), respectively with a time resolution of 1 h. The concentration data were available in >85% of the yearly time intervals, and >98% of them were above the limit of determinations. It is worth mentioning that concentration of SO_2 in the Budapest area is ordinarily distributed without larger spatial (and temporal) gradients (Salma et al., 2011). For the present study, this was proved by evaluating the concentration ratios from 2 different municipal stations which are in the closest distance from the BpART in 2 different directions with an angle of 60° between them. The mean SO_2 concentration ratio and standard deviation (SD) for the 2 stations were 81±20% over the 5-year

167 long measurement time interval. The assumption can also be justified indirectly by a conclusion

168 on the monthly distribution of SO_2 concentration in Sect. 4.2.

169

170 **3 Data treatment**

171

172 The measured DMPS data were evaluated according to the procedure protocol recommended

173 by Kulmala et al. (2012) with some refinements that are related to urban features (see Sect. 3.1).

174 Particle number concentrations in the diameter ranges from 6 to 1000 nm (N), from 6 to 25 nm

175 (N_{6-25}) and from 6 to 100 nm (N_{6-100} or UF particles) were calculated from the measured and

176 inverted DMPS concentrations. Particle number size distribution surface plots showing jointly

177 the variation in particle diameter and particle number concentration density in time were also

178 derived. Identification and classification of NPF and growth events was accomplished on these

179 surface plots (Dal Maso et al., 2005; Németh et al., 2018) on a daily basis into the following

180 main classes: NPF event days, non-event days, days with undefined character, and days with

181 missing data (for more than 4 h during the midday). Relative occurrence frequency of events

182 was determined for each month and year as the ratio of the number of event days to the total

183 number of relevant (i.e. all−missing) days. A subset of NPF events with uninterrupted evolution

184 in time, which are called quantifiable (class 1A) events, were further separated because the time

185 evolution of their size distribution functions was utilised to determine the dynamic and timing

186 properties with good accuracy and reliability.

187

188 **3.1 Dynamic and timing properties**

189

190 Growth rate (GR) of nucleation-mode particles was calculated by mode-fitting method

191 (Kulmala et al., 2012). Particle number median mobility diameter (NMMD) of the nucleation

192 mode were obtained from fitting the individual size distributions by DoFit algorithm (Hussein

193 et al., 2004). The growth rate was determined as the slope of the linear line fitted to the time

194 series of the NMMD data within a time interval around a diameter d, where the dependency

195 could be satisfactorily approximated by linear fit. Since the nucleation mode was mostly

196 estimated by N_{6-25} in the calculations of the formation rate (see below), and since the median

197 of the related diameter interval (from 6 to 25 nm) is close to d=10 nm, GRs for particles with a

198 diameter of 10 nm were determined (GR_{10}). This type of GR can be interpreted as an average

199 GR as far as the given particle diameter range is concerned, but it actually expresses the

200   beginning of the growth process only, which may have considerable effects on the formation

201   rate calculations in specific cases (see later).

202

203   Time evolution of an aerosol population is described by the general dynamic equation which

204   was rearranged, simplified and approximated by several quantities (Kulmala et al., 2001; Dal

205   Maso et al., 2002; Kulmala et al., 2012; Cai and Jiang, 2017) to express the formation rate J_6

206   of particles with the smallest detected diameter of $d_{min}=6$ nm in a form utilised in the present

207   evaluation as

208

209   $$J_6 = \frac{dN_{6\text{-}25}}{dt} + \text{CoagS}_{10} N_{6\text{-}25} + \frac{\text{GR}_{10}}{(25-6)} N_{6\text{-}25} - \frac{dN_{\text{Ai},<25}}{dt}. \tag{1}$$

210

211   The first term on the right side of Eq. 1 expresses the concentration increment. The particle

212   number concentration in the size range from 6 to 25 nm (i.e. $N_{6\text{--}25}$) was selected to approximate

213   the nucleation-mode particles $N_{\text{nuc}} \approx N_{6\text{--}25}$. This is a usual and reasonable choice because it was

214   proved to be advantageous and effective way in handling fluctuating data sets since $N_{6\text{--}25}$ often

215   exhibits less sensitivity and smaller scatter in time than the fitted area of the nucleation mode.

216   It is implicitly assumed that the intensity of the NPF is constant for a certain time interval, and,

217   therefore, $dN_{6\text{--}25}/dt$ can be determined as the slope of the linear function of $N_{6\text{--}25}$ versus time t

218   within an interval where the dependence could be satisfactorily approximated by linear fit. A

219   limitation of the relatively wide size range (6–25 nm) selected can be manifested by

220   disturbances from primary particles particularly in urban environments. This is taken into

221   account by the last term of Eq. 1 and is discussed later.

222

223   The second term on the right side of Eq. 1 represents the loss of particles due to coagulation

224   scavenging (with pre-existing particles). The coagulation scavenging efficiency for particles

225   with a diameter of 10 nm (CoagS_{10}) was selected to approximate the mean coagulation

226   efficiency of nucleation-mode particles ($\text{CoagS}_{\text{nuc}}$). This diameter was chosen by considering

227   the median of the related diameter range, which was discussed above for GR. The coagulation

228   efficiency was calculated from classical aerosol mechanics with adopting a mass

229   accommodation coefficient of 1 and utilizing the Fuchs' transition-regime correction factor

230   (Kulmala et al., 2001; Dal Maso et al., 2005; Kulmala et al., 2013) by using computation scripts

231   developed at the University of Helsinki. Self-coagulation within the nucleation mode was

232   neglected due to its limited concentration. Hygroscopic growth of particles was not considered

233   since this depends on chemical composition of particles, which is unknown.

234

235   The third term on the right side of Eq. 1 expresses the particle growth out of the considered size

236   range by condensation of vapours. The GR_{10} was selected to approximate a representative value

237   at the median of the particle diameter range considered (Vuollekoski et al., 2012). It is implicitly

238   assumed that GR_{10} can be regarded to be constant over the time interval under consideration.

239   Nevertheless, the growth of nucleation-mode particles in time is occasionally limited (Fig. S1a).

240   In these specific cases, the mean relative area of the nucleation mode below 25 nm was

241   determined by fitting the individual size distributions around the time of the maximum

242   nucleation-mode NMMD, and the ratios were averaged. A correction in form of the mean

243   relative area was adopted as a multiplication factor for the growth out term in Eq. 1. On very

244   few days, the growth of newly formed particles was followed by a decrease in nucleation-mode

245   NMMD (Salma et al., 2016a). In these cases, the shrinkage rate (with a formal $GR_{10}<0$) was

246   derived and adopted in Eq. 1.

247

248   The fourth term on the right side of Eq. 1 expresses the contribution of high-temperature

249   emission sources, usually of vehicular road traffic (Paasonen et al., 2016; Salma et al., 2017) to

250   N_{6-25}, which can provisionally disturb the assumption of $N_{nuc} \approx N_{6-25}$. A typical example of such

251   a situation is shown in Fig. S1b from 10:09 to 12:23 LT. In these specific cases, the contribution

252   of primary emissions was estimated from the slope of the time series of the fitted peak area of

253   the Aitken mode below $d<25$ nm ($N_{Ai,<25}$) in the time region under consideration. Reliable

254   separation of the nucleation and Aitken modes from each other was hindered or was not possible

255   for a few individual size distributions due to overlapping modes and the scatter in the

256   concentration data, and these individual Aitken-mode areas were excluded from or skipped in

257   the time series. Relative contributions of the concentration increment coagulation loss and

258   growth out from the diameter interval to J_6 are decreasing in this order with mean values of

259   71%, 17% and 12%, respectively (Table S1).

260

261   The formation and growth rates for the measurement years of 2008–2009 and 2012–2013 were

262   calculated earlier by a slightly different way and neglecting the urban features discussed above

263   (Salma et al., 2011, 2016b). To obtain consistent data sets, the dynamic properties for these 2

264   years were re-evaluated by adopting the present improved protocol and implementing the

265   experience gained over the years. The mean new-to-old rate ratios with SDs for the GR_{10} and

J_6 were 1.06±0.32 and 1.23±0.37, respectively in the city centre (2008–2009) and 1.04±0.21 and 1.20±0.35, respectively in the near-city background (2012–2013). It was the smaller rates that were primarily and sometimes substantially impacted. The modifications were simultaneously adopted. The subtraction of particle number concentrations emitted by road traffic from N_{6-25}, which usually leads to a decrease in the coagulation loss and loss due to growth out from the diameter range of 6–25 nm, and which can influence the slope of the concentration change in time (dN_{6-25}/dt) in a positive or negative manner depending on the actual time evolution of perturbing emission source. In addition to that, the time interval in which this slope is considered to be constant was set in a new treatment. It is mentioned that the relative contributions of the concentration increment, coagulation loss and growth out from the diameter interval to J_6 have different weights in propagating their effects. Furthermore, J_6 itself also depends on the GR_{10}, which makes the relationships even more complex. These explain why the changes resulted in overall increments. The re-calculation is considered as a methodological improvement over the years of research.

The assumptions and estimations above usually represent a reasonable approximation to reality. The N_{6-25} is derived from the experimental data in a straightforward way, the GR_{10} and the corrections for primary particles and limited particle growth depend on the quality of the size distribution fitting as well, while the $CoagS_{10}$ is determined by using a theoretical model. The resulting accuracies of the dynamic properties, in particular of J_6, look rather complicated. They also depend on the spatial heterogeneity in the air masses measured particularly for the observations performed at the fixed site, size and time resolution of the concentrations measured, diameter range of the size distributions, fluctuations in the experimental data, selection of the particle diameter interval, choice of the time interval of interest (for linear fits), sensitivity of the models to the input uncertainties (Vuollekoski et al., 2012), and also on the extent of the validity of the assumptions applied under highly polluted conditions (Cai and Jiang, 2017). The situation is further complicated with the fact that the dynamic (and also the timing) properties are connected to each other. Finally, it is important to recognise that some NPF and growth curves on the surface plots have rather broad starting time interval (Fig. S1a and S1c). They occur in a considerable abundance in cities, e.g. in 40% of all quantifiable events in Budapest (Sect. 4.4). This may yield badly defined or composite dynamic properties, whose uncertainty can have principle limitations which can prevail on the experimental and model uncertainties.

300 Timing properties of NPF and growth events are increasingly recognised, and they can provide
301 valuable information even if they are estimated indirectly from the observed diameter interval
302 >1.5 nm (Sect. 1). The earliest estimated time of the beginning of a nucleation (t_1) and the latest
303 estimated time of the beginning of a nucleation (t_2) were derived by a comparative method
304 (Németh and Salma, 2014) based on the variation in the content of the first size channel of the
305 DMPS system. Both time parameters include a time shift that accounts for the particle growth
306 from the stable neutral cluster mode at approximately 2 nm to the smallest detectable diameter
307 limit of the DMPS systems (6 nm in our case) by adopting the GR value in the size window
308 nearest to it in size space. The difference $\Delta t = t_2 - t_1$ is considered as the duration time interval of
309 the nucleation process. It represents the time interval during which new aerosol particles are
310 generated in the air. The timing properties are expressed in UTC+1, and their uncertainty is
311 regarded to be ca. 30 min under ordinary NPF and growth situations.

312

3.2 Sources and sink

314

315 Relative effects and role of gas-phase H_2SO_4 were estimated by its proximity measure (proxy
316 value) containing both its major source and sink terms under steady-state conditions according
317 to Petäjä et al. (2009). It was calculated for GRad>10 W m^{-2}. Formaly, it is possible to convert
318 the H_2SO_4 proxy values to H_2SO_4 concentrations by an empirical scaling factor of $k=1.4\times10^{-7}\times GRad^{-0.70}$, where GRad is expressed in a unit of W m^{-2} (Petäjä et al., 2009). The factor was,
320 however, derived for a remote boreal site, and, therefore, we prefer not to perform the
321 conversion since urban areas are expected to differ from the boreal regions, and adopting the
322 factor could distort the dynamic relationships or time trends investigated. The conversion was
323 applied only to estimate the order of average H_2SO_4 atmospheric concentration levels. The
324 results derived by utilising the proxy are subject to larger uncertainties than for the other
325 properties because of these limitations, but they may indicate well gross tendencies.

326

327 Condensation sink for vapour molecules onto the surface of existing aerosol particles was
328 computed for discrete size distributions as described in earlier papers (Kulmala et al., 2001; Dal
329 Maso et al., 2002, 2005) and summarised by Kulmala et al. (2013). The equilibrium vapour
330 pressure of the condensing species was assumed to be negligible at the surface of the particles,
331 so similar to sulfuric acid. Dry particle diameters were considered in the calculations.

332

4 Results and discussion

Annual median particle number concentrations based on the individual data in the near-city background in 2012–2013, and in the city centre for the separate measurement years of 2008–2009, 2013–2014, 2014–2015, 2015–2016 and 2017–2018 were 3.4×10^3, and 11.5×10^3, 9.7×10^3, 9.3×10^3, 7.5×10^3 and 10.6×10^3 cm^{-3}, respectively. The data for the city centre indicate a decreasing trend. The first 4 values unambiguously show a decrease, while the last data point may look somewhat differently. Rigorous statistical evaluation of the joint data set of particle number concentrations in various size fractions over a decennial time interval from November 2008 to November 2018 is in progress, and its preliminary results in the one hand, confirm the decreasing tendency, and in the other hand, reveal some fine structure to this dependency. The mean UF/N ratio with SD for the same measurement time intervals were 67±14%, and 79±6%, 75±10%, 75±11%, 76±11% and 80±10%, respectively. The values correspond to ordinary urban atmospheric environments in Europe (Putaud et al., 2010).

An overview on the number of classified days separately for the 1-year long measurement time intervals is given in Table 1. The availability of the daily size distribution surface plots with respect to all days ensures that the data are representative on yearly and monthly time scales, except for the months August and September 2015, when there were missing days in larger ratios. The number of quantifiable event days (248 cases) is also considerable, which establishes to arrive at firm conclusion on the NPF and growth events as well.

Table 1. Number of days with new aerosol particle formation and growth event, quantifiable (class 1A) event days, non-event days, undefined days, missing days and the coverage of relevant days with respect to all days in the near-city background and city centre separately for the 1-year long measurement time intervals.
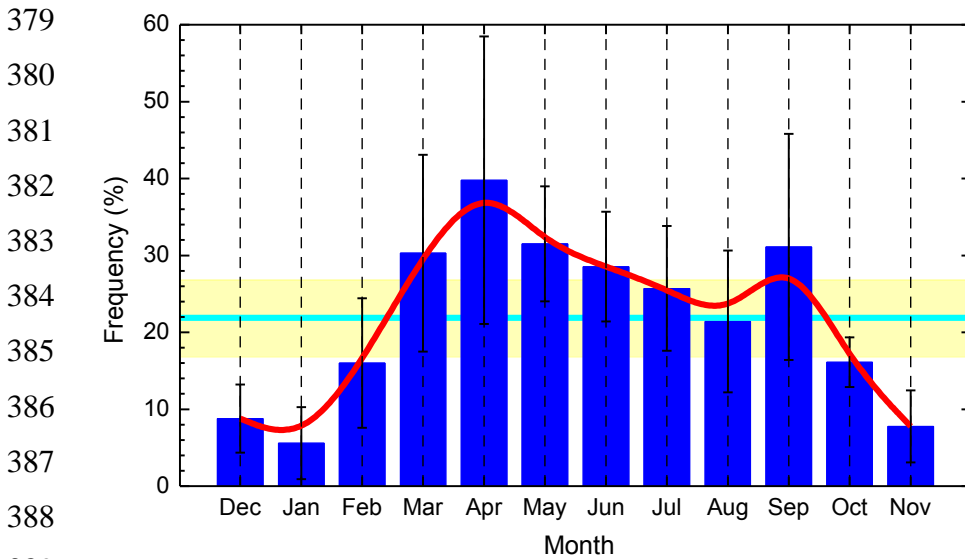
Environment	Background	Centre				
Time interval	2012–2013	2008–2009	2013–2014	2014–2015	2015–2016	2017–2018
Event days	96	83	72	81	35	83
Quantifiable days	43	31	48	56	18	52
Undefined days	19	34	24	25	8	23
Non-event days	231	229	267	240	226	257
Coverage (%)	95	95	99	95	73	99
Missing days	20	19	2	19	97	2

It was previously shown that the NPF and growth events observed in the city centre of Budapest and its background ordinarily happen above a larger territory or region in the Carpathian Basin (Salma et al., 2011; Németh and Salma, 2014), and they are linked to each other (Salma et al., 2016b). From the point of the occurrence frequency distribution, they can, therefore, be evaluated jointly in the first approximation. An overall monthly mean relative occurrence frequency of nucleation days derived for all 6 measurement years is shown in Fig. 1. The annual mean frequency with SD was 22±5%, which is considerable and is in line with other urban sites (Sect. 1). The monthly mean frequency has a temporal variation, which can be characterised by a noteworthy pattern. The mean monthly dependency exhibits an absolute and a local minimum in January (5.6%) and August (21%), respectively, and an absolute and a local maximum in April (40%), and September (31%), respectively. Nevertheless, the SDs of the monthly (and annual) means indicate prominent variability from year to year. The pattern can be related to multivariate relationships and complex interplay among the influencing factors, which include the air temperature (January is the coldest month, while August is the warmest month in the Carpathian Basin) and enhanced emission of biogenic VOCs in springtime (March–April) and early autumn (September) as well (Salma et al., 2016b).

Figure 1. Monthly mean relative occurrence frequency of new aerosol particle formation and consecutive particle diameter growth events with respect to the number of relevant days for the joint 6-year long data set. The error bars show ±1 standard deviation, the horizontal line in cyan indicates the overall annual mean frequency, the yellow bands represent ±1 standard deviation of the annual mean, and the smooth curve in red serves to guide the eye.

The properties and variables studied were derived in full time resolution. They were averaged in several ways for different conditions and for various purposes to obtain typical average descriptive characteristics. In 1 case (31–08–2016), the NPF and growth event could reliable be identified, while the measured absolute particle number concentrations could not be validated due to some experimental troubles, and, therefore, it was left out from the further calculations. Similarly, there were 1 and 4 events with unusually/extraordinarily large dynamic properties in the measurement years 2014–2015 and 2017–2018, respectively. More specifically, 5 individual J_6 data when expressed in a unit of cm^{-3} s^{-1} and 1 individual GR$_{10}$ data when given in nm h^{-1} were >20 (Table 3). These extremes were left out from the overview statistics to maintain the representativity (they could be influenced by some unknown extra or very local sources) and to fulfil better the basic requirements of correlation analysis. If an event showed a double beginning then the dynamic properties for the first onset were considered in the basic overview since this onset is of regional relevance (Salma et al., 2016b). The extreme NPF and growth events and the characteristics for the second onsets were, however, evaluated separately and are discussed in detail and interpreted in Sect. 4.4.

4.1 Ranges and averages

Ranges and averages with SDs of formation rate J_6, growth rate GR_{10}, starting time of nucleation (t_1) and duration time interval of nucleation (Δt) are summarised in Table 2 for separate measurement years and for the joint 5-year long city centre data set. In the city centre, nucleation generally starts at 09:15 UTC+1, and it is typically maintained for approximately 3 h. The NPF and growth events ordinarily produce 5.6 new aerosol particles with a diameter of 6 nm in 1 cm^3 of air in 1 s, and cause the particles with a diameter of 10 nm to grow with a typical rate of 7.6 nm h^{-1}. The statistics for J_6 and GR_{10} are based on 199 and 203 events, respectively. The corresponding data for the separate years show considerable variability without obvious trends or tendencies. The differences between the years can likely be related to changes in actual atmospheric chemical and physical situations and conditions, and to the resulting modifications in the sensitive balance and delicate coupling among them from year to year. Spread of the individual data for GR_{10} is smaller than for J_6; the relative SDs for the joint 5-year long city centre data set were 38% and 68%, respectively, while the (external) relative SDs calculated from the annual mean values were 4.2% and 14.0%, respectively.

The dynamic properties and t_1 data tend to be smaller in the near-city background than in the city centre. In general, nucleation starts 1 h earlier in the background, and the events typically show significantly smaller J_6 (with a median of 2.0 cm^{-3} s^{-1}) and GR_{10} (with a median of 5.0 nm h^{-1}). Duration of the nucleation is very similar to that in the city centre. All starting times of nucleation were larger than (in a few cases, very close to) the time of the sunrise. This implies that no nocturnal NPF and growth event has been identified in Budapest so far. The particle growth process (the so-called banana curve) could be traced usually for a longer time interval (up to 1.5 d) in the background than in the centre.

These results are in line with the ideas on atmospheric nucleation and consecutive particle growth process (e.g. Kulmala et al., 2014; Zhang et al., 2015; Kerminen et al., 2018). It was observed in a recent overview study (Nieminen et al., 2018) that the formation rate of 10–25 nm particles increased with the extent of anthropogenic influence, and in general, it was 1–2 orders of magnitude larger in cities than at sites in remote and clean environments. This highlights the importance of some anthropogenic vapours such as SO$_2$, NH$_3$ and amines to NPF and growth. The data also confirm our earlier findings with respect to Budapest and its regional

445 background within the Carpathian Basin achieved with shorter, 2-year long data sets (Salma et

446 al., 2016b)

447

448 **Table 2.** Ranges, averages and standard deviations of aerosol particle formation rate J_6, particle diameter

449 growth rate GR_{10}, starting time (t_1) and duration time interval ($\Delta t = t_2 - t_1$) of nucleation process of

450 quantifiable (class 1A) new particle formation and growth events in the near-city background and city

451 centre separately for the 1-year long measurement time intervals and for the joint 5-year long city centre

452 data set.

453

Environment	Background	Centre					
Time interval	2012– 2013	2008– 2009	2013– 2014	2014– 2015	2015– 2016	2017– 2018	All 5 years
Formation rate J_6 (cm^{-3} s^{-1})							
Minimum	0.48	1.47	1.13	0.81	1.19	1.60	0.81
Median	2.0	4.2	3.5	4.4	4.6	6.3	4.6
Maximum	5.6	15.9	17.8	18.0	15.3	17.3	18.0
Mean	2.2	4.7	5.2	5.6	5.0	6.6	5.6
St. deviation	1.3	2.6	3.7	4.2	3.7	3.3	3.8
Growth rate GR_{10} (nm h^{-1})							
Minimum	3.0	3.7	3.1	2.8	3.2	3.3	2.8
Median	5.0	7.6	6.6	6.5	8.0	7.5	7.3
Maximum	9.8	17.4	19.0	18.0	15.5	19.8	19.8
Mean	5.2	7.8	7.2	7.3	7.7	8.0	7.6
St. deviation	1.4	2.6	2.8	3.2	3.0	2.8	2.9
Starting time, t_1 (HH:mm UTC+1)							
Minimum	05:51	07:14	06:44	05:48	07:31	05:57	05:48
Median	08:19	09:26	09:22	08:48	09:45	09:18	09:15
Maximum	11:09	11:38	12:21	11:23	12:45	12:15	12:45
Mean	08:17	09:27	09:25	08:49	10:02	09:24	09:19
St. deviation	01:11	01:05	01:26	01:22	01:23	01:36	01:26
Duration time, Δt (HH:mm)							
Minimum	01:23	00:52	00:42	00:31	01:03	01:26	00:31
Median	03:16	02:36	02:04	03:53	02:31	03:49	02:57
Maximum	06:44	06:04	05:34	07:46	06:05	07:55	07:55
Mean	03:30	02:44	02:14	03:52	02:58	03:57	03:18
St. deviation	01:40	01:11	01:01	01:40	01:47	01:39	01:40

454

455 Ranges and averages with SDs of some related atmospheric properties, namely of mean CS

456 averaged for the time interval from t_1 to t_2, daily maximum gas-phase H_2SO_4 proxy, daily mean

457 T and RH (Table S2), and of daily median concentrations of SO_2 (as the major precursor of gas-

458   phase H_2SO_4), O_3 (as an indicator of photochemical activity), NO_x and CO gases (as indicators

459   of anthropogenic combustion activities and road vehicle emissions) (Table S3) were also

460   derived for quantifiable NPF and growth event days, and are further evaluated. The annual

461   mean CS values exhibited decreasing tendency in the city centre over the years (as can be

462   expected from the particle number concentrations as well). The individual values remained

463   below approximately 20×10^{-3} s^{-1}, which agrees well with the results of our earlier study (Salma

464   et al., 2016b) according to which the CS suppresses NPF above this level in the Carpathian

465   Basin. Maximum H_2SO_4 proxy values reached substantially higher levels (by a factor of

466   approximately 2) in the near-city background than in the city centre due mainly to the

467   differences in the CS and [SO_2]. The differences between the 2 sites are particularly evident

468   when considering their smallest values. The largest variability in the annual average values

469   were observed for the proxy. Median concentration of H_2SO_4 molecules was roughly estimated

470   to be approximately 5×10^5 cm^{-3} by adopting the scaling factor (Sect. 3.2). ~~The dynamic~~

471   ~~properties seem to be not very sensitive to air T~~ The air T displayed quite similar and comparable

472   values over the years at both sites. The discussion of its overall effect on the dynamic properties

473   is accomplished in Sec. 4.2, where the monthly distributions are presented. Some events

474   happened at daily mean temperatures below zero. The daily mean RH and its SD for the city

475   centre and near-city background were 54±11% and 64±12%, respectively. There were events

476   that occurred at RHs as high as 90%. Relationships of the dynamic properties with T and RH

477   are also obscured with strong seasonal cycle of these meteorological data and with the fact that

478   air masses arriving to the receptor site in different trajectories are often characterised by distinct

479   levels of meteorological data.

480

481   As far as the pollutant gases are concerned (Table S3), SO_2 showed somewhat smaller daily

482   median values, and O_3 exhibited substantially smaller levels on event days in the city centre

483   than in the near-city background, while concentrations of NO_x and CO were obviously larger

484   in the city than in its close background. The differences can primarily be explained by the

485   intensity and spatial distribution of their major sources and atmospheric chemical reactions, and

486   the joined concentration data resembles typical situations without photochemical smog

487   episodes in cities. There was no obvious decrease in SO_2 concentration during these years in

488   contrast with an earlier decreasing trend from mid-1980s till about 2000. ~~No evident or sensitive~~

489   ~~effect of atmospheric gases on the dynamic or timing properties could be deduced from the~~

490   ~~averaged data. This can probably be explained by a dedicated balance between the intensifying~~

491 and suppressing effects, which were averaged out on a yearly time scale. Relationships on
492 shorter scales are further investigated and discussed in more detail in the following sections.

493

494 **4.2 Monthly distributions**

495

496 Distributions of the monthly mean J_6, GR_{10}, daily maximum gas-phase H_2SO_4 proxy, mean CS,
497 daily mean air T and RH, and daily median SO_2, O_3, NO_x and CO concentrations for quantifiable
498 NPF and growth events for the joint 5-year long city centre data sets are shown in Fig. 2. The
499 distributions – eminently for J_6, GR_{10}, H_2SO_4 proxy and SO_2 – do not follow the monthly pattern
500 of the event occurrence frequency at all (cf. Fig. 1). Instead, the J_6, GR_{10} and H_2SO_4 proxy tend
501 to exhibit larger values in summer months, and they temporal changes over the other months
502 are smooth and do not show distinctive features. The elevations are substantial; the estimated
503 maximum level was larger than the baseline by a factor of 2.1 for the J_6, and by a factor of
504 approximately 1.4 for the GR_{10} and H_2SO_4 proxy. The intensity of solar radiation at the surface,
505 its seasonal cycling, concentration of atmospheric precursors in different months, biogenic
506 processes, anthropogenic activities and the fact that rate coefficients of many thermal
507 chemical/physicochemical processes in the nature (including GR, Paasonen et al., 2018)
508 increase with T could play an important role in explained the distributions. A more
509 comprehensive study involving chemicals and their photochemistry is required for more
510 detailed explanation.

511

512 It is worth mentioning that [SO2] did not change substantially for the NPF event and non-event
513 days, while GRad was typically larger by a factor of ca. 2 and CS was smaller by approximately
514 30% on event days than on non-event days. The differences in the GRad (and some other
515 properties) are, however, biased by the seasonal cycle of solar electromagnetic radiation via the
516 seasonal variation of NPF occurrence frequency, while the CS indicated a modest seasonal
517 dependency. Interpretation of their joint effect should be approached by care, requires further
518 evaluations and is to be realised fully in a further study. Nevertheless, the misalignment among
519 the monthly distributions of NPF and growth event occurrence frequency and all the other
520 properties indicates that the occurrence or its basic causes are not linked with the dynamic
521 properties in a straightforward or linear manner, and 2) gas-phase H_2SO_4 does not seem to be
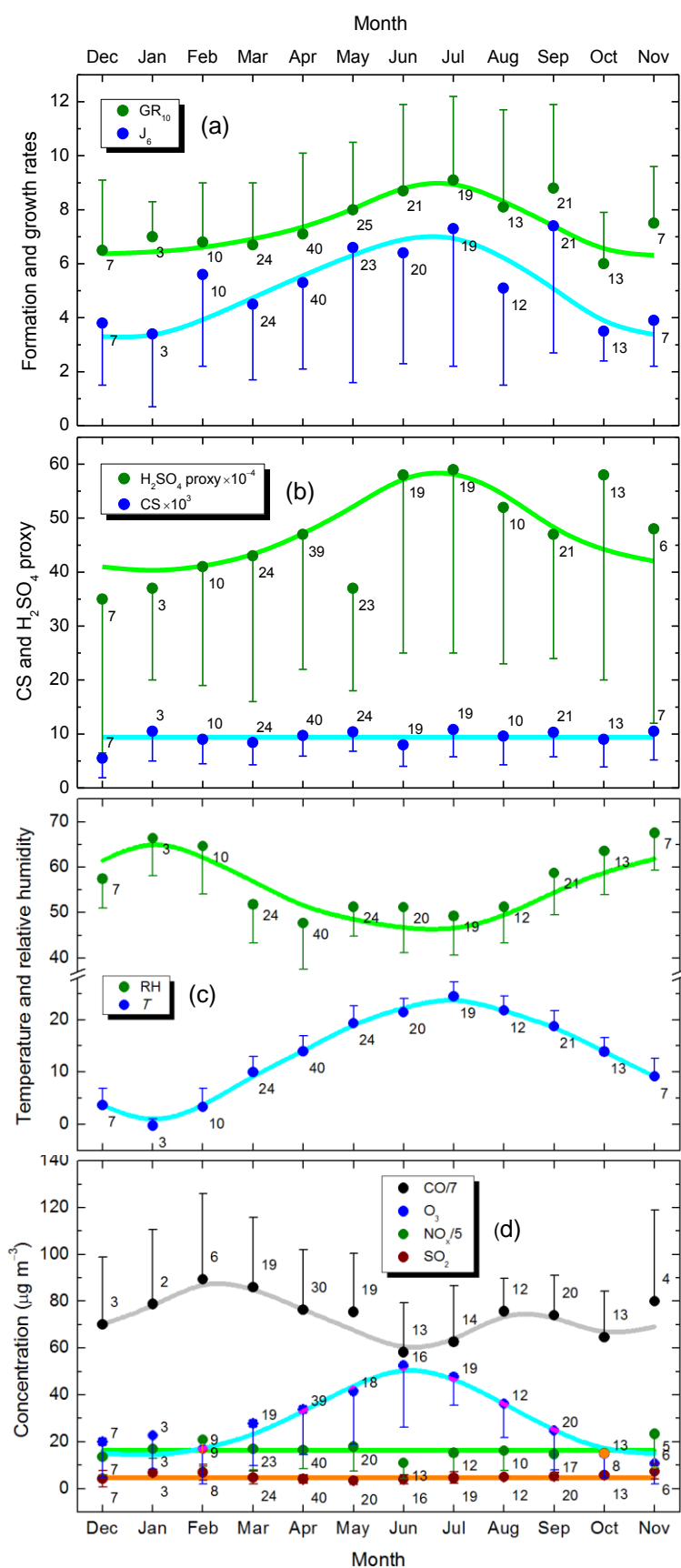522 the controlling factor of NPF occurrence in the Carpathian Basin including Budapest.

523

Some of our results are in line with other observations according to which GR exhibited almost exclusively a summer maximum, while some other finding are different in the sense that the seasonal variability in particle formation rate was quite modest and could not be established earlier (Nieminen et al., 2018). There is one more aspect which may be worth realising in this respect. A large fraction of compounds contributing to NPF and growth in cities can originate from anthropogenic precursors (Vakkari et al., 2015). Their emissions may peak any time of year depending on human habits and requirements (Nieminen et al., 2018). Nevertheless, the fact that our monthly distributions of the dynamic properties in urban environments follow the universal summer maximum behaviour may indicate the overall prevailing role of atmospheric photochemistry coupled with biogenic emissions of aerosol precursor vapours.

The monthly mean J_6, GR_{10} and H_2SO_4 proxy data still have considerable uncertainty, which makes their interpretation not yet completely conclusive. The uncertainties are influenced by inherent fluctuations in the primary data sets, enhancing effects caused by combining some individual primary data into compound variables (such as H_2SO_4 proxy), number of data items available for different properties and months, variations in other or unknown relevant environmental conditions, and by the variability in relative nucleation occurrence frequency from year to year. The resulting uncertainties are expected to decrease with the length of the available data sets, which emphasized the need to continue the measurements.

The monthly distributions of CS, and SO_2 and NO_x concentrations could be represented by constant values of the overall means and SDs of $(9.4\pm4.3)\times10^{-3}$ s^{-1}, 4.7 ± 2.1 µg m^{-3} and 81 ± 38 µg m^{-3}, respectively with an acceptable accuracy. This suggests that CS, SO_2 and NO_x in Budapest do not critically or substantially affect either the dynamic properties (or the event occurrence). Monthly distributions of air T and O_3 concentration showed a maximum over summer months, while RH reflected the T tendency. The monthly variation of T on event days and on non-event days were similar. More importantly, higher biogenic emissions and typically stronger photochemistry are expected during the summer, which both enhance the production rate of nucleating and condensing vapours, while there is practically nothing extra that would suppress the dynamical properties (Kerminen et al., 2018). As a result of these, the dynamic rates show a summer maximum. This is completely consistent with the results from other urban and non-urban studies (Nieminen et al., 2018). Distribution of CO was more changing and without obvious tendentious temporal structure or feature than for the other gases, and, therefore, its interpretation is encumbered so far. However, it doesn't seem to substantially affect the dynamic properties.

Figure 2. Distribution of monthly mean aerosol particle formation rate J_6 in a unit of cm^{-3} s^{-1} and particle diameter growth rate GR_{10} in a unit of $nm\ h^{-1}$ (a), mean condensation sink for vapours (CS) in a unit of s^{-1} averaged over the nucleation time interval (t_1, t_2) and daily maximum gas-phase H_2SO_4 proxy in a unit of $\mu g\ m^{-5}\ W\ s$ (b), daily mean air temperature (T) in a unit of °C and daily mean relative humidity (RH) in % (c), and daily median concentrations of SO_2, O_3, NO_x and CO for quantifiable (class 1A) new particle formation and growth events in the city centre for the joint 5-year long time interval. The error bars are shown for one side for clarity and indicate 1 standard deviation. Number of the individual data averaged in each month is displayed next to the symbols. The horizontal lines indicate the overall mean. The nonlinear curves assist to guide the eye.

4.3 Relationships
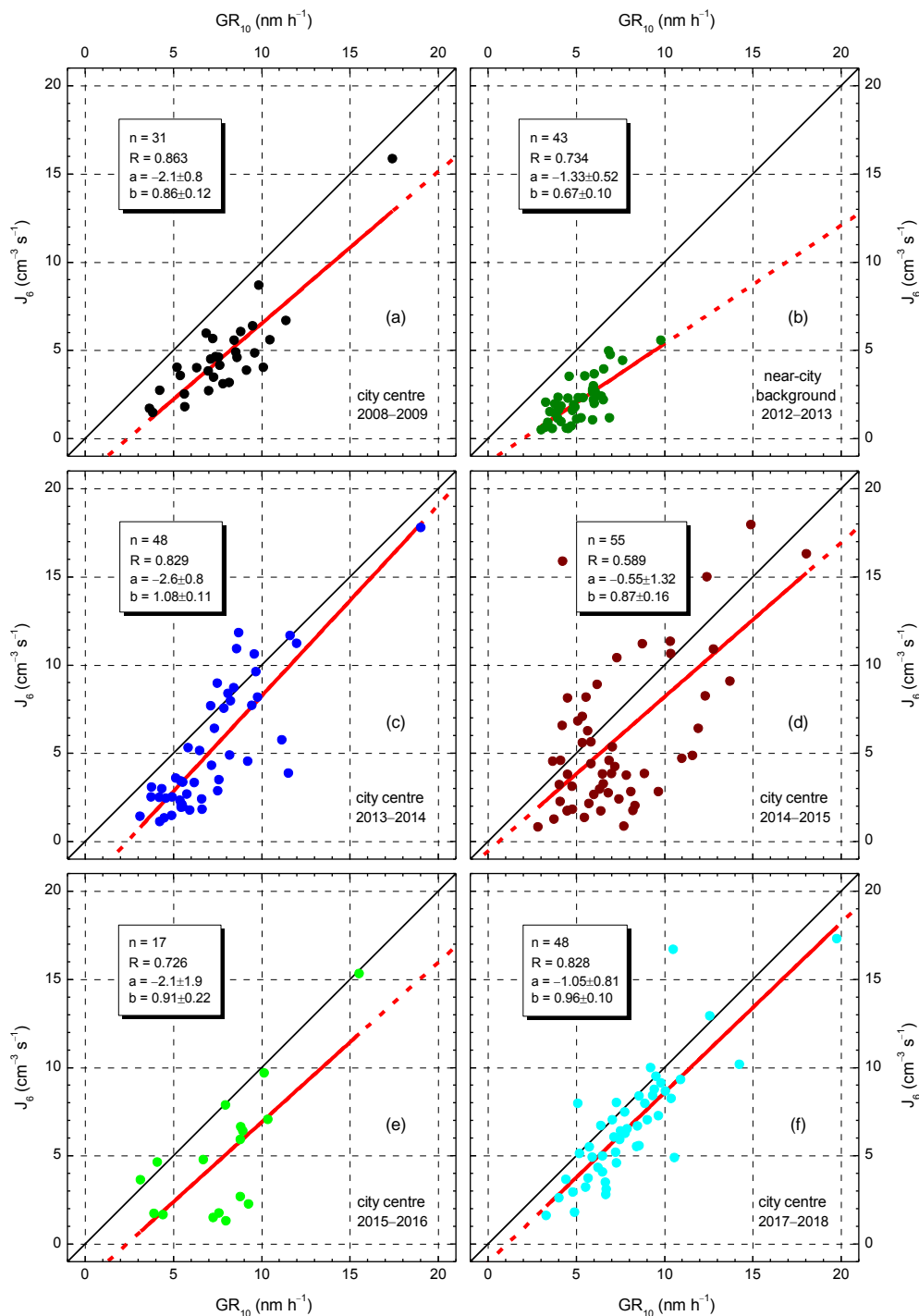
Pearson's coefficients of correlation (R) between J_6 and GR_{10} revealed significant linear relationship between them for all annual data sets (the mean R and SD were 0.768 ± 0.099, number of data pairs $n=243$). This confirms that formation of new aerosol particle and their growth to larger sizes in the atmosphere are tightly and positively linked together. It should be noted that J_6 and GR_{10} are not completely independent variables (see Eq. 1 and Table S1). The linear relationship between the dynamic properties was observed under different atmospheric conditions in many environments (Nieminen et al., 2018). At some sites, this relationship could not be proved due to the weak variability in the variables.

The dynamic properties can also be coupled to the concentrations of aerosol precursor compounds and properties of a pre-existing particle population, thus to atmospheric environment (Kerminen et al., 2018). It is, therefore, sensible to investigate the city centre and near-city background data separately. Scatter plots between J_6 and GR_{10} for the 1-year long measurement time intervals are shown in Fig. 3. For the city centre, the regression lines follow the line with a slope of 1 in all 5 years. The mean slope (b) with SD for the joint 5-year long city centre data set was $b=0.94\pm0.07$ expressed formally in a unit of cm^{-3} s^{-1} nm^{-1} h. ~~This implies that the relevant chemical species and/or their processes in the air of the city centre contribute equally to the formation of 6-nm particles and to their growth process.~~ At the same time, the regression line for the near-city background deviated significantly with a $b=0.67\pm0.10$ cm^{-3} s^{-1} nm^{-1} h from the J_6 vs. GR_{10} dependency for the city centre. This can imply that NPF and growth processes advance in a different manner in these 2 environments~~, and that the chemical compounds available and their processes power particle growth more than new particle formation in the near-city background~~. This can be related to the differences between the city and its close environment as far as the atmospheric composition (for instance, the VOC and NO_x concentrations), chemistry and physics, and other delicate conditions are concerned (Paasonen et al., 2018). The narrower range and smaller number of individual dynamic properties available for the near-city background relative to those in the city centre represent some inherent limitation or weakness in the explanation, and, therefore, it can strictly be regarded as a working hypothesis because a rigorous statistical treatment would require larger variability in the near-city background data.

Figure 3. Scatter plots for aerosol particle formation rate J_6 and consecutive particle diameter growth rate GR_{10} in city centre (a and c–f) and near-city background (b) separately for the 1-year long measurement time intervals. Number of data point (n), their coefficient of correlation (R) and the intercept (a) and slope (b) of the regression line with standard deviations are also indicated. The lines in black represent the line with a slope of 1, the solid lines in red show the regression lines, while the dashed parts in red are extrapolated from the regression line.

21

660

661   The intercepts (a) of the regression lines were identical for all data sets within their uncertainty

662   interval. The mean intercept and SD were estimated to be -1.7 ± 0.8 cm^{-3} s^{-1}. This finding is

663   interpreted as the existence of a minimum GR or more exactly of a minimally required GR that

664   leads to $J_6>0$. Particles that exhibit at least this level of GR can escape coagulation mainly with

665   larger particles and reach the detectable diameter (6 nm in our case) by condensational growth.

666   The minimal GR was derived as GR$_{min}=-a/b$, and its mean and SD are 1.8 ± 1.0 nm h^{-1} for the

667   conditions ordinarily present in the Budapest air. Nucleation processes which are initiated under

668   circumstances that cause the newly formed particle with a diameter of 10 nm to grow with a

669   rate <GR$_{min}$ are normally not observed. Anyway, these are expected to be events with relatively

670   small J_6 (weak phenomena) due to the relationship between GR$_{10}$ and J_6. The events with GR

671   larger but close to this limit could be still masked by fluctuating experimental data. Their

672   identification and evaluation can be made feasible by decreasing the lower measurement

673   diameter limit of DMPS systems down to 3 nm, or by different instruments such as particle size

674   magnifier or neutral cluster and air ions spectrometer.

675

676   Correlations between individual H$_2$SO$_4$ proxy values on one side and J_6 or GR$_{10}$ on the other

677   side were not significant. This is consistent with the corresponding conclusion of Sect. 4.2 and

678   with the earlier results according to which the mean contribution of H$_2$SO$_4$ condensation to the

679   particle GR$_{10}$ was only 12.3% in Budapest (Salma et al., 2016b). The lack of correlation and

680   the average concentrations of SO$_2$ derived separately for the NPF and growth event and non-

681   event days suggest that this precursor gas is ordinarily available in excess and, therefore, the

682   formation of H$_2$SO$_4$ is likely governed by photochemical conditions, and that other chemical

683   species than H$_2$SO$_4$ can have larger influence on the particle growth. The role of H$_2$SO$_4$ in the

684   nucleation process and early particle growth could be still relevant or determinant.

685

686   Coefficients of correlation between CS on one side and J_6 or GR$_{10}$ on the other side for the joint

687   city centre data sets were modest (R=0.41 and 0.32, respectively with n=194 and 197,

688   respectively). This is simply related to the fact that larger GR values are typical for polluted

689   urban air (Kulmala et al., 2017) since particles capable of escaping coagulation scavenging need

690   to grow faster in comparison to cleaner environments, and the enhanced requirements for the

691   growth are linked to increased formation rates as well. It should be noted here that the GR of

692   newly formed particles to larger sizes is primarily coupled to 1) CS, which is further linked to

693   the entire aerosol particle population (including the newly formed particles, thus the NPF itself),

22

694　2) to the total concentration and some physicochemical properties of non-volatile gaseous
695　compounds and 3) to their production rate in the gas phase from aerosol precursor compounds
696　(e.g. Kerminen et al., 2018). These couplings could result in rather complex behaviour, and
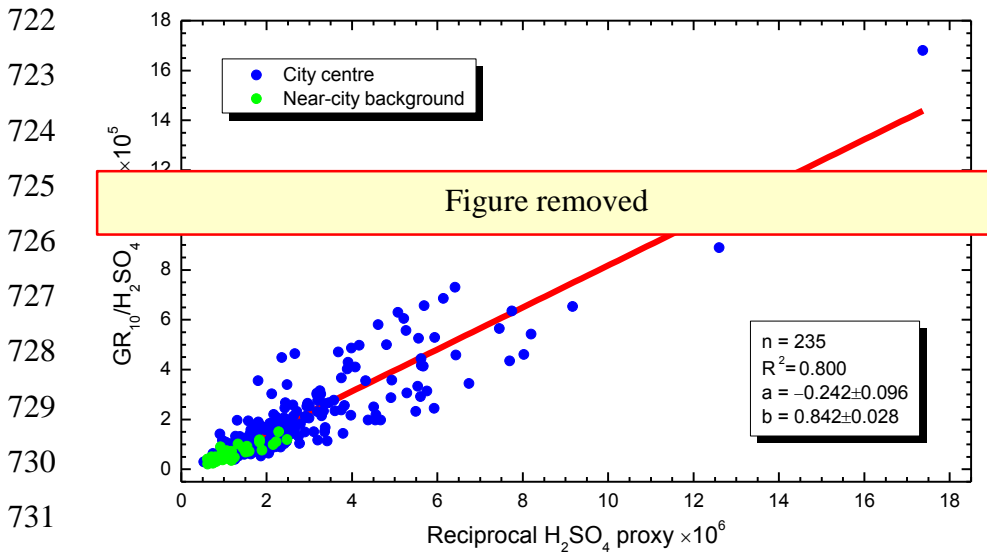697　their understanding is essential when analysing atmospheric observations.
698

699　As far as the pollutant gases are concerned, no correlation could be identified between J_6 or
700　GR_{10} on one side and the gas concentrations on the other side. The coefficients of correlation
701　between CS and NO_x or CO were modest (R=0.37 and 0.42, respectively with n=164 and 152,
702　respectively), while correlation of NO_x and CO on one side with WS was also modest but
703　negative (R= –0.32 and –0.42, respectively with n=167 and 155, respectively). The former
704　relationships can be explained by the fact that vehicular road traffic in cities is a considerable
705　and common source of NO_x, CO and primary particles (Paasonen et al., 2016), and the emitted
706　particles largely contribute to CS levels. The latter relationships are linked to the effect of large-
707　scale air mass transport (often connected to high WSs) on urban air pollution or air quality.
708

709　~~Importance and contribution of condensing vapours other than H_2SO_4 are further demonstrated~~
710　~~in Fig. 4. The data for the city centre and near-city background were presented in a linearized~~
711　~~form and separately for the 2 sites. Nevertheless, the fitting of the correlation line was~~
712　~~accomplished for the joint 6-year long data set. It can be demonstrated in particular on non-~~
713　~~linearized plot of the GR_{10}/H_2SO_4-proxy as function of H_2SO_4-proxy (not shown here) that the~~
714　~~2 data sets merge into each other without any relevant structure, and, therefore, that they can be~~
715　~~regarded to be coherent. This approach seems sensible when considering also the limited~~
716　~~accuracy of the values. The relationship between the 2 composite variables in Fig. 4 was~~
717　~~significant (R^2=0.800, p<0.05). It can be interpreted as the increasing atmospheric concentration~~
718　~~of gas-phase H_2SO_4 can be related to larger contributions of other vapours than H_2SO_4 to~~
719　~~particle growth. The other or competing compounds may include oxidation products and their~~
720　~~dimers from photooxidation of VOC precursors from both biogenic and anthropogenic sources.~~
721

Figure 4. ~~Dependence of the growth rate GR_{10} (in a unit of nm h^{-1}) of new particle formation and growth events normalised to the daily maximum gas-phase H$_2$SO$_4$-proxy (µg m^{-5} W s) on the reciprocal proxy value in the city centre and near-city background. The linear line in red represents the line fitted to the joint data set. Number of individual data considered (n), their coefficient of determination (R^2) and the intercept (a) and slope (b) of the fitted regression line with standard deviations are also shown.~~

4.4 Extreme and multiple events

The joint 6-year long data sets of J_6, GR_{10} and Δt containing all, 247 individual data each could be characterised by lognormal distribution function. This is demonstrated by log-probability graph for J_6 in Fig. S2 as example. The coefficient of determination, median and geometric standard deviation for J_6, GR_{10} and Δt data sets were 0.990, 4.0 cm^{-3} and 2.3; 0.993, 6.8 nm h^{-1} and 1.46; and 0.998, 02:57 (0.123 d) and 1.74, respectively.

One of the major properties of this distribution type is that it contains relatively large individual data with considerably high abundances. There were 5 individual J_6 and 5 individual GR_{10} data above the 98% percentile of the data sets, which belonged to 9 separate NPF and growth events (days). Their specifications, properties and parameters are summarised in Table 3. All these events occurred in the city centre from April to September. ~~Their number in the separate consecutive measurement years (Sect. 2) were 1, 0, 1, 2, 0 and 5, respectively.~~ The medians of J_6, GR_{10}, CS and air T for the subsets of these 9 extreme event days were larger by factors of 5.2, 2.4, 1.5 and 1.4, respectively than for the city centre data. At the same time, the medians of the other atmospheric properties and concentrations in these 2 respective data sets agreed within approximately 10%. There was a single event associated with an extreme H$_2$SO$_4$ proxy

24

756 (of 23×10^5 µg m^{-5} W s) and relatively low NO$_x$ concentration (44 µg m^{-3}), which indicate

757 exceptionally favourable conditions for NPF and growth. In addition to this case, there were

758 only a few days that were characterised by an unusually large CS (23×10^{-3} s^{-1}) – which could

759 in turn be linked to higher dynamic rates (Sect. 4.3) – or by somewhat larger SO$_2$ (8.1 µg m^{-3})

760 or lower NO$_x$ concentration (34 µg m^{-3}). For all the other events, however, no simple or

761 compound property of the investigated variables could explain the extreme rates. Instead, they

762 may be related to some other chemical species and/or atmospheric processes, which were not

763 including in the present study. ~~Since the extreme NPF and growth events usually resembled the~~

764 ~~time evolution for regional events (well-developed banana curves) – sometimes with multiple~~

765 ~~onsets –, the missing atmospheric players in increased concentrations or their relevant processes~~

766 ~~are expected to appear on a larger horizontal spatial scale.~~

767

768 **Table 3.** Date (in a format of dd–MM–yyyy), new particle formation rate J_6 (in a unit of cm^{-3} s^{-1}),

769 particle diameter growth rate GR$_{10}$ (nm h^{-1}), starting time t_1 of nucleation (HH:mm UTC+1), duration

770 time interval $\Delta t = t_2 - t_1$ of nucleation (HH:mm), mean condensation sink CS during the nucleation process

771 (10^{-3} s^{-1}), daily maximum gas-phase H$_2$SO$_4$ proxy (10^4 µg m^{-5} W s), daily mean air temperature T (°C),

772 daily mean relative humidity RH (%), daily median concentrations of SO$_2$, O$_3$, NO$_x$ (µg m^{-3}) and CO

773 (mg m^{-3}) gases, and the type of the onset for extreme quantifiable (class 1A) new particle formation and

774 growth events. The cells in yellow indicate the values which are above the 98% percentile of the

775 corresponding data sets. N.a.: not available.

776

Date/ property	15–09–2009	20–04–2014	19–05–2015	04–07–2015	28–05–2017	25–06–2017	02–08–2017	31–08–2017	09–09–2017
J_6	15.9	17.8	24	16.3	27	33	30	47	17.3
GR$_{10}$	17.4	19.0	12.2	18.0	9.2	17.0	11.8	21	19.8
t_1	10:20	08:52	08:52	09:38	06:34	10:18	07:39	10:06	11:38
Δt	01:23	01:42	03:57	02:06	07:15	02:46	06:58	06:19	02:06
Proxy	38	42	25	16	229	41	69	92	45
CS	13.4	8.9	13.7	11.9	6.9	10.5	23	18.2	15.5
T	20	13.0	22	26	20	24	29	23	19.1
RH	60	62	48	40	40	68	49	47	58
SO$_2$	6.1	2.5	4.4	2.3	3.4	3.1	5.6	8.1	6.6
O$_3$	16.3	43	n.a.	33	61	56	34	24	12.9
NO$_x$	69	34	174	70	44	66	n.a.	109	112
CO	0.42	n.a.	0.71	0.33	0.31	0.50	0.97	0.62	0.71
Onset	ordinary	double	broad	ordinary	broad	broad	broad	broad	ordinary

777

778

779 Each quantifiable NPF and growth event was labelled as ordinary or broad by visual inspection

780 of its beginning part. If the width of the beginning was smaller than approximately 2 h or there

781 was a determinant single growth curve (rib) on the size distribution surface plot then the onset

782 was labelled as ordinary, otherwise as broad (Fig. S1a and S1c for broad onsets). Broad onsets

783 can be generated by 1) long-lasting nucleation process, 2) disrupted and started over nucleation

784 due to changing atmospheric and meteorological conditions or 3) multiple nucleation processes

785 close to each other in time (Salma et al., 2016b). The broad onsets were specified as doublets

786 if the nucleation mode could be separated into 2 submodes by size distribution fitting.

787 Approximately 40% of all quantifiable events had a broad onset. This indicates that NPF and

788 growth events with broad/multiple onsets are abundant in the urban environment, which could

789 be an important difference from remote or clean atmospheres.

790

791 For 9% of all quantifiable days, it was feasible to calculate 2 sets of dynamic properties for

792 onsets 1 and 2 with a reasonable accuracy. In the near-city background, the medians of J_6 and

793 GR_{10} for the onset 1 were similar ~~or somewhat smaller~~ than the corresponding medians for the

794 whole near-city background data set, while for the onset 2, they were substantially larger,

795 namely 4.1 cm^{-3} s^{-1} and 10.0 nm h^{-1}, respectively (cf. Table 2). Actually, the latter values were

796 closer to the medians of the city centre than for the near-city background. ~~The dynamic~~

797 ~~properties for the city centre for both the onset 1 and onset 2 were somewhat larger than for the~~

798 ~~whole the city centre data set.~~ Approximately 75% of the doublets resulted in individual

799 onset2/onset1 ratios larger than unity. Their overall median ratios for J_6 and GR_{10} were similar

800 and approximately 1.4, while for the near-city background, they were about 2. The results are

801 in line with ~~and confirm~~ our earlier conclusion according to which the second onsets (if it is a

802 new formation process and not just a started over event) ~~often generate new particles more~~

803 ~~intensively~~ are more intensive than the first onsets (Salma et al., 2016b). These particles also

804 grow faster. This can be explained by the fact that the first event is ~~often or likely~~ of regional

805 scale since its dynamic properties resemble those of the regional background ~~process~~ (Yli-Juuti

806 et al., 2009), while the later event can be characterised by values typical for the city centre

807 (Salma et al., 2016b). The later event (or events) are mainly caused and governed by sub-

808 regional processes. These findings are also coherent with a previous observation of NPF and

809 growth events with multiple onsets in semi-clean savannah and industrial environments

810 (Hirsikko et al., 2013), and they also fit well into the existing ideas on mixing regional and

26

811 urban air parcels that exhibit different properties such as precursor concentrations, T and RH

812 (Kulmala et al., 2017).

813

814 **5 Conclusions**

815

816 Magnitude of the particle number concentration level produced solely by NPF and growth

817 (strength of the events) can roughly be estimated by considering the median J_6, median duration

818 of nucleation Δt (their distribution function is lognormal; Table 2) and the mean coagulation

819 loss of these particles F_{coag} (0.17; Sect. 3.1 and Table S1) as: $J_6 \times \Delta t \times (1 - F_{coag})$. In central

820 Budapest, it yields a concentration of 10^4 cm^{-3}. This is in line with another result achieved by

821 nucleation strength factor (Salma et al., 2017). More importantly, the estimated concentration

822 from NPF and growth process is comparable to the annual median atmospheric concentrations

823 (Sect. 4). This simple example indicates that the phenomenon is not only relevant for aerosol

824 load and climate issues on regional or global spatial scales – which were first recognised – but

825 it can affect the urban climate and the health risk of inhabitants of cities as well.

826

827 Similar recognitions have led to the emerge of urban atmospheric nucleation studies. As part of

828 this international progress, we presented here a considerable variety of contributions, which

829 became feasible thank to gradually generating, multi-year long, critically evaluated, complex

830 and coherent data sets. Dynamic and timing properties of 247 NPF and growth events were

831 studied together with supporting aerosol properties, meteorological data and pollutant gas

832 concentrations in near-city background and city centre of Budapest for 6 years. The results and

833 conclusions derived form in important component that is based on atmospheric observations.

834 The present study can also be considered as the first step toward a larger statistical evaluation

835 process. The results are to be combine with results from laboratory experiments and finally,

836 with theoretical models to further improve our understanding on the atmospheric processes in

837 cities. Specialities and features of the urban atmospheric NPF and growth phenomena are finally

838 to be also considered when assessing their potentials to increase UF and CCN concentrations

839 or their health implications.

840

841 The present research based on ambient atmospheric measurements provided evidence that some

842 important chemical players in the NPF and growth events are still missing. Considering the

843 results and conclusions of cloud chamber experiments, these factors are expected to be related

844 mainly to oxidation products of VOCs and/or their processes. Further dedicated research

845 including sophisticated measurements, data evaluations and modelling studies is required to

846 find and identify these species and their processes, and to account their multifactorial role in

847 more detail. Such measurement campaign focusing on chemical composition of molecular

848 clusters, precursors and nucleating vapours by applying recent expedient instruments in

849 Budapest over the months of the highest expected event occurrence has been just realised within

850 a frame of an international cooperation. Its perspective results can hopefully provide additional

851 valuable information for some of the conclusion base on indirect evidence for the time being

852 and can further clarify the overall picture on urban multicomponent nucleation and growth

853 phenomenon.

854

858

860

865

866 **References**

867 Alam, A., Shi, J. P., and Harrison, R. M.: Observations of new particle formation in urban air, J.

868   Geophys. Res., 108 (D3), 4093, doi:10.1029/2001JD001417, 2003.

869 Almeida, J., Schobesberger, S., Kurten, A., Ortega, I. K., Kupiainen-Maatta, O., Praplan, A. P.,

870   Adamov, A., Amorim, A., Bianchi, F., Breitenlechner, M., David, A., Dommen, J., Donahue, N.

871   M., Downard, A., Dunne, E., Duplissy, J., Ehrhart, S., Flagan, R. C., Franchin, A., Guida, R.,

872   Hakala, J., Hansel, A., Heinritzi, M., Henschel, H., Jokinen, T., Junninen, H., Kajos, M.,

873   Kangasluoma, J., Keskinen, H., Kupc, A., Kurten, T., Kvashin, A. N., Laaksonen, A., Lehtipalo,

874   K., Leiminger, M., Leppa, J., Loukonen, V., Makhmutov, V., Mathot, S., McGrath, M. J.,

875   Nieminen, T., Olenius, T., Onnela, A., Petäjä, T., Riccobono, F., Riipinen, I., Rissanen, M., Rondo,

876   L., Ruuskanen, T., Santos, F. D., Sarnela, N., Schallhart, S., Schnitzhofer, R., Seinfeld, J. H.,

877   Simon, M., Sipilä, M., Stozhkov, Y., Stratmann, F., Tome, A., Tröstl, J., Tsagkogeorgas, G.,

878   Vaattovaara, P., Viisanen, Y., Virtanen, A., Vrtala, A., Wagner, P. E., Weingartner, E., Wex, H.,

879   Williamson, C., Wimmer, D., Ye, P. L., Yli-Juuti, T., Carslaw, K. S., Kulmala, M., Curtius, J.,

880   Baltensperger, U., Worsnop, D. R., Vehkamäki, H., and Kirkby, J.: Molecular understanding of

881   sulphuric acid–amine particle nucleation in the atmosphere, Nature, 502, 359–363, 2013.

882   Baltensperger, U., Streit, N., Weingartner, E., Nyeki, S., Prévôt, A. S. H., Van Dingenen, R., Virkkula,

883   A., Putaud, J. P., Even, A., Brink, H., Blatter, A., Neftel, A., and Gaggeler, H. W.: Urban and rural

884   aerosol characterization of summer smog events during the PIPAPO field campaign in Milan, Italy,

885   J. Geophys. Res., 107(D22), 8193, doi:10.1029/2001JD001292, 2002.

886   Bianchi, F., Tröstl, J., Junninen, H., Frege, C., Henne, S., Hoyle, C. R., Molteni, U., Herrmann, E.,

887   Adamov, A., Bukowiecki, N., Chen, X., Duplissy, J., Gysel, M., Hutterli, M. Kangasluoma, J.,

888   Kontkanen, J., Kürten, A. Manninen, H. E., Münch, S., Peräkylä, O., Petäjä, T., Rondo, L.,

889   Williamson, C., Weingartner, E. Curtius, J., Worsnop, D. R., Kulmala, M., Dommen, J., and

890   Baltensperger, U.: New particle formation in the free troposphere: A question of chemistry and

891   timing, Science, 352, 1109–1112, https://doi.org/10.1126/science.aad5456, 2016.

892   Braakhuis, H. M., Park, M. V., Gosens, I., De Jong, W. H., and Cassee, F. R.: Physicochemical

893   characteristics of nanomaterials that affect pulmonary inflammation, Part. Fibre Toxicol., 11:18,

894   doi: 10.1186/1743-8977-11-18, 2014.

895   Cai, R. and Jiang, J.: A new balance formula to estimate new particle formation rate: reevaluating the

896   effect of coagulation scavenging, Atmos. Chem. Phys., 17, 12659–12675, 2017.

897   Carslaw, K. S., Lee, L. A., Reddington, C. L., Pringle, K. J., Rap, A., Forster, P. M., Mann, G. W.,

898   Spracklen, D. V., Woodhouse, M. T., Regayre, L. A., and Pierce, J. R: Large contribution of

899   natural aerosols to uncertainty in indirect forcing, Nature, 503, 67–71, 2013.

900   Crounse, J. D., Nielsen, L. B., Jørgensen, S., Kjaergaard, H. G., and Wennberg, P. O.: Autoxidation of

901   organic compounds in the atmosphere, J. Phys. Chem. Lett., 4, 20, 3513–3520, 2013.

902   Dal Maso, M., Kulmala, M., Lehtinen, K. E. J., Mäkelä, J. M., Aalto, P. P., and O'Dowd, C.:

903   Condensation and coagulation sinks and formation of nucleation mode particles in coastal and

904   boreal forest boundary layers, J. Geophys. Res., 107(19D), 8097, 10.1029/2001jd001053, 2002.

905   Dal Maso, M., Kulmala, M., Riipinen, I., Wagner, R., Hussein, T., Aalto, P. P., and Lehtinen, K. E. J.:

906   Formation and growth of fresh atmospheric aerosols: eight years of aerosol size distribution data

907   from SMEAR II, Hyytiälä, Finland, Boreal Environ. Res., 10, 323–336, 2005.

908   Dall'Osto, M., Querol, X., Alastuey, A., O'Dowd, C., Harrison, R. M., Wenger, J., and Gómez-

909   Moreno, F. J.: On the spatial distribution and evolution of ultrafine particles in Barcelona, Atmos.

910   Chem. Phys., 13, 741–759, 2013.

911   Ehn, M., Thornton, J. A., Kleist, E., Sipilä, M., Junninen, H., Pullinen, I., Springer, M., Rubach, F.,

912   Tillmann, R., Lee, B., Lopez-Hilfiker, F., Andres, S., Acir, I. H., Rissanen, M., Jokinen, T.,

913   Schobesberger, S., Kangasluoma, J., Kontkanen, J., Nieminen, T., Kurten, T., Nielsen, L. B.,

914   Jorgensen, S., Kjaergaard, H. G., Canagaratna, M., Dal Maso, M., Berndt, T., Petäjä, T., Wahner,

915   A., Kerminen, V. M., Kulmala, M., Worsnop, D. R., Wildt, J., and Mentel, T. F.: A large source of

916   low-volatility secondary organic aerosol, Nature, 506, 476–479, 2014.

917 Gordon, H., Sengupta, K., Rap, A., Duplissy, J., Frege, C., Williamson, C., Heinritzi, M., Simon, M.,
918 Yan, C., Almeida, J., Tröstl, J., Nieminen, T., Ortega, I. K., Wagner, R., Dunne, E. M., Adamov,
919 A., Amorim, A., Bernhammer, A. K., Bianchi, F., Breitenlechner, M., Brilke, S., Chen, X., Craven,
920 J. S., Dias, A., Ehrhart, S., Fischer, L., Flagan, R. C., Franchin, A., Fuchs, C., Guida, R., Hakala, J.,
921 Hoyle, C. R., Jokinen, T., Junninen, H., Kangasluoma, J., Kim, J., Kirkby, J., Krapf, M., Kürten,
922 A., Laaksonen, A., Lehtipalo, K., Makhmutov, V., Mathot, S., Molteni, U., Monks, S. A., Onnela,
923 A., Peräkylä, O., Piel, F., Petäjä, T., Praplan, A. P., Pringle, K. J., Richards, N. A. D., Rissanen, M.
924 P., Rondo, L., Sarnela, N., Schobesberger, S., Scott, C. E., Seinfeld, J. H., Sharma, S., Sipilä, M.,
925 Steiner, G., Stozhkov, Y., Stratmann, F., Tomé, A., Virtanen, A., Vogel, A. L., Wagner, A. C.,
926 Wagner, P. E., Weingartner, E., Wimmer, D., Winkler, P. M., Ye, P., Zhang, X., Hansel, A.,
927 Dommen, J., Donahue, N. M., Worsnop, D. R., Baltensperger, U., Kulmala, M., Curtius, J., and
928 Carslaw, K. S.: Reduced anthropogenic aerosol radiative forcing caused by biogenic new particle
929 formation, Proc. Natl. Acad. Sci. U.S.A., 113, 12053–12058,
930 https://doi.org/10.1073/pnas.1602360113, 2016.
931 Hirsikko, A., Vakkari, V., Tiitta, P., Hatakka, J., Kerminen, V.-M., Sundström, A.-M., Beukes, J. P.,
932 Manninen, H. E., Kulmala, M., and Laakso, L.: Multiple daytime nucleation events in semi-clean
933 savannah and industrial environments in South Africa: analysis based on observations, Atmos.
934 Chem. Phys., 13, 5523–5532, 2013.
935 Hussein, T., Puustinen, A., Aalto, P. P., Mäkelä, J. M., Hämeri, K., and Kulmala, M.: Urban aerosol
936 number size distributions, Atmos. Chem. Phys., 4, 391–411, 2004.
937 Hussein, T., Martikainen, J., Junninen, H., Sogacheva, L., Wagner, R., Dal Maso, M., Riipinen, I.,
938 Aalto, P. P., and Kulmala, M.: Observation of regional new particle formation in the urban
939 atmosphere, Tellus 60B, 509–521, 2008.
940 Jokinen, T., Berndt, T., Makkonen, R., Kerminen, V.-M., Junninen, H., Paasonen, P., Stratmann, F.,
941 Herrmann, H., Guenther, A. B., Worsnop, D. R., Kulmala, M., Ehn, M. and Sipilä, M.: Production
942 of extremely low volatile organic compounds from biogenic emissions: Measured yields and
943 atmospheric implications, Proc. Natl. Acad. Sci. U.S.A., 112, 7123–7128, 2015.
944 Kerminen, V.-M., Paramonov, M., Anttila, T., Riipinen, I., Fountoukis, C., Korhonen, H., Asmi, E.,
945 Laakso, L., Lihavainen, H., Swietlicki, E., Svenningsson, B., Asmi, A., Pandis, S. N., Kulmala, M.,
946 and Petäjä, T.: Cloud condensation nuclei production associated with atmospheric nucleation: a
947 synthesis based on existing literature and new results, Atmos. Chem. Phys., 12, 12037–12059,
948 2012.
949 Kerminen, V.-M., Chen, X., Vakkari, V., Petäjä, T., Kulmala, M., and Bianchi, F.: Atmospheric new
950 particle formation and growth: review of field observations, Environ. Res. Lett., 13 (2018) 103003,
951 2018.
952 Kirkby, J., Curtius, J., Almeida, J., Dunne, E., Duplissy, J., Ehrhart, S., Franchin, A., Gagné, S., Ickes,
953 L., Kürten, A., Kupc, A., Metzger, A., Riccobono, F., Rondo, L., Schobesberger, S.,
954 Tsagkogeorgas, G., Wimmer, D., Amorim, A., Bianchi, F., Breitenlechner, M., David, A.,

955 Dommen, J., Downard, A., Ehn, M., Flagan, R. C., Haider, S., Hansel, A., Hauser, D., Jud, W.,
956 Junninen, H., Kreissl, F., Kvashin, A., Laaksonen, A., Lehtipalo, K., Lima, J., Lovejoy, E. R.,
957 Makhutov, V., Mathot, S., Mikkilä, J., Minginette, P., Mogo, S., Nieminen, T., Onnela, A., Pereira,
958 A., Petäjä, T., Schnitzhofer, R., Seinfeld, J. H., Sipilä, M., Stozhkov, Y., Stratmann, F., Tome, A.,
959 Vanhanen, J., Viisanen Y., Vrtala, A., Wagner, P.E., Walther, H., Weingartner, E., Wex, H.,
960 Winkler, P.M., Carslaw, K. S., Worsnop, D. R., Baltensperger, U., and Kulmala, M.: The role of
961 sulfuric acid, ammonia and galactic cosmic rays in atmospheric aerosol nucleation, Nature, 476,
962 429–433, 2011.
963 Kirkby, J., Duplissy, J., Sengupta, K., Frege, C., Gordon, H., Williamson, C., Heinritzi, M., Simon,
964 M., Yan, C., Almeida, J., Tröstl, J., Nieminen, T., Ortega, I. K., Wagner, R., Adamov, A., Amorim,
965 A., Bernhammer, A.-K., Bianchi, F., Breitenlechner, M., Brilke, S., Chen, X., Craven, J., Dias, A.,
966 Ehrhart, S., Flagan, R. C., Franchin, A., Fuchs, C., Guida, R., Hakala, J., Hoyle, C. R., Jokinen, T.,
967 Junninen, H., Kangasluoma, J., Kim, J., Krapf, M., Kürten, A., Laaksonen, A., Lehtipalo, K.,
968 Makhmutov, V., Mathot, S., Molteni, U., Onnela, A., Peräkylä, O., Piel, F., Petäjä, T., Praplan, A.
969 P., Pringle, K., Rap, A., Richards, N. A. D., Riipinen, I., Rissanen, M. P., Rondo, L., Sarnela, N.,
970 Schobesberger, S., Scott, C. E., Seinfeld, J. H., Sipilä, M., Steiner, G., Stozhkov, Y., Stratmann, F.,
971 Tomé, A., Virtanen, A., Vogel, A. L., Wagner, A., Wagner, P. E., Weingartner, E., Wimmer, D.,
972 Winkler, P. M., Ye, P., Zhang, X., Hansel, A., Dommen, J., Donahue, N. M., Worsnop, D. R.,
973 Baltensperger, U., Kulmala, M., Carslaw, K. S., and Curtius, J.: Ion-induced nucleation of pure
974 biogenic particles, Nature, 533, 521–526, https://doi.org/10.1038/nature17953, 2016.
975 Kulmala, M., Dal Maso, M., Mäkelä, J. M., Pirjola, L., Väkevä, M., Aalto, P., Miikkulainen, P.,
976 Hämeri, K., and O'Dowd, C. D.: On the formation, growth and composition of nucleation mode
977 particles, Tellus B53, 479–490, 2001.
978 Kulmala, M., Vehkamäki, H., Petäjä, T., Dal Maso, M., Lauri, A., Kerminen, V.-M., Birmili, W., and
979 McMurry, P.: Formation and growth rates of ultrafine atmospheric particles: a review of
980 observations, J. Aerosol Sci., 35, 143–176, 2004.
981 Kulmala, M., Petäjä, T., Nieminen, T., Sipilä, M., Manninen, H. E., Lehtipalo, K., Dal Maso, M.,
982 Aalto, P. P., Junninen, H., Paasonen, P., Riipinen, I., Lehtinen, K. E. J., Laaksonen, A., and
983 Kerminen, V.-M.: Measurement of the nucleation of atmospheric aerosol particles, Nat. Protoc., 7,
984 1651–1667, doi:10.1038/nprot.2012.091, 2012.
985 Kulmala, M., Kontkanen, J., Junninen, H., Lehtipalo, K., Manninen, H. E., Nieminen, T., Petäjä, T.,
986 Sipilä, M., Schobesberger, S., Rantala, P., Franchin, A., Jokinen, T., Järvinen, E., Äijälä, M.,
987 Kangasluoma, J., Hakala, J., Aalto, P.P., Paasonen, P., Mikkilä, J., Vanhanen, J., Aalto, J., Hakola,
988 H., Makkonen, U., Ruuskanen, T., Mauldin, R. L. III, Duplissy, J., Vehkamäki, H., Bäck, J.,
989 Kortelainen, A., Riipinen, I., Kurtén, T., Johnston, M. V., Smith, J. N., Ehn, M., Mentel, T. F.,
990 Lehtinen, K. E. J., Laaksonen, A., Kerminen, V.-M., and Worsnop, D. R.: Direct observations of
991 atmospheric aerosol nucleation, Science, 339, 943–946, 2013.

992   Kulmala, M., Petäjä, T., Ehn, M., Thornton, J., Sipilä, M., Worsnop, D. R., and Kerminen, V.-M.:
993   Chemistry of atmospheric nucleation: On the recent advances on precursor characterization and
994   atmospheric cluster composition in connection with atmospheric new particle formation, Annu.
995   Rev. Phys. Chem., 65, 21−37, 2014.

996   Kulmala, M., Kerminen, V. M., Petäjä, T., Ding, A. J., and Wang, L.: Atmospheric gas-to-particle
997   conversion: why NPF events are observed in megacities, Faraday Discuss.,
998   doi:10.1039/C6FD00257A, 2017.

999   Makkonen, R., Asmi, A., Korhonen, H., Kokkola, H., Järvenoja, S., Räisänen, P., Lehtinen, K. E. J.,
1000   Laaksonen, A., Kerminen, V.-M., Järvinen, H., Lohmann, U., Bennartz, R., Feichter, J., and
1001   Kulmala, M.: Sensitivity of aerosol concentrations and cloud properties to nucleation and
1002   secondary organic distribution in ECHAM5-HAM global circulation model, Atmos. Chem. Phys.,
1003   9, 1747–1766, 2009.

1004   Makkonen, R., Asmi, A., Kerminen, V.-M., Boy, M., Arneth, A., Hari, P., and Kulmala, M.: Air
1005   pollution control and decreasing new particle formation lead to strong climate warming, Atmos.
1006   Chem. Phys., 12, 1515–1524, 2012.

1007   Merikanto, J., Spracklen, D. V., Mann, G. W., Pickering, S. J., and Carslaw, K. S.: Impact of
1008   nucleation on global CCN, Atmos. Chem. Phys., 9, 8601–8616, 2009.

1009   Metzger, A., Verheggen, B., Dommen, J., Duplissy, J., Prévôt, A. S. H., Weingartner, E., Riipinen, I.,
1010   Kulmala, M., Spracklen, D. V., Carslaw, K. S., and Baltensperger, U.: Evidence for the role of
1011   organics in aerosol particle formation under atmospheric conditions, Proc. Natl. Acad. Sci. U. S.
1012   A., 107, 6646–6651, 2010.

1013   Németh, Z. and Salma, I.: Spatial extension of nucleating air masses in the Carpathian Basin, Atmos.
1014   Chem. Phys., 14, 8841–8848, 2014.

1015   Németh, Z., Rosati, B., Zíková, N., Salma, I., Bozó, L., Dameto de España, C., Schwarz, J., Ždímal,
1016   V., and Wonaschütz, A.: Comparison of atmospheric new particle formation and growth events in
1017   three Central European cities, Atmos. Environ., 178, 191–197, 2018.

1018   Nieminen, T., Kerminen, V.-M., Petäjä, T., Aalto, P. P., Arshinov, M., Asmi, E., Baltensperger, U.,
1019   Beddows, D. C. S., Beukes, J. P., Collins, D., Ding, A., Harrison, R. M., Henzing, B., Hooda, R.,
1020   Hu, M., Hõrrak, U., Kivekäs, N., Komsaare, K., Krejčí, R., Kristensson, A., Laakso, L., Laaksonen,
1021   A., Leaitch, W. R., Lihavainen, H., Mihalopoulos, N., Németh, Z., Nie, W., O'Dowd, C., Salma, I.,
1022   Sellegri, K., Svenningsson, B., Swietlicki, E., Tunved, P., Ulevicius, V., Vakkari, V., Vana, M.,
1023   Wiedensohler, A., Wu, Z., Virtanen, A., and Kulmala, M.: Global analysis of continental boundary
1024   layer new particle formation based on long-term measurements, Atmos. Chem. Phys., 18, 14737–
1025   14756, 2018.

1026   Oberdörster, G., Oberdörster, E., and Oberdörster, J.: Nanotoxicology: an emerging discipline
1027   evolving from studies of ultrafine particles, Environ. Health Perspect., 113, 823–839, 2005.

1028 O'Dowd, C. D., Jimenez, J. L., Bahreini, R. Flagan, R. C., Seinfeld, J. H., Hämeri, K., Pirjola, L.,

1029   Kulmala, M., Jennings, S. G., and Hoffmann, Th.: Marine aerosol formation from biogenic iodine

1030   emissions, Nature 417, 632–636, 2002.

1031 Paasonen, P., Kupiainen, K., Klimont, Z., Visschedijk, A., Denier van der Gon, H. A. C., and Amann,

1032   M.: Continental anthropogenic primary particle number emissions, Atmos. Chem. Phys., 16, 6823–

1033   6840, 2016.

1034 Paasonen, P., Peltola, M., Kontkanen, J., Junninen, H., Kerminen, V.-M., and Kulmala, M.:

1035   Comprehensive analysis of particle growth rates from nucleation mode to cloud condensation

1036   nuclei in Boreal forest, Atmos. Chem. Phys. Discuss., https://doi.org/10.5194/acp-2018-169, in

1037   review, 2018.

1038 Petäjä, T., Mauldin, III, R. L., Kosciuch, E., McGrath, J., Nieminen, T., Paasonen, P., Boy, M.,

1039   Adamov, A., Kotiaho, T., and Kulmala, M.: Sulfuric acid and OH concentrations in a boreal forest

1040   site, Atmos. Chem. Phys., 9, 7435–7448, 2009.

1041 Putaud, J.-P., Van Dingenen, R., Alastuey, A., Bauer, H., Birmili, W., Cyrys, J., Flentje, H., Fuzzi, S.,

1042   Gehrig, R., Hansson, H. C., Harrison, R. M., Herrmann, H., Hitzenberger, R., Hüglin, C., Jones,

1043   A.M., Kasper-Giebl, A., Kiss, G., Kousa, A., Kuhlbusch, T. A. J., Löschau, G., Maenhaut, W.,

1044   Molnár, A., Moreno, T., Pekkanen, J., Perrino, C., Pitz, M., Puxbaum, H., Querol, X., Rodriguez,

1045   S., Salma, I., Schwarz, J., Smolík, J., Schneider, J., Spindler, G., ten Brink, H., Turšič, J., Viana,

1046   M., Wiedensohler, and A., Raes, F.: A European Aerosol Phenomenology - 3: physical and

1047   chemical characteristics of particulate matter from 60 rural, urban, and kerbside sites across

1048   Europe, Atmos. Environ., 44, 1308–1320, 2010.

1049 Riccobono, F., Schobesberger, S., Scott, C., Dommen, J., Ortega, I., Rondo, L., Almeida, J., Amorim,

1050   A., Bianchi, F., Breitenlechner, M., David, A., Downard, A., Dunne, E., Duplissy, J., Ehrhart, S.,

1051   Flagan, R., Franchin, A., Hansel, A., Junninen, H., Kajos, M., Keskinen, H., Kupc, A., Kurten, A.,

1052   Kvashin, A., Laaksonen, A., Lehtipalo, K., Makhmutov, V., Mathot, S., Nieminen, T., Onnela, A.,

1053   Petäjä, T., Praplan, A., Santos, F., Schallhart, S., Seinfeld, J., Sipila, M., Spracklen, D., Stozhkov,

1054   Y., Stratmann, F., Tome, A., Tsagkogeorgas, G., Vaattovaara, P., Viisanen, Y., Vrtala, A., Wagner,

1055   P., Weingartner, E., Wex, H., Wimmer, D., Carslaw, K., Curtius, J., Donahue, N., Kirkby, J.,

1056   Kulmala, M., Worsnop, D., and Baltensperger, U.: Oxidation products of biogenic emissions

1057   contribute to nucleation of atmospheric particles, Science, 344, 717–721, 2014.

1058 Riipinen, I., Pierce, J. R., Yli-Juuti, T., Nieminen, T., Häkkinen, S., Ehn, M., Junninen, H., Lehtipalo,

1059   K., Petäjä, T., Slowik, J., Chang, R., Shantz, N. C., Abbatt, J., Leaitch, W. R., Kerminen, V.-M.,

1060   Worsnop, D. R., Pandis, S. N., Donahue, N. M., and Kulmala, M.: Organic condensation: a vital

1061   link connecting aerosol formation to cloud condensation nuclei (CCN) concentrations, Atmos.

1062   Chem. Phys., 11, 3865–3878, 2011.

1063 Salma, I., Borsós, T., Weidinger, T., Aalto, P., Hussein, T., Dal Maso, M., and Kulmala, M.:

1064   Production, growth and properties of ultrafine atmospheric aerosol particles in an urban

1065   environment, Atmos. Chem. Phys., 11, 1339–1353, 2011.

1066 Salma, I., Borsós, T., Németh, Z., Weidinger, T., Aalto, T., and Kulmala, M.: Comparative study of
1067   ultrafine atmospheric aerosol within a city, Atmos. Environ., 92, 154–161, 2014.
1068 Salma, I., Füri, P., Németh, Z., Farkas, Á., Balásházy, I., Hofmann, W., and Farkas, Á.: Lung burden
1069   and deposition distribution of inhaled atmospheric urban ultrafine particles as the first step in their
1070   health risk assessment, Atmos. Environ., 104, 39–49, 2015.
1071 Salma, I., Németh, Z., Weidinger, T., Kovács, B., and Kristóf, G.: Measurement, growth types and
1072   shrinkage of newly formed aerosol particles at an urban research platform, Atmos. Chem. Phys.,
1073   16, 7837–7851, 2016a.
1074 Salma, I., Németh, Z., Kerminen, V. M., Aalto, P., Nieminen, T., Weidinger, T., Molnár, Á., Imre, K.,
1075   and Kulmala, M.: Regional effect on urban atmospheric nucleation, Atmos. Chem. Phys., 16,
1076   8715–8728, 2016b.
1077 Salma, I., Varga, V., and Németh, Z.: Quantification of an atmospheric nucleation and growth process
1078   as a single source of aerosol particles in a city, Atmos. Chem. Phys., 17, 15007–15017, 2017.
1079 Schobesberger, S., Junninen, H., Bianchi, F., Lonn, G., Ehn, M., Lehtipalo, K., Dommen, J., Ehrhart,
1080   S., Ortega, I. K., Franchin, A., Nieminen, T., Riccobono, F., Hutterli, M., Duplissy, J., Almeida, J.,
1081   Amorim, A., Breitenlechner, M., Downard, A. J., Dunne, E. M., Flagan, R. C., Kajos, M.,
1082   Keskinen, H., Kirkby, J., Kupc, A., Kurten, A., Kurten, T., Laaksonen, A., Mathot, S., Onnela, A.,
1083   Praplan, A. P., Rondo, L., Santos, F. D., Schallhart, S., Schnitzhofer, R., Sipilä, M., Tome, A.,
1084   Tsagkogeorgas, G., Vehkamäki, H., Wimmer, D., Baltensperger, U., Carslaw, K. S., Curtius, J.,
1085   Hansel, A., Petäjä, T., Kulmala, M., Donahue, N. M., and Worsnop, D. R.: Molecular
1086   understanding of atmospheric particle formation from sulfuric acid and large oxidized organic
1087   molecules, Proc. Natl. Acad. Sci. U.S.A., 110, 17223–17228, 10.1073/pnas.1306973110, 2013.
1088 Sihto, S.-L., Mikkilä, J., Vanhanen, J., Ehn, M., Liao, L., Lehtipalo, K., Aalto, P. P., Duplissy, J.,
1089   Petäjä, T., Kerminen, V.-M., Boy, M., and Kulmala, M.: Seasonal variation of CCN concentrations
1090   and aerosol activation properties in boreal forest, Atmos. Chem. Phys., 11, 13269–13285, 2011.
1091 Sipilä, M., Berndt, T., Petäjä, T., Brus, D., Vanhanen, J., Stratmann, F., Patokoski, J., Mauldin, R. L.
1092   3rd, Hyvärinen, A. P., Lihavainen, H., and Kulmala, M.: The role of sulfuric acid in atmospheric
1093   nucleation, Science, 327(5970), 1243-6. doi: 10.1126/science.1180315, 2010.
1094 Spracklen, D. V., Carslaw, K. S., Merikanto, J., Mann, G. W., Reddington, C. L., Pickering, S., Ogren,
1095   J. A., Andrews, E., Baltensperger, U., Weingartner, E., Boy, M., Kulmala. M., Laakso, L.,
1096   Lihavainen, H., Kivekäs, N., Komppula, M., Mihalopoulos, N., Kouvarakis, G., Jennings, S. G.,
1097   O'Dowd, C., Birmili, W., Wiedensohler, A., Weller, R., Gras, J., Laj, P., Sellegri, K., Bonn, B.,
1098   Krejčí, R., Laaksonen, A., Hamed, A., Minikin, A., Harrison, R. M., Talbot, R., and Sun, J.: The
1099   contribution of boundary layer nucleation events to total particle concentrations on regional and
1100   global scales, Atmos. Chem. Phys., 6, 5631–5648, 2006.
1101 Tröstl, J., Chuang, W. K., Gordon, H., Heinritzi, M., Yan, C., Molteni, U., Ahlm, L., Frege, C.,
1102   Bianchi, F., Wagner, R., Simon, M., Lehtipalo, K., Williamson, C., Craven, J. S., Duplissy, J.,
1103   Adamov, A., Almeida, J., Bernhammer, A. K., Breitenlechner, M., Brilke, S., Dias, A., Ehrhart, S.,

Flagan, R. C., Franchin, A., Fuchs, C., Guida, R., Gysel, M., Hansel, A., Hoyle, C. R., Jokinen, T., Junninen, H., Kangasluoma, J., Keskinen, H., Kim, J., Krapf, M., Kürten, A., Laaksonen, A., Lawler, M., Leiminger, M., Mathot, S., Möhler, O., Nieminen, T., Onnela, A., Petäjä, T., Piel, F. M., Miettinen, P., Rissanen, M. P., Rondo, L., Sarnela, N., Schobesberger, S., Sengupta, K., Sipilä, M., Smith, J. N., Steiner, G., Tomè, A., Virtanen, A., Wagner, A. C., Weingartner, E., Wimmer, D., Winkler, P. M., Ye, P. L., Carslaw, K. S., Curtius, J., Dommen, J., Kirkby, J., Kulmala, M., Riipinen, I., Worsnop, D. R., Donahue, N. M., and Baltensperger, U.: The role of low-volatility organic compounds in initial particle growth in the atmosphere, Nature, 533, 527, 10.1038/nature18271, 2016.

Vakkari, V., Tiitta, P., Jaars, K., Croteau, P., Beukes, J. P., Josipovic, M., Kerminen, V.-M., Kulmala, M., Venter, A. D., van Zyl, P. G., Worsnop, D. R., and Laakso, L.: Reevaluating the contribution of sulfuric acid and the origin of organic compounds in atmospheric nanoparticle growth, Geophys. Res. Lett., 42, 10486−10493, 2015.

Vuollekoski, H., Sihto, S.-L., Kerminen, V.-M., Kulmala, M., and Lehtinen, K. E. J.: A numerical comparison of different methods for determining the particle formation rate, Atmos. Chem. Phys., 12, 2289–2295, 2012.

Wehner, B., Wiedensohler, A., Tuch, T. M., Wu, Z. J., Hu, M., Slanina, J., and Kiang, C. S.: Variability of the aerosol number size distribution in Beijing, China: new particle formation, dust storms, and high continental background, Geophys. Res. Lett., 31, L22108, 2004.

Wiedensohler, A., Cheng, Y. F., Nowak, A., Wehner, B., Achtert, P., Berghof, M., Birmili, W., Wu, Z. J., Hu, M., Zhu, T., Takegawa, N., Kita, K., Kondo, Y., Lou, S. R., Hofzumahaus, A., Holland, F., Wahner, A., Gunthe, S. S., Rose, D., Su, H., and Pöschl, U.: Mobility particle size spectrometers: harmonization of technical standards and data structure to facilitate high quality long-term observations of atmospheric particle number size distributions, Atmos. Meas. Tech., 5, 657–685, 2012.

Woo, K. S., Chen, D. R., Pui, D. Y. H., and McMurry, P. H.: Measurement of Atlanta aerosol size distributions: observations of ultrafine particle events, Aerosol Sci. Technol., 34, 75–87, 2001.

Xiao, S., Wang, M. Y., Yao, L., Kulmala, M., Zhou, B., Yang, X., Chen, J. M., Wang, D. F., Fu, Q. Y., Worsnop, D. R., and Wang, L.: Strong atmospheric new particle formation in winter in urban Shanghai, China, Atmos. Chem. Phys., 15, 1769–1781, 2015.

Yli-Juuti, T., Riipinen, I., Aalto, P. P., Nieminen, T., Maenhaut, W., Janssens, I. A., Claeys, M., Salma, I., Ocskay, R., Hoffer, A., Imre, K., and Kulmala, M.: Characteristics of new particle formation events and cluster ions at K-puszta, Hungary. Boreal Environ. Res., 14, 683–698, 2009.

Zhang, R., Wang, G., Guo, S., Zamora, M. L., Ying, Q., Lin, Y., Wang, W., Hu, M., and Wang, Y.: Formation of urban fine particulate matter, Chem. Rev., 115, 3803−3855, 2015.

1139 **Supplementary material**

1140

1141 **Table S1.** Relative contributions of particle number concentration increment ($dN_{nuc}/dt=dN_{6-25}/dt-$
1142 $dN_{Ai,<25}/dt$), coagulation scavenging loss (F_{coag}) and growth out of particles from the diameter interval
1143 of 6–25 nm (F_{growth}) relative to the formation rate J_6 in the near-city background and city centre
1144 separately for 1-year long measurement time intervals. The measurement year and number of
1145 quantifiable (class 1A) new aerosol particle formation and growth events (n) are also shown.

1146

Environment and year/ statistics	Contribution in %		
	dN_{nuc}/dt	F_{coag}	F_{growth}
Background, 2012–2013, n=43			
Minimum	45	4	2
Maximum	93	38	26
Mean	76	14	10
St. deviation	12	9	5
Centre, 2008–2009, n=31			
Minimum	32	13	3
Maximum	84	44	38
Mean	54	29	18
St. deviation	13	8	9
Centre, 2013–2014, n=48			
Minimum	43	9	3
Maximum	86	37	30
Mean	63	22	15
St. deviation	11	7	7
Centre, 2014–2015, n=56			
Minimum	45	6	2
Maximum	91	46	32
Mean	70	17	14
St. deviation	12	7	8
Centre, 2015–2016, n=17			
Minimum	50	4	2
Maximum	92	43	30
Mean	74	14	11
St. deviation	11	9	8
Centre, 2017–2018, n=52			
Minimum	44	4	3
Maximum	93	41	31
Mean	70	17	13
St. deviation	11	8	7

1147

1148 **Table S2.** Ranges, averages and standard deviations of condensation sink value during the nucleation
1149 process, daily maximum gas-phase H_2SO_4 proxy, daily mean air temperature and daily mean relative
1150 humidity on quantifiable (class 1A) new particle formation and growth events in the near-city
1151 background and city centre separately for the 1-year long measurement time intervals and for the joint
1152 5-year long city centre data set.

1153

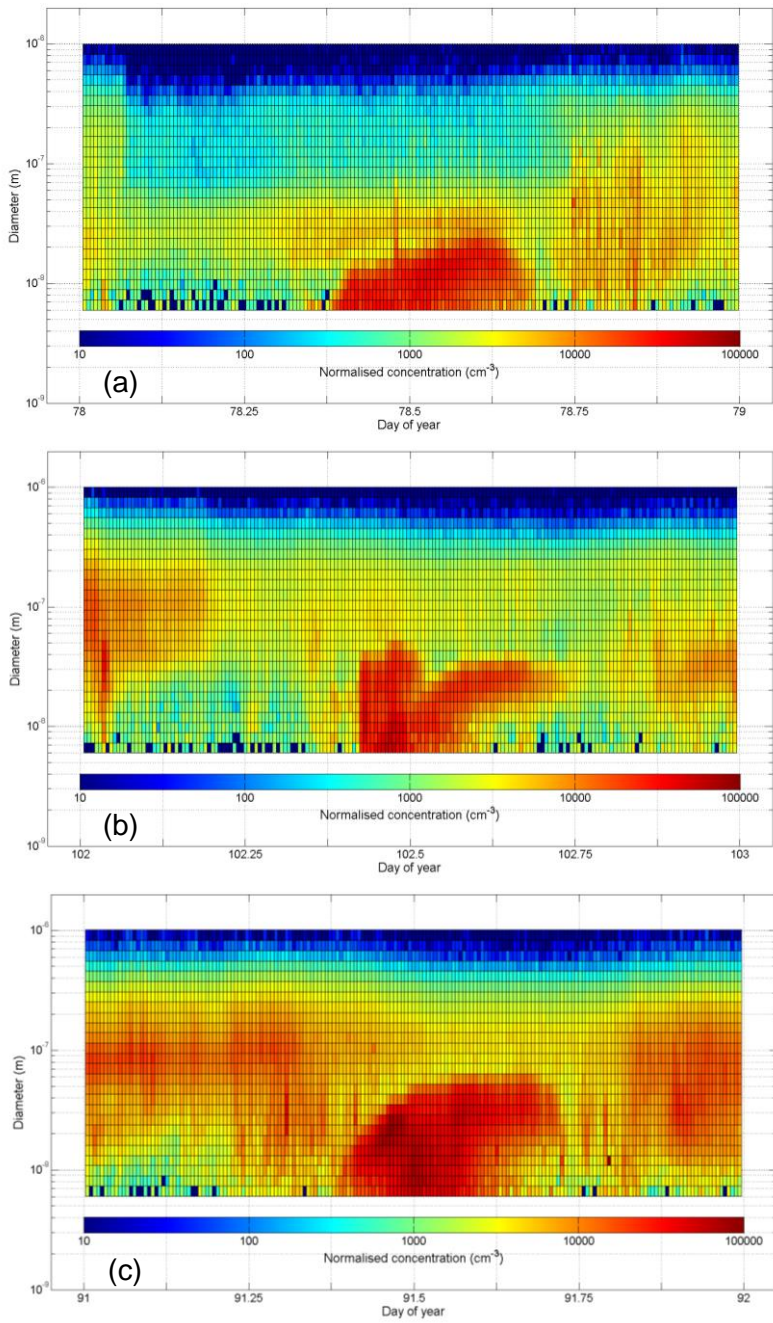| Environment	Background	Centre					
Time interval	2012–2013	2008–2009	2013–2014	2014–2015	2015–2016	2017–2018	All 5 years
Condensation sink, CS (10^{-3} s^{-1})							
Minimum	1.63	3.1	2.0	2.4	1.69	2.1	1.69
Median	5.6	9.5	9.9	8.6	5.0	8.4	8.9
Maximum	14.6	21	17.8	21	18.4	18.5	21
Mean	6.2	11.0	10.4	9.4	6.8	8.7	9.4
St. deviation	3.1	4.9	3.7	4.2	4.2	4.6	4.3
Gas-phase H_2SO_4 proxy (10^4 µg m^{-5} W s)							
Minimum	40	10.9	12.2	5.8	34	7.3	5.8
Median	93	39	40	38	79	46	41
Maximum	163	96	139	135	190	134	190
Mean	93	39	45	42	82	50	48
St. deviation	32	17	27	23	38	31	29
Air temperature, T (°C)							
Minimum	-5.2	-0.46	-1.78	-1.19	-1.07	1.21	-1.78
Median	11.5	17.1	16.8	15.3	14.2	16.7	16.1
Maximum	27	23	28	28	28	27	28
Mean	11.5	16.3	15.7	15.0	13.6	16.4	15.5
St. deviation	8.1	5.6	6.9	7.2	8.3	6.5	6.8
Relative humidity, RH (%)							
Minimum	41	32	41	31	39	36	31
Median	63	49	60	50	55	52	53
Maximum	91	74	78	77	89	73	89
Mean	64	51	60	50	56	52	54
St. deviation	12	11	10	9	12	9	11

1154

1155 **Table S3.** Ranges, averages and standard deviations of daily median concentrations of SO_2, O_3, NO_x

1156 and CO gases on quantifiable (class 1A) new particle formation and growth event days in the near-city

1157 background and city centre separately for the 1-year long measurement time intervals and for the joint
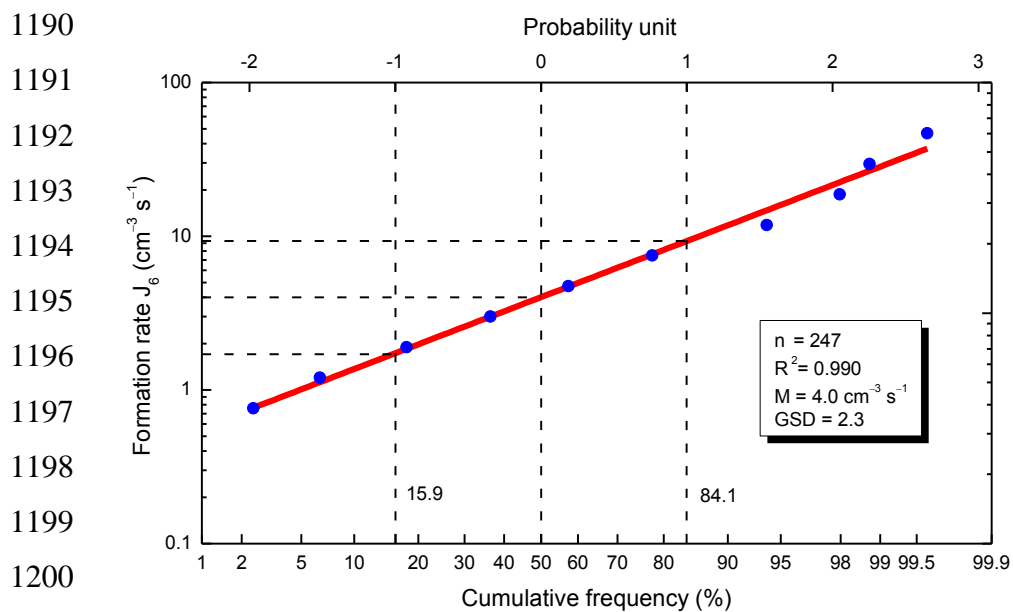
1158 5-year long city centre data set.

1159

Environment	Background	Centre					
Time interval	2012–2013	2008–2009	2013–2014	2014–2015	2015–2016	2017–2018	All 5 years
SO_2 concentration ($\mu g\ m^{-3}$)							
Minimum	4.4	3.4	2.0	0.90	3.3	0.80	0.80
Median	6.2	5.3	5.1	3.9	5.2	3.7	4.8
Maximum	11.7	8.3	8.2	10.4	11.4	7.0	11.4
Mean	6.5	5.4	5.1	4.4	5.9	3.9	4.7
St. deviation	1.4	1.2	1.8	2.4	2.4	1.8	2.1
O_3 concentration ($\mu g\ m^{-3}$)							
Minimum	8.7	1.80	0.80	10.3	13.0	3.7	0.80
Median	61	44	25	35	36	29	31
Maximum	85	93	67	66	61	68	93
Mean	55	39	28	33	37	31	33
St. deviation	21	28	19	14	14	17	19
NO_x concentration ($\mu g\ m^{-3}$)							
Minimum	4.9	13.0	34	32	30	17.8	13.0
Median	12.2	49	72	87	72	75	74
Maximum	66	213	143	186	120	167	213
Mean	15.8	62	77	96	76	79	81
St. deviation	12.1	42	28	41	24	33	38
CO concentration ($mg\ m^{-3}$)							
Minimum	0.167	0.26	0.30	0.26	0.29	0.20	0.198
Median	0.31	0.48	0.56	0.54	0.42	0.52	0.51
Maximum	0.87	0.76	0.79	0.95	0.88	0.86	0.95
Mean	0.38	0.47	0.54	0.55	0.46	0.51	0.52
St. deviation	0.18	0.13	0.14	0.16	0.16	0.15	0.15

1160

Figure S1. Size distribution surface plots for new aerosol particle formation and consecutive particle diameter growth process as banana-shape plot with limited growth of particles on 19–03–2017 (a), with an emission interference on 12–04–2015 (b) and with a broad unresolvable onset on 01–04–2017 (c) in the city centre.

Figure S2. Log-probability graph of the formation rate J_6 and its cumulative frequency distribution for n individual data in the joint overall 6-year long data set. The linear line in red represents the apparent fit to the data. Coefficient of determination (R^2), median J_6 value (M) and its geometric standard deviation (GSD) obtained from the fitted line are also shown.

Consequences of dynamic and timing properties of new aerosol particle formation and consecutive growth events

Imre Salma and Zoltán Németh

Institute of Chemistry, Eötvös University, H-1518 Budapest, P.O. Box 32, Hungary

Correspondence to: Imre Salma (salma@chem.elte.hu)

Abstract. A variety of contributions to the emerging research field of urban atmospheric new particle formation (NPF) and consecutive particle diameter growth based on gradually generating, several-year long, semi-continuous, critically evaluated, complex and coherent data sets are presented here. Dynamic properties, i.e. particle formation rate J_6 and particle diameter growth rate GR_{10}, and timing properties, i.e. starting time (t_1) and duration time interval (Δt) of 247 quantifiable atmospheric NPF and growth events identified in the city centre and near-city background of Budapest over 6 full measurement years together with related gas-phase H_2SO_4 proxy, condensation sink (CS) of vapours, basic meteorological data and concentrations of criteria pollutant gases were derived, evaluated, discussed and interpreted. In the city centre, nucleation ordinarily starts at 09:15 UTC+1, and it is maintained for approximately 3 h. The NPF and growth events produce 4.6 aerosol particles with a diameter of 6 nm in 1 cm^3 of air in 1 s, and cause the particles with a diameter of 10 nm to grow with a typical rate of 7.3 nm h^{-1}. Nucleation starts approximately 1 h earlier in the near-city background, it shows substantially smaller J_6 (with a median of 2.0 cm^{-3} s^{-1}) and GR_{10} values (with a median of 5.0 nm h^{-1}), while the duration of nucleation is similar to that in the centre. Monthly distributions of the dynamic properties and daily maximum H_2SO_4 proxy do not follow the mean monthly pattern of the event occurrence frequency. The factors that control the event occurrence and that govern the intensity of particle formation and growth are not directly linked. ~~Condensing atmospheric chemical species and/or their processes in the city centre seem to contribute equally to new particle formation and particle growth. In the near-city background, however, chemical compounds available and their processes power particle growth more than particle formation.~~ New particle formation and growth processes advance in a different manner in the city and its close environment. This could mainly be related to diversities in atmospheric composition, chemistry and physics. We showed that there is a minimum growth rate (1.8 nm h^{-1} is our case) that is required for nucleated particles to reach the lower end of the diameter interval measured (in our case 6 nm). Monthly distributions and relationships among the properties mentioned

32   provided indirect evidence that chemical species other than H_2SO_4 largely influence the particle

33   growth and possibly atmospheric NPF process as well. The J_6, GR_{10} and Δt can be described

34   by log-normal distribution function. Most of the extreme dynamic properties could not be

35   explained by H_2SO_4 proxy, CS, meteorological data or pollutant gas concentrations.

36   Approximately 40% of the NPF and growth events exhibited broad beginning, which can be an

37   urban feature. For 9% of all quantifiable days, it was feasible to calculate 2 separate sets of

38   dynamic properties. The later onset frequently shows more intensive particle formation and

39   growth than the first onset by a typical factor of approximately 1.4. The first event is attributed

40   to regional type, while the second event, superimposed on the first, is often associated with sub-

41   regional, thus urban NPF and growth process.

42

43   **1 Introduction**

44

45   Molecules and molecular fragments in the air collide randomly and can form electrically neutral

46   or charged clusters. Most clusters decompose shortly. Chemical stabilising interactions among

47   certain components within a cluster can enhance its lifetime, during which it can grow further

48   by additional molecular collisions through some distinguishable size regimes (Kulmala et al.,

49   2014). If the diameter of these clusters reaches a critical value of 1.5±0.3 nm (Kulmala et al.,

50   2013), they become thermodynamically stable, and their further growth turns into a spontaneous

51   process. Supersaturation is a necessary atmospheric condition for this principal transformation.

52   It is essentially a phase transition, which takes place in a dispersed manner in the atmosphere,

53   so it generates an aerosol system. The newly formed particles grow further by condensation to

54   larger sizes in most cases due to the existing supersaturation. Photochemical oxidation products

55   such as H_2SO_4 (Sipilä et al., 2010), extremely low-volatile organic compounds (ELVOCs, Ehn

56   et al., 2014; Jokinen et al., 2015) and highly oxygenated molecules (HOMs, Bianchi et al., 2016;

57   Kirkby et al., 2016; Tröstl et al., 2016) together with H_2O vapour, NH_3 (Kirkby et al., 2011),

58   amines (Almeida et al., 2013), other oxidation products of volatile organic compounds (VOCs;

59   Metzger et al., 2010; Schobesberger et al., 2013; Riccobono et al., 2014) and NO_2 can play an

60   important role in both the particle formation and growth. The VOCs include compounds of both

61   anthropogenic and biogenic origin, mainly isoprenoids such as α-pinene (Kirkby et al., 2016).

62   In some specific coastal regions, iodine oxides produced from marine biota are involved

63   (O'Dowd et al., 2002). Atmospheric concentration of these key compounds at a level that is

64   smaller by 12–14 orders of magnitude than the concentration of air molecules is already

65   sufficient for the phenomenon (Kulmala et al., 2014). Relative importance of the organics

2

increases with particle size (Riipinen et al., 2011; Ehn et al., 2014), and their supersaturation is maintained by fast gas-phase autooxidation reactions of VOCs (Crounse et al., 2013). The overall phenomenon is ordinarily confined in time for 1 day or so, and, therefore, it can be regarded as an event in time, and is referred as new aerosol particle formation (NPF) and consecutive particle growth event.

Such events appear to take place almost everywhere in the world and anytime (Kulmala et al., 2004; Kerminen et al., 2018; Nieminen et al., 2018). Their occurrence frequency and, more importantly, their contribution to particle number concentrations were found to be substantial or determinant in the global troposphere (Spracklen et al., 2006; Kulmala et al., 2014). Moreover, their contribution to the number of cloud condensation nuclei (CCN) can be 50% or even more (Makkonen et al., 2009; Merikanto et al, 2009; Sihto et al., 2011), which links the events to climate system, and emphasizes their global relevance (Kerminen et al., 2012; Makkonen et al., 2012; Carslaw et al., 2013; Gordon et al., 2016). New particle formation and growth events were proved to be common in polluted air of large cities as well with a typical relative occurrence frequency between 10% and 30% (Woo et al., 2001; Baltensperger et al., 2002; Alam, et al., 2003; Wehner et al., 2004; Salma et al., 2011; Dall'Osto et al., 2013; Xiao et al., 2015; Zhang et al., 2015; Kulmala et al., 2017, Nieminen et al., 2018). The coupling and relationships between regional and urban (sub-regional) NPF were demonstrated at least under favourable orographic conditions (Salma et al., 2016b). New particle formation can increase the existing particle number concentrations in city centres by a factor of approximately 2 on nucleation days, while it can produce approximately 28% of ultrafine (UF) particles on a longer (e.g. annual) time scale (Salma et al., 2017). Particle concentrations from NPF are also important when compared to the (primary) particles emitted by their dominant source in cities, namely by road vehicles with internal combustion engines (Paasonen et al., 2016). These results jointly suggest that particles from NPF and growth events in cities can influence not only the urban climate but can contribute to the public's excess health risk from particle number exposures (Oberdörster et al., 2005; Braakhuis et al., 2014; Salma et al., 2015), and, furthermore, could be linked to the role of human actions in all these effects.

Despite these potentials, conclusive interpretation of the data obtained, and results derived specifically for cities remained hindered so far. Several-year long, semi-continuous, critically evaluated, complex and coherent data sets are required for this purpose, which have been generating gradually. As part of this international progress, investigations dedicated to urban

NPF and growth events in Budapest have been going on since November 2008. Measurements for 5 full years were realised in the city centre at a fixed location, 1 full year was devoted to measurements in a near-city background environment, and some other measurements were accomplished in different urban microenvironments for time intervals of a few months. The main objectives of this study are to determine, present and analyse the dynamic properties, i.e. particle formation rate and particle diameter growth rate, timing properties, i.e. starting time and duration time interval of nucleation process of NPF and growth events together with the major sources and sink of condensing vapours, basic meteorological data and criteria pollutant gases for 6 years, to investigate and interpret their relationships, to discuss their monthly distributions, to evaluate and detect some of their features specific for urban atmospheric environments, and to demonstrate some specific urban influence on the calculation of the properties. These quantities and relationships are of basic importance in many atmospheric processes for several reasons. Our goals are in line with the research needs for global atmospheric nucleation studies (Kerminen et al., 2018; Nieminen et al., 2018).

2 Experimental methods

The measurements took place at two urban locations in Budapest, Hungary. Most measurements were realised at the Budapest platform for Aerosol Research and Training (BpART) facility (N 47° 28' 29.9", E 19° 3' 44.6", 115 m above mean sea level (a.s.l.; Salma et al., 2016a). This site represents a well-mixed, average atmospheric environment for the city centre. The other location was situated at the NW border of Budapest in a wooded area of the Konkoly Astronomical Observatory of the Hungarian Academy of Sciences (N 47° 30' 00.0", E 18° 57' 46.8", 478 m a.s.l.). This site characterises the air masses entering the city since the prevailing wind direction in the area is NW. The measurements were accomplished for 6 full-year long time intervals, i.e. from 03–11–2008 to 02–11–2009, from 19–01–2012 to 18–01–2013, from 13–11–2013 to 12–11–2014, from 13–11–2014 to 12–11–2015, from 13–11–2015 to 12–11–2016 and from 28–01–2017 to 27–01–2018. In the measurement year 2012–2013, the instruments were set up in the near-city background, while in all other years, they were installed in the city centre. Local time (LT=UTC+1 or daylight-saving time, UTC+2) was chosen as the time base of the data unless otherwise indicated because it had been observed in earlier investigations that the daily activity time pattern of inhabitants substantially influences the atmospheric processes in cities (Salma et al., 2014).

The main measuring system was a flow-switching type differential mobility particle sizer (DMPS). It consists of a radioactive (^{60}Ni) bipolar charger, a Nafion semi-permeable membrane dryer, a 28-cm long Vienna-type differential mobility analyser and a butanol-based condensation particle counter (TSI, model CPC3775). The sample flow was 2.0 L min^{-1} in the high-flow mode, and 0.31 L min^{-1} in the low-flow mode with sheath air flow rates 10 times larger than for the sample flows. The DMPS measures particle number concentrations in an electrical mobility diameter range from 6 to 1000 nm in the dry state of particles (with a relative humidity of RH<30%) in 30 channels, which finally yields 27 channels after averaging 3 overlapping channels when joining the data for the 2 flow modes. The time resolution of the measurements was approximately 10 min till 18–01–2013, and 8 min from 13–11–2013 (after a planned update of the DMPS system). There was no upper size cut-off inlet applied to the sampling line, and a weather shield and insect net were only attached. The sampling inlet was installed at a height of 12.5 m above the street level in the city centre, and of approximately 1.7 m in the near-city background. The measurements were performed according to the international technical standard (Wiedensohler et al., 2012). The availability of the DMPS data over 1-year long time intervals are summarised in Table 1. Synoptic meteorological data for air temperature (*T*), RH, wind speed (WS) and wind direction (WD) were obtained from a measurement station of the Hungarian Meteorological Service (HMS, no. 12843) by standardised methods with a time resolution of 1 h. Global solar radiation (GRad) data were measured by the HMS at a distance of 10 km in E direction with a time resolution of 1 h. Meteorological data were available in >90% of the possible cases in each year. Concentrations of SO_2, O_3, NO_x and CO were obtained from measurement stations of the National Air Quality Network in Budapest (in a distance of 4.5 km from the urban site, and of 6.9 km from the near-city background site) located in the upwind prevailing direction from the measurement sites. They are measured by UV fluorescence (Ysselbach 43C), UV absorption (Ysselbach 49C), chemiluminescence (Thermo 42C) and IR absorption methods (Thermo 48i), respectively with a time resolution of 1 h. The concentration data were available in >85% of the yearly time intervals, and >98% of them were above the limit of determinations. It is worth mentioning that concentration of SO_2 in the Budapest area is ordinarily distributed without larger spatial (and temporal) gradients (Salma et al., 2011). For the present study, this was proved by evaluating the concentration ratios from 2 different municipal stations which are in the closest distance from the BpART in 2 different directions with an angle of 60° between them. The mean SO_2 concentration ratio and standard deviation (SD) for the 2 stations were 81±20% over the 5-year

167 long measurement time interval. The assumption can also be justified indirectly by a conclusion

168 on the monthly distribution of SO_2 concentration in Sect. 4.2.

169

170 **3 Data treatment**

171

172 The measured DMPS data were evaluated according to the procedure protocol recommended

173 by Kulmala et al. (2012) with some refinements that are related to urban features (see Sect. 3.1).

174 Particle number concentrations in the diameter ranges from 6 to 1000 nm (N), from 6 to 25 nm

175 (N_{6-25}) and from 6 to 100 nm (N_{6-100} or UF particles) were calculated from the measured and

176 inverted DMPS concentrations. Particle number size distribution surface plots showing jointly

177 the variation in particle diameter and particle number concentration density in time were also

178 derived. Identification and classification of NPF and growth events was accomplished on these

179 surface plots (Dal Maso et al., 2005; Németh et al., 2018) on a daily basis into the following

180 main classes: NPF event days, non-event days, days with undefined character, and days with

181 missing data (for more than 4 h during the midday). Relative occurrence frequency of events

182 was determined for each month and year as the ratio of the number of event days to the total

183 number of relevant (i.e. all−missing) days. A subset of NPF events with uninterrupted evolution

184 in time, which are called quantifiable (class 1A) events, were further separated because the time

185 evolution of their size distribution functions was utilised to determine the dynamic and timing

186 properties with good accuracy and reliability.

187

188 **3.1 Dynamic and timing properties**

189

190 Growth rate (GR) of nucleation-mode particles was calculated by mode-fitting method

191 (Kulmala et al., 2012). Particle number median mobility diameter (NMMD) of the nucleation

192 mode were obtained from fitting the individual size distributions by DoFit algorithm (Hussein

193 et al., 2004). The growth rate was determined as the slope of the linear line fitted to the time

194 series of the NMMD data within a time interval around a diameter d, where the dependency

195 could be satisfactorily approximated by linear fit. Since the nucleation mode was mostly

196 estimated by N_{6-25} in the calculations of the formation rate (see below), and since the median

197 of the related diameter interval (from 6 to 25 nm) is close to d=10 nm, GRs for particles with a

198 diameter of 10 nm were determined (GR_{10}). This type of GR can be interpreted as an average

199 GR as far as the given particle diameter range is concerned, but it actually expresses the

200   beginning of the growth process only, which may have considerable effects on the formation

201   rate calculations in specific cases (see later).

202

203   Time evolution of an aerosol population is described by the general dynamic equation which

204   was rearranged, simplified and approximated by several quantities (Kulmala et al., 2001; Dal

205   Maso et al., 2002; Kulmala et al., 2012; Cai and Jiang, 2017) to express the formation rate J_6

206   of particles with the smallest detected diameter of d_{min}=6 nm in a form utilised in the present

207   evaluation as

208

209 $$J_6 = \frac{dN_{6\text{-}25}}{dt} + CoagS_{10}N_{6\text{-}25} + \frac{GR_{10}}{(25-6)}N_{6\text{-}25} - \frac{dN_{Ai,<25}}{dt}. \tag{1}$$

210

211   The first term on the right side of Eq. 1 expresses the concentration increment. The particle

212   number concentration in the size range from 6 to 25 nm (i.e. $N_{6\text{–}25}$) was selected to approximate

213   the nucleation-mode particles $N_{nuc} \approx N_{6\text{–}25}$. This is a usual and reasonable choice because it was

214   proved to be advantageous and effective way in handling fluctuating data sets since $N_{6\text{–}25}$ often

215   exhibits less sensitivity and smaller scatter in time than the fitted area of the nucleation mode.

216   It is implicitly assumed that the intensity of the NPF is constant for a certain time interval, and,

217   therefore, $dN_{6\text{–}25}/dt$ can be determined as the slope of the linear function of $N_{6\text{–}25}$ versus time t

218   within an interval where the dependence could be satisfactorily approximated by linear fit. A

219   limitation of the relatively wide size range (6–25 nm) selected can be manifested by

220   disturbances from primary particles particularly in urban environments. This is taken into

221   account by the last term of Eq. 1 and is discussed later.

222

223   The second term on the right side of Eq. 1 represents the loss of particles due to coagulation

224   scavenging (with pre-existing particles). The coagulation scavenging efficiency for particles

225   with a diameter of 10 nm ($CoagS_{10}$) was selected to approximate the mean coagulation

226   efficiency of nucleation-mode particles ($CoagS_{nuc}$). This diameter was chosen by considering

227   the median of the related diameter range, which was discussed above for GR. The coagulation

228   efficiency was calculated from classical aerosol mechanics with adopting a mass

229   accommodation coefficient of 1 and utilizing the Fuchs' transition-regime correction factor

230   (Kulmala et al., 2001; Dal Maso et al., 2005; Kulmala et al., 2013) by using computation scripts

231   developed at the University of Helsinki. Self-coagulation within the nucleation mode was

232   neglected due to its limited concentration. Hygroscopic growth of particles was not considered

233   since this depends on chemical composition of particles, which is unknown.

234

235   The third term on the right side of Eq. 1 expresses the particle growth out of the considered size

236   range by condensation of vapours. The GR_{10} was selected to approximate a representative value

237   at the median of the particle diameter range considered (Vuollekoski et al., 2012). It is implicitly

238   assumed that GR_{10} can be regarded to be constant over the time interval under consideration.

239   Nevertheless, the growth of nucleation-mode particles in time is occasionally limited (Fig. S1a).

240   In these specific cases, the mean relative area of the nucleation mode below 25 nm was

241   determined by fitting the individual size distributions around the time of the maximum

242   nucleation-mode NMMD, and the ratios were averaged. A correction in form of the mean

243   relative area was adopted as a multiplication factor for the growth out term in Eq. 1. On very

244   few days, the growth of newly formed particles was followed by a decrease in nucleation-mode

245   NMMD (Salma et al., 2016a). In these cases, the shrinkage rate (with a formal $GR_{10}<0$) was

246   derived and adopted in Eq. 1.

247

248   The fourth term on the right side of Eq. 1 expresses the contribution of high-temperature

249   emission sources, usually of vehicular road traffic (Paasonen et al., 2016; Salma et al., 2017) to

250   $N_{6–25}$, which can provisionally disturb the assumption of $N_{nuc} \approx N_{6–25}$. A typical example of such

251   a situation is shown in Fig. S1b from 10:09 to 12:23 LT. In these specific cases, the contribution

252   of primary emissions was estimated from the slope of the time series of the fitted peak area of

253   the Aitken mode below $d<25$ nm ($N_{Ai,<25}$) in the time region under consideration. Reliable

254   separation of the nucleation and Aitken modes from each other was hindered or was not possible

255   for a few individual size distributions due to overlapping modes and the scatter in the

256   concentration data, and these individual Aitken-mode areas were excluded from or skipped in

257   the time series. Relative contributions of the concentration increment coagulation loss and

258   growth out from the diameter interval to J_6 are decreasing in this order with mean values of

259   71%, 17% and 12%, respectively (Table S1).

260

261   The formation and growth rates for the measurement years of 2008–2009 and 2012–2013 were

262   calculated earlier by a slightly different way and neglecting the urban features discussed above

263   (Salma et al., 2011, 2016b). To obtain consistent data sets, the dynamic properties for these 2

264   years were re-evaluated by adopting the present improved protocol and implementing the

265   experience gained over the years. The mean new-to-old rate ratios with SDs for the GR_{10} and

266   J_6 were 1.06±0.32 and 1.23±0.37, respectively in the city centre (2008–2009) and 1.04±0.21

267   and 1.20±0.35, respectively in the near-city background (2012–2013). It was the smaller rates

268   that were primarily and sometimes substantially impacted. The modifications were

269   simultaneously adopted. The subtraction of particle number concentrations emitted by road

270   traffic from N_{6-25}, which usually leads to a decrease in the coagulation loss and loss due to

271   growth out from the diameter range of 6–25 nm, and which can influence the slope of the

272   concentration change in time (dN_{6-25}/dt) in a positive or negative manner depending on the

273   actual time evolution of perturbing emission source. In addition to that, the time interval in

274   which this slope is considered to be constant was set in a new treatment. It is mentioned that

275   the relative contributions of the concentration increment, coagulation loss and growth out from

276   the diameter interval to J_6 have different weights in propagating their effects. Furthermore, J_6

277   itself also depends on the GR_{10}, which makes the relationships even more complex. These

278   explain why the changes resulted in overall increments. The re-calculation is considered as a

279   methodological improvement over the years of research.

280

281   The assumptions and estimations above usually represent a reasonable approximation to reality.

282   The N_{6-25} is derived from the experimental data in a straightforward way, the GR_{10} and the

283   corrections for primary particles and limited particle growth depend on the quality of the size

284   distribution fitting as well, while the $CoagS_{10}$ is determined by using a theoretical model. The

285   resulting accuracies of the dynamic properties, in particular of J_6, look rather complicated. They

286   also depend on the spatial heterogeneity in the air masses measured particularly for the

287   observations performed at the fixed site, size and time resolution of the concentrations

288   measured, diameter range of the size distributions, fluctuations in the experimental data,

289   selection of the particle diameter interval, choice of the time interval of interest (for linear fits),

290   sensitivity of the models to the input uncertainties (Vuollekoski et al., 2012), and also on the

291   extent of the validity of the assumptions applied under highly polluted conditions (Cai and

292   Jiang, 2017). The situation is further complicated with the fact that the dynamic (and also the

293   timing) properties are connected to each other. Finally, it is important to recognise that some

294   NPF and growth curves on the surface plots have rather broad starting time interval (Fig. S1a

295   and S1c). They occur in a considerable abundance in cities, e.g. in 40% of all quantifiable events

296   in Budapest (Sect. 4.4). This may yield badly defined or composite dynamic properties, whose

297   uncertainty can have principle limitations which can prevail on the experimental and model

298   uncertainties.

299

300   Timing properties of NPF and growth events are increasingly recognised, and they can provide

301   valuable information even if they are estimated indirectly from the observed diameter interval

302   >1.5 nm (Sect. 1). The earliest estimated time of the beginning of a nucleation (t_1) and the latest

303   estimated time of the beginning of a nucleation (t_2) were derived by a comparative method

304   (Németh and Salma, 2014) based on the variation in the content of the first size channel of the

305   DMPS system. Both time parameters include a time shift that accounts for the particle growth

306   from the stable neutral cluster mode at approximately 2 nm to the smallest detectable diameter

307   limit of the DMPS systems (6 nm in our case) by adopting the GR value in the size window

308   nearest to it in size space. The difference $\Delta t = t_2 - t_1$ is considered as the duration time interval of

309   the nucleation process. It represents the time interval during which new aerosol particles are

310   generated in the air. The timing properties are expressed in UTC+1, and their uncertainty is

311   regarded to be ca. 30 min under ordinary NPF and growth situations.

312

313   **3.2 Sources and sink**

314

315   Relative effects and role of gas-phase H_2SO_4 were estimated by its proximity measure (proxy

316   value) containing both its major source and sink terms under steady-state conditions according

317   to Petäjä et al. (2009). It was calculated for $GRad > 10$ W m^{-2}. Formaly, it is possible to convert

318   the H_2SO_4 proxy values to H_2SO_4 concentrations by an empirical scaling factor of $k = 1.4 \times 10^{-7} \times GRad^{-0.70}$, where GRad is expressed in a unit of W m^{-2} (Petäjä et al., 2009). The factor was,

319

320   however, derived for a remote boreal site, and, therefore, we prefer not to perform the

321   conversion since urban areas are expected to differ from the boreal regions, and adopting the

322   factor could distort the dynamic relationships or time trends investigated. The conversion was

323   applied only to estimate the order of average H_2SO_4 atmospheric concentration levels. The

324   results derived by utilising the proxy are subject to larger uncertainties than for the other

325   properties because of these limitations, but they may indicate well gross tendencies.

326

327   Condensation sink for vapour molecules onto the surface of existing aerosol particles was

328   computed for discrete size distributions as described in earlier papers (Kulmala et al., 2001; Dal

329   Maso et al., 2002, 2005) and summarised by Kulmala et al. (2013). The equilibrium vapour

330   pressure of the condensing species was assumed to be negligible at the surface of the particles,

331   so similar to sulfuric acid. Dry particle diameters were considered in the calculations.

332

4 Results and discussion

Annual median particle number concentrations based on the individual data in the near-city background in 2012–2013, and in the city centre for the separate measurement years of 2008–2009, 2013–2014, 2014–2015, 2015–2016 and 2017–2018 were 3.4×10^3, and 11.5×10^3, 9.7×10^3, 9.3×10^3, 7.5×10^3 and 10.6×10^3 cm^{-3}, respectively. The data for the city centre indicate a decreasing trend. The first 4 values unambiguously show a decrease, while the last data point may look somewhat differently. Rigorous statistical evaluation of the joint data set of particle number concentrations in various size fractions over a decennial time interval from November 2008 to November 2018 is in progress, and its preliminary results in the one hand, confirm the decreasing tendency, and in the other hand, reveal some fine structure to this dependency. The mean UF/N ratio with SD for the same measurement time intervals were 67±14%, and 79±6%, 75±10%, 75±11%, 76±11% and 80±10%, respectively. The values correspond to ordinary urban atmospheric environments in Europe (Putaud et al., 2010).
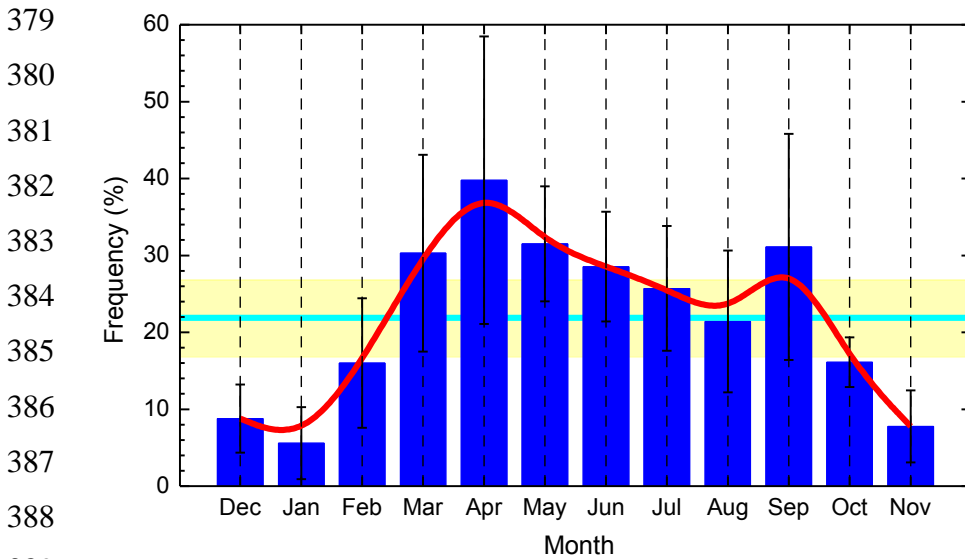
An overview on the number of classified days separately for the 1-year long measurement time intervals is given in Table 1. The availability of the daily size distribution surface plots with respect to all days ensures that the data are representative on yearly and monthly time scales, except for the months August and September 2015, when there were missing days in larger ratios. The number of quantifiable event days (248 cases) is also considerable, which establishes to arrive at firm conclusion on the NPF and growth events as well.

Table 1. Number of days with new aerosol particle formation and growth event, quantifiable (class 1A) event days, non-event days, undefined days, missing days and the coverage of relevant days with respect to all days in the near-city background and city centre separately for the 1-year long measurement time intervals.

Environment	Background	Centre				
Time interval	2012–2013	2008–2009	2013–2014	2014–2015	2015–2016	2017–2018
Event days	96	83	72	81	35	83
Quantifiable days	43	31	48	56	18	52
Undefined days	19	34	24	25	8	23
Non-event days	231	229	267	240	226	257
Coverage (%)	95	95	99	95	73	99
Missing days	20	19	2	19	97	2

It was previously shown that the NPF and growth events observed in the city centre of Budapest and its background ordinarily happen above a larger territory or region in the Carpathian Basin (Salma et al., 2011; Németh and Salma, 2014), and they are linked to each other (Salma et al., 2016b). From the point of the occurrence frequency distribution, they can, therefore, be evaluated jointly in the first approximation. An overall monthly mean relative occurrence frequency of nucleation days derived for all 6 measurement years is shown in Fig. 1. The annual mean frequency with SD was $22\pm5\%$, which is considerable and is in line with other urban sites (Sect. 1). The monthly mean frequency has a temporal variation, which can be characterised by a noteworthy pattern. The mean monthly dependency exhibits an absolute and a local minimum in January (5.6%) and August (21%), respectively, and an absolute and a local maximum in April (40%), and September (31%), respectively. Nevertheless, the SDs of the monthly (and annual) means indicate prominent variability from year to year. The pattern can be related to multivariate relationships and complex interplay among the influencing factors, which include the air temperature (January is the coldest month, while August is the warmest month in the Carpathian Basin) and enhanced emission of biogenic VOCs in springtime (March–April) and early autumn (September) as well (Salma et al., 2016b).

Figure 1. Monthly mean relative occurrence frequency of new aerosol particle formation and consecutive particle diameter growth events with respect to the number of relevant days for the joint 6-year long data set. The error bars show ±1 standard deviation, the horizontal line in cyan indicates the overall annual mean frequency, the yellow bands represent ±1 standard deviation of the annual mean, and the smooth curve in red serves to guide the eye.

The properties and variables studied were derived in full time resolution. They were averaged in several ways for different conditions and for various purposes to obtain typical average descriptive characteristics. In 1 case (31–08–2016), the NPF and growth event could reliable be identified, while the measured absolute particle number concentrations could not be validated due to some experimental troubles, and, therefore, it was left out from the further calculations. Similarly, there were 1 and 4 events with unusually/extraordinarily large dynamic properties in the measurement years 2014–2015 and 2017–2018, respectively. More specifically, 5 individual J_6 data when expressed in a unit of cm^{-3} s^{-1} and 1 individual GR_{10} data when given in nm h^{-1} were >20 (Table 3). These extremes were left out from the overview statistics to maintain the representativity (they could be influenced by some unknown extra or very local sources) and to fulfil better the basic requirements of correlation analysis. If an event showed a double beginning then the dynamic properties for the first onset were considered in the basic overview since this onset is of regional relevance (Salma et al., 2016b). The extreme NPF and growth events and the characteristics for the second onsets were, however, evaluated separately and are discussed in detail and interpreted in Sect. 4.4.

4.1 Ranges and averages

Ranges and averages with SDs of formation rate J_6, growth rate GR_{10}, starting time of nucleation (t_1) and duration time interval of nucleation (Δt) are summarised in Table 2 for separate measurement years and for the joint 5-year long city centre data set. In the city centre, nucleation generally starts at 09:15 UTC+1, and it is typically maintained for approximately 3 h. The NPF and growth events ordinarily produce 5.6 new aerosol particles with a diameter of 6 nm in 1 cm^3 of air in 1 s, and cause the particles with a diameter of 10 nm to grow with a typical rate of 7.6 nm h^{-1}. The statistics for J_6 and GR_{10} are based on 199 and 203 events, respectively. The corresponding data for the separate years show considerable variability without obvious trends or tendencies. The differences between the years can likely be related to changes in actual atmospheric chemical and physical situations and conditions, and to the resulting modifications in the sensitive balance and delicate coupling among them from year to year. Spread of the individual data for GR_{10} is smaller than for J_6; the relative SDs for the joint 5-year long city centre data set were 38% and 68%, respectively, while the (external) relative SDs calculated from the annual mean values were 4.2% and 14.0%, respectively.

The dynamic properties and t_1 data tend to be smaller in the near-city background than in the city centre. In general, nucleation starts 1 h earlier in the background, and the events typically show significantly smaller J_6 (with a median of 2.0 cm^{-3} s^{-1}) and GR_{10} (with a median of 5.0 nm h^{-1}). Duration of the nucleation is very similar to that in the city centre. All starting times of nucleation were larger than (in a few cases, very close to) the time of the sunrise. This implies that no nocturnal NPF and growth event has been identified in Budapest so far. The particle growth process (the so-called banana curve) could be traced usually for a longer time interval (up to 1.5 d) in the background than in the centre.

These results are in line with the ideas on atmospheric nucleation and consecutive particle growth process (e.g. Kulmala et al., 2014; Zhang et al., 2015; Kerminen et al., 2018). It was observed in a recent overview study (Nieminen et al., 2018) that the formation rate of 10–25 nm particles increased with the extent of anthropogenic influence, and in general, it was 1–2 orders of magnitude larger in cities than at sites in remote and clean environments. This highlights the importance of some anthropogenic vapours such as SO_2, NH_3 and amines to NPF and growth. The data also confirm our earlier findings with respect to Budapest and its regional

background within the Carpathian Basin achieved with shorter, 2-year long data sets (Salma et al., 2016b)

Table 2. Ranges, averages and standard deviations of aerosol particle formation rate J_6, particle diameter growth rate GR_{10}, starting time (t_1) and duration time interval ($\Delta t = t_2 - t_1$) of nucleation process of quantifiable (class 1A) new particle formation and growth events in the near-city background and city centre separately for the 1-year long measurement time intervals and for the joint 5-year long city centre data set.

Environment	Background	Centre					
Time interval	2012–2013	2008–2009	2013–2014	2014–2015	2015–2016	2017–2018	All 5 years
Formation rate J_6 (cm^{-3} s^{-1})							
Minimum	0.48	1.47	1.13	0.81	1.19	1.60	0.81
Median	2.0	4.2	3.5	4.4	4.6	6.3	4.6
Maximum	5.6	15.9	17.8	18.0	15.3	17.3	18.0
Mean	2.2	4.7	5.2	5.6	5.0	6.6	5.6
St. deviation	1.3	2.6	3.7	4.2	3.7	3.3	3.8
Growth rate GR_{10} (nm h^{-1})							
Minimum	3.0	3.7	3.1	2.8	3.2	3.3	2.8
Median	5.0	7.6	6.6	6.5	8.0	7.5	7.3
Maximum	9.8	17.4	19.0	18.0	15.5	19.8	19.8
Mean	5.2	7.8	7.2	7.3	7.7	8.0	7.6
St. deviation	1.4	2.6	2.8	3.2	3.0	2.8	2.9
Starting time, t_1 (HH:mm UTC+1)							
Minimum	05:51	07:14	06:44	05:48	07:31	05:57	05:48
Median	08:19	09:26	09:22	08:48	09:45	09:18	09:15
Maximum	11:09	11:38	12:21	11:23	12:45	12:15	12:45
Mean	08:17	09:27	09:25	08:49	10:02	09:24	09:19
St. deviation	01:11	01:05	01:26	01:22	01:23	01:36	01:26
Duration time, Δt (HH:mm)							
Minimum	01:23	00:52	00:42	00:31	01:03	01:26	00:31
Median	03:16	02:36	02:04	03:53	02:31	03:49	02:57
Maximum	06:44	06:04	05:34	07:46	06:05	07:55	07:55
Mean	03:30	02:44	02:14	03:52	02:58	03:57	03:18
St. deviation	01:40	01:11	01:01	01:40	01:47	01:39	01:40

Ranges and averages with SDs of some related atmospheric properties, namely of mean CS averaged for the time interval from t_1 to t_2, daily maximum gas-phase H_2SO_4 proxy, daily mean T and RH (Table S2), and of daily median concentrations of SO_2 (as the major precursor of gas-

458   phase H_2SO_4), O_3 (as an indicator of photochemical activity), NO_x and CO gases (as indicators

459   of anthropogenic combustion activities and road vehicle emissions) (Table S3) were also

460   derived for quantifiable NPF and growth event days, and are further evaluated. The annual

461   mean CS values exhibited decreasing tendency in the city centre over the years (as can be

462   expected from the particle number concentrations as well). The individual values remained

463   below approximately 20×10^{-3} s^{-1}, which agrees well with the results of our earlier study (Salma

464   et al., 2016b) according to which the CS suppresses NPF above this level in the Carpathian

465   Basin. Maximum H_2SO_4 proxy values reached substantially higher levels (by a factor of

466   approximately 2) in the near-city background than in the city centre due mainly to the

467   differences in the CS and $[SO_2]$. The differences between the 2 sites are particularly evident

468   when considering their smallest values. The largest variability in the annual average values

469   were observed for the proxy. Median concentration of H_2SO_4 molecules was roughly estimated

470   to be approximately 5×10^5 cm^{-3} by adopting the scaling factor (Sect. 3.2). ~~The dynamic~~

471   ~~properties seem to be not very sensitive to air T~~ The air T displayed quite similar and comparable

472   values over the years at both sites. The discussion of its overall effect on the dynamic properties

473   is accomplished in Sec. 4.2, where the monthly distributions are presented. Some events

474   happened at daily mean temperatures below zero. The daily mean RH and its SD for the city

475   centre and near-city background were 54±11% and 64±12%, respectively. There were events

476   that occurred at RHs as high as 90%. Relationships of the dynamic properties with T and RH

477   are also obscured with strong seasonal cycle of these meteorological data and with the fact that

478   air masses arriving to the receptor site in different trajectories are often characterised by distinct

479   levels of meteorological data.

480

481   As far as the pollutant gases are concerned (Table S3), SO_2 showed somewhat smaller daily

482   median values, and O_3 exhibited substantially smaller levels on event days in the city centre

483   than in the near-city background, while concentrations of NO_x and CO were obviously larger

484   in the city than in its close background. The differences can primarily be explained by the

485   intensity and spatial distribution of their major sources and atmospheric chemical reactions, and

486   the joined concentration data resembles typical situations without photochemical smog

487   episodes in cities. There was no obvious decrease in SO_2 concentration during these years in

488   contrast with an earlier decreasing trend from mid-1980s till about 2000. ~~No evident or sensitive~~

489   ~~effect of atmospheric gases on the dynamic or timing properties could be deduced from the~~

490   ~~averaged data. This can probably be explained by a dedicated balance between the intensifying~~

491　~~and suppressing effects, which were averaged out on a yearly time scale. Relationships on~~
492　~~shorter scales are further investigated and discussed in more detail in the following sections.~~
493

494　**4.2 Monthly distributions**

495

496　Distributions of the monthly mean J_6, GR_{10}, daily maximum gas-phase H_2SO_4 proxy, mean CS,

497　daily mean air T and RH, and daily median SO_2, O_3, NO_x and CO concentrations for quantifiable

498　NPF and growth events for the joint 5-year long city centre data sets are shown in Fig. 2. The

499　distributions – eminently for J_6, GR_{10}, H_2SO_4 proxy and SO_2 – do not follow the monthly pattern

500　of the event occurrence frequency at all (cf. Fig. 1). Instead, the J_6, GR_{10} and H_2SO_4 proxy tend

501　to exhibit larger values in summer months, and they temporal changes over the other months

502　are smooth and do not show distinctive features. The elevations are substantial; the estimated

503　maximum level was larger than the baseline by a factor of 2.1 for the J_6, and by a factor of

504　approximately 1.4 for the GR_{10} and H_2SO_4 proxy. The intensity of solar radiation at the surface,

505　its seasonal cycling, concentration of atmospheric precursors in different months, biogenic

506　processes, anthropogenic activities and the fact that rate coefficients of many thermal

507　chemical/physicochemical processes in the nature (including GR, Paasonen et al., 2018)

508　increase with T could play an important role in explained the distributions. A more

509　comprehensive study involving chemicals and their photochemistry is required for more

510　detailed explanation.

511

512　It is worth mentioning that [SO2] did not change substantially for the NPF event and non-event

513　days, while GRad was typically larger by a factor of ca. 2 and CS was smaller by approximately

514　30% on event days than on non-event days. The differences in the GRad (and some other

515　properties) are, however, biased by the seasonal cycle of solar electromagnetic radiation via the

516　seasonal variation of NPF occurrence frequency, while the CS indicated a modest seasonal

517　dependency. Interpretation of their joint effect should be approached by care, requires further

518　evaluations and is to be realised fully in a further study. Nevertheless, the misalignment among

519　the monthly distributions of NPF and growth event occurrence frequency and all the other

520　properties indicates that the occurrence or its basic causes are not linked with the dynamic

521　properties in a straightforward or linear manner~~, and 2) gas-phase H₂SO₄ does not seem to be~~

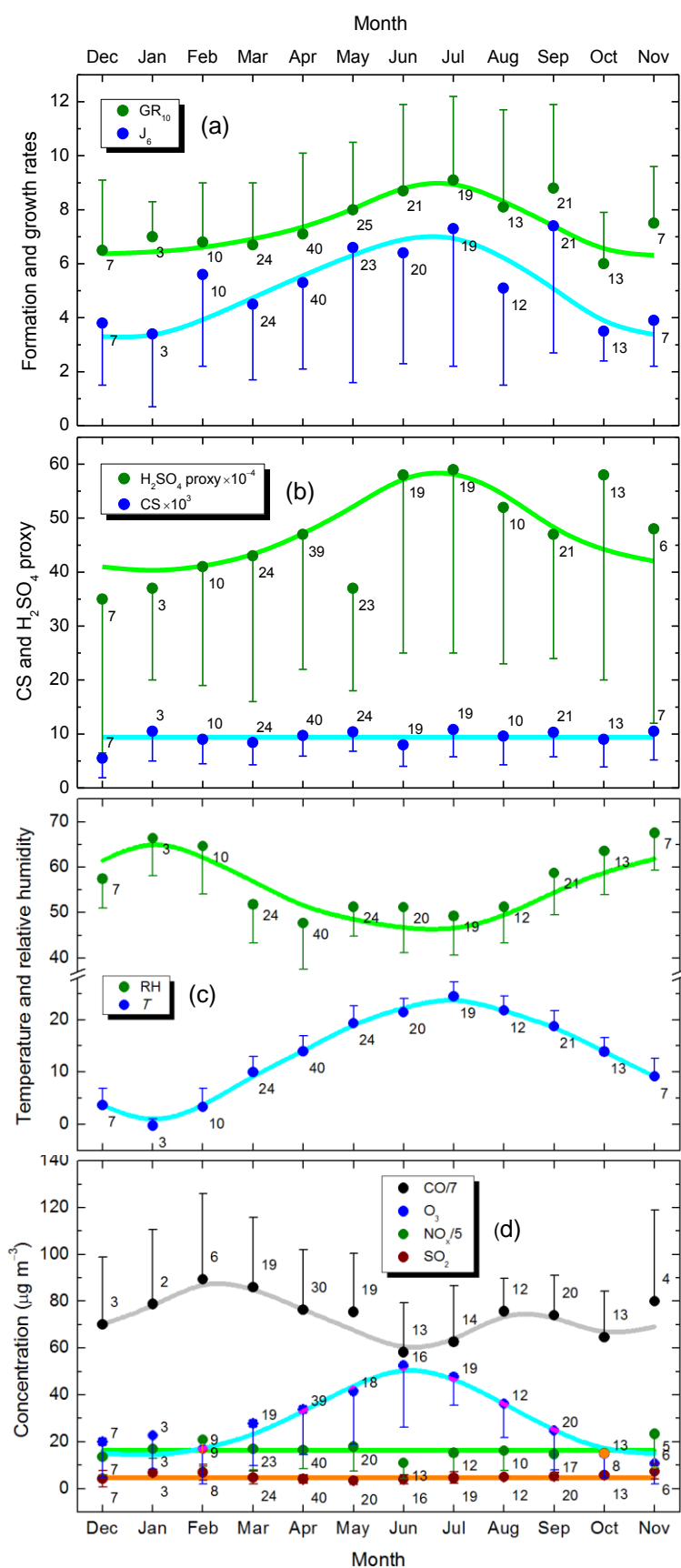522　~~the controlling factor of NPF occurrence~~ in the Carpathian Basin including Budapest.

523

17

Some of our results are in line with other observations according to which GR exhibited almost exclusively a summer maximum, while some other finding are different in the sense that the seasonal variability in particle formation rate was quite modest and could not be established earlier (Nieminen et al., 2018). There is one more aspect which may be worth realising in this respect. A large fraction of compounds contributing to NPF and growth in cities can originate from anthropogenic precursors (Vakkari et al., 2015). Their emissions may peak any time of year depending on human habits and requirements (Nieminen et al., 2018). Nevertheless, the fact that our monthly distributions of the dynamic properties in urban environments follow the universal summer maximum behaviour may indicate the overall prevailing role of atmospheric photochemistry coupled with biogenic emissions of aerosol precursor vapours.

The monthly mean J_6, GR_{10} and H_2SO_4 proxy data still have considerable uncertainty, which makes their interpretation not yet completely conclusive. The uncertainties are influenced by inherent fluctuations in the primary data sets, enhancing effects caused by combining some individual primary data into compound variables (such as H_2SO_4 proxy), number of data items available for different properties and months, variations in other or unknown relevant environmental conditions, and by the variability in relative nucleation occurrence frequency from year to year. The resulting uncertainties are expected to decrease with the length of the available data sets, which emphasized the need to continue the measurements.

The monthly distributions of CS, and SO_2 and NO_x concentrations could be represented by constant values of the overall means and SDs of $(9.4\pm4.3)\times10^{-3}$ s^{-1}, 4.7 ± 2.1 µg m^{-3} and 81 ± 38 µg m^{-3}, respectively with an acceptable accuracy. This suggests that CS, SO_2 and NO_x in Budapest do not critically or substantially affect either the dynamic properties (or the event occurrence). Monthly distributions of air T and O_3 concentration showed a maximum over summer months, while RH reflected the T tendency. The monthly variation of T on event days and on non-event days were similar. More importantly, higher biogenic emissions and typically stronger photochemistry are expected during the summer, which both enhance the production rate of nucleating and condensing vapours, while there is practically nothing extra that would suppress the dynamical properties (Kerminen et al., 2018). As a result of these, the dynamic rates show a summer maximum. This is completely consistent with the results from other urban and non-urban studies (Nieminen et al., 2018). Distribution of CO was more changing and without obvious tendentious temporal structure or feature than for the other gases, and, therefore, its interpretation is encumbered so far. However, it doesn't seem to substantially affect the dynamic properties.

Figure 2. Distribution of monthly mean aerosol particle formation rate J_6 in a unit of cm^{-3} s^{-1} and particle diameter growth rate GR_{10} in a unit of nm h^{-1} (a), mean condensation sink for vapours (CS) in a unit of s^{-1} averaged over the nucleation time interval (t_1, t_2) and daily maximum gas-phase H_2SO_4 proxy in a unit of μg m^{-5} W s (b), daily mean air temperature (T) in a unit of °C and daily mean relative humidity (RH) in % (c), and daily median concentrations of SO_2, O_3, NO_x and CO for quantifiable (class 1A) new particle formation and growth events in the city centre for the joint 5-year long time interval. The error bars are shown for one side for clarity and indicate 1 standard deviation. Number of the individual data averaged in each month is displayed next to the symbols. The horizontal lines indicate the overall mean. The nonlinear curves assist to guide the eye.
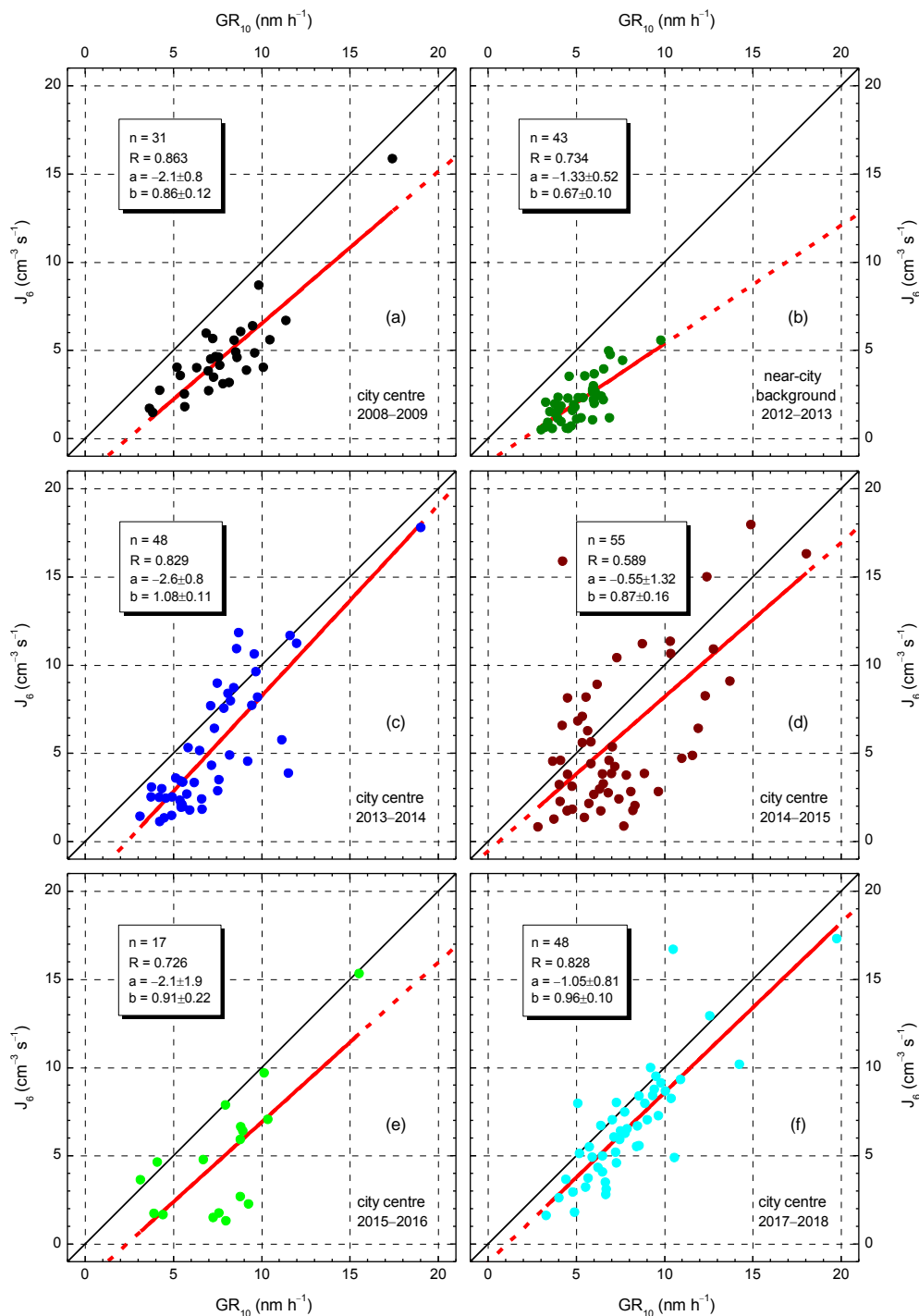
4.3 Relationships

Pearson's coefficients of correlation (R) between J_6 and GR_{10} revealed significant linear relationship between them for all annual data sets (the mean R and SD were 0.768 ± 0.099, number of data pairs n=243). This confirms that formation of new aerosol particle and their growth to larger sizes in the atmosphere are tightly and positively linked together. It should be noted that J_6 and GR_{10} are not completely independent variables (see Eq. 1 and Table S1). The linear relationship between the dynamic properties was observed under different atmospheric conditions in many environments (Nieminen et al., 2018). At some sites, this relationship could not be proved due to the weak variability in the variables.

The dynamic properties can also be coupled to the concentrations of aerosol precursor compounds and properties of a pre-existing particle population, thus to atmospheric environment (Kerminen et al., 2018). It is, therefore, sensible to investigate the city centre and near-city background data separately. Scatter plots between J_6 and GR_{10} for the 1-year long measurement time intervals are shown in Fig. 3. For the city centre, the regression lines follow the line with a slope of 1 in all 5 years. The mean slope (b) with SD for the joint 5-year long city centre data set was b=0.94 ± 0.07 expressed formally in a unit of cm^{-3} s^{-1} nm^{-1} h. ~~This implies that the relevant chemical species and/or their processes in the air of the city centre contribute equally to the formation of 6-nm particles and to their growth process.~~ At the same time, the regression line for the near-city background deviated significantly with a b=0.67 ± 0.10 cm^{-3} s^{-1} nm^{-1} h from the J_6 vs. GR_{10} dependency for the city centre. This can imply that NPF and growth processes advance in a different manner in these 2 environments~~, and that the chemical compounds available and their processes power particle growth more than new particle formation in the near-city background~~. This can be related to the differences between the city and its close environment as far as the atmospheric composition (for instance, the VOC and NO$_x$ concentrations), chemistry and physics, and other delicate conditions are concerned (Paasonen et al., 2018). The narrower range and smaller number of individual dynamic properties available for the near-city background relative to those in the city centre represent some inherent limitation or weakness in the explanation, and, therefore, it can strictly be regarded as a working hypothesis because a rigorous statistical treatment would require larger variability in the near-city background data.

Figure 3. Scatter plots for aerosol particle formation rate J_6 and consecutive particle diameter growth rate GR_{10} in city centre (a and c–f) and near-city background (b) separately for the 1-year long measurement time intervals. Number of data point (n), their coefficient of correlation (R) and the intercept (a) and slope (b) of the regression line with standard deviations are also indicated. The lines in black represent the line with a slope of 1, the solid lines in red show the regression lines, while the dashed parts in red are extrapolated from the regression line.

660

The intercepts (a) of the regression lines were identical for all data sets within their uncertainty interval. The mean intercept and SD were estimated to be -1.7 ± 0.8 cm^{-3} s^{-1}. This finding is interpreted as the existence of a minimum GR or more exactly of a minimally required GR that leads to $J_6>0$. Particles that exhibit at least this level of GR can escape coagulation mainly with larger particles and reach the detectable diameter (6 nm in our case) by condensational growth. The minimal GR was derived as $GR_{min}=-a/b$, and its mean and SD are 1.8 ± 1.0 nm h^{-1} for the conditions ordinarily present in the Budapest air. Nucleation processes which are initiated under circumstances that cause the newly formed particle with a diameter of 10 nm to grow with a rate $<GR_{min}$ are normally not observed. Anyway, these are expected to be events with relatively small J_6 (weak phenomena) due to the relationship between GR_{10} and J_6. The events with GR larger but close to this limit could be still masked by fluctuating experimental data. Their identification and evaluation can be made feasible by decreasing the lower measurement diameter limit of DMPS systems down to 3 nm, or by different instruments such as particle size magnifier or neutral cluster and air ions spectrometer.

Correlations between individual H$_2$SO$_4$ proxy values on one side and J_6 or GR_{10} on the other side were not significant. This is consistent with the corresponding conclusion of Sect. 4.2 and with the earlier results according to which the mean contribution of H$_2$SO$_4$ condensation to the particle GR_{10} was only 12.3% in Budapest (Salma et al., 2016b). The lack of correlation and the average concentrations of SO$_2$ derived separately for the NPF and growth event and non-event days suggest that this precursor gas is ordinarily available in excess and, therefore, the formation of H$_2$SO$_4$ is likely governed by photochemical conditions, and that other chemical species than H$_2$SO$_4$ can have larger influence on the particle growth. The role of H$_2$SO$_4$ in the nucleation process and early particle growth could be still relevant or determinant.

Coefficients of correlation between CS on one side and J_6 or GR_{10} on the other side for the joint city centre data sets were modest ($R=0.41$ and 0.32, respectively with $n=194$ and 197, respectively). This is simply related to the fact that larger GR values are typical for polluted urban air (Kulmala et al., 2017) since particles capable of escaping coagulation scavenging need to grow faster in comparison to cleaner environments, and the enhanced requirements for the growth are linked to increased formation rates as well. It should be noted here that the GR of newly formed particles to larger sizes is primarily coupled to 1) CS, which is further linked to the entire aerosol particle population (including the newly formed particles, thus the NPF itself),

22

2) to the total concentration and some physicochemical properties of non-volatile gaseous

695 compounds and 3) to their production rate in the gas phase from aerosol precursor compounds

696 (e.g. Kerminen et al., 2018). These couplings could result in rather complex behaviour, and

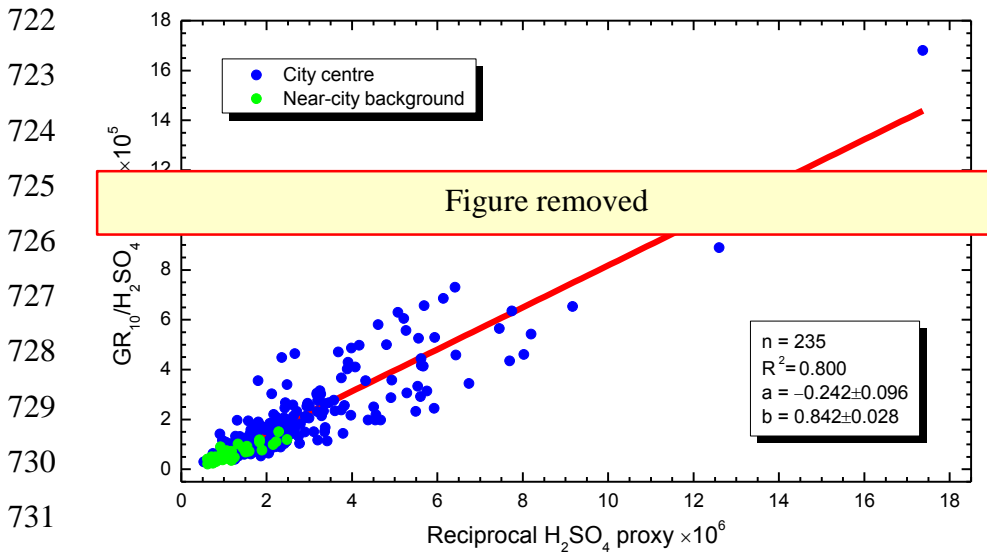697 their understanding is essential when analysing atmospheric observations.

698

699 As far as the pollutant gases are concerned, no correlation could be identified between J_6 or

700 GR_{10} on one side and the gas concentrations on the other side. The coefficients of correlation

701 between CS and NO_x or CO were modest (R=0.37 and 0.42, respectively with n=164 and 152,

702 respectively), while correlation of NO_x and CO on one side with WS was also modest but

703 negative (R= –0.32 and –0.42, respectively with n=167 and 155, respectively). The former

704 relationships can be explained by the fact that vehicular road traffic in cities is a considerable

705 and common source of NO_x, CO and primary particles (Paasonen et al., 2016), and the emitted

706 particles largely contribute to CS levels. The latter relationships are linked to the effect of large-

707 scale air mass transport (often connected to high WSs) on urban air pollution or air quality.

708

709 ~~Importance and contribution of condensing vapours other than H_2SO_4 are further demonstrated~~

710 ~~in Fig. 4. The data for the city centre and near-city background were presented in a linearized~~

711 ~~form and separately for the 2 sites. Nevertheless, the fitting of the correlation line was~~

712 ~~accomplished for the joint 6-year long data set. It can be demonstrated in particular on non-~~

713 ~~linearized plot of the GR_{10}/H_2SO_4-proxy as function of H_2SO_4-proxy (not shown here) that the~~

714 ~~2 data sets merge into each other without any relevant structure, and, therefore, that they can be~~

715 ~~regarded to be coherent. This approach seems sensible when considering also the limited~~

716 ~~accuracy of the values. The relationship between the 2 composite variables in Fig. 4 was~~

717 ~~significant (R^2=0.800, p<0.05). It can be interpreted as the increasing atmospheric concentration~~

718 ~~of gas-phase H_2SO_4 can be related to larger contributions of other vapours than H_2SO_4 to~~

719 ~~particle growth. The other or competing compounds may include oxidation products and their~~

720 ~~dimers from photooxidation of VOC precursors from both biogenic and anthropogenic sources.~~

721

Figure 4. ~~Dependence of the growth rate GR₁₀ (in a unit of nm h⁻¹) of new particle formation and growth events normalised to the daily maximum gas-phase H₂SO₄ proxy (μg m⁻⁵ W s) on the reciprocal proxy value in the city centre and near-city background. The linear line in red represents the line fitted to the joint data set. Number of individual data considered (*n*), their coefficient of determination (*R*²) and the intercept (*a*) and slope (*b*) of the fitted regression line with standard deviations are also shown.~~

4.4 Extreme and multiple events

The joint 6-year long data sets of J_6, GR_{10} and Δt containing all, 247 individual data each could be characterised by lognormal distribution function. This is demonstrated by log-probability graph for J_6 in Fig. S2 as example. The coefficient of determination, median and geometric standard deviation for J_6, GR_{10} and Δt data sets were 0.990, 4.0 cm⁻³ and 2.3; 0.993, 6.8 nm h⁻¹ and 1.46; and 0.998, 02:57 (0.123 d) and 1.74, respectively.

One of the major properties of this distribution type is that it contains relatively large individual data with considerably high abundances. There were 5 individual J_6 and 5 individual GR_{10} data above the 98% percentile of the data sets, which belonged to 9 separate NPF and growth events (days). Their specifications, properties and parameters are summarised in Table 3. All these events occurred in the city centre from April to September. ~~Their number in the separate consecutive measurement years (Sect. 2) were 1, 0, 1, 2, 0 and 5, respectively.~~ The medians of J_6, GR_{10}, CS and air *T* for the subsets of these 9 extreme event days were larger by factors of 5.2, 2.4, 1.5 and 1.4, respectively than for the city centre data. At the same time, the medians of the other atmospheric properties and concentrations in these 2 respective data sets agreed within approximately 10%. There was a single event associated with an extreme H₂SO₄ proxy

24

756 (of 23×10^5 µg m^{-5} W s) and relatively low NO$_x$ concentration (44 µg m^{-3}), which indicate

757 exceptionally favourable conditions for NPF and growth. In addition to this case, there were

758 only a few days that were characterised by an unusually large CS (23×10^{-3} s^{-1}) – which could

759 in turn be linked to higher dynamic rates (Sect. 4.3) – or by somewhat larger SO$_2$ (8.1 µg m^{-3})

760 or lower NO$_x$ concentration (34 µg m^{-3}). For all the other events, however, no simple or

761 compound property of the investigated variables could explain the extreme rates. Instead, they

762 may be related to some other chemical species and/or atmospheric processes, which were not

763 including in the present study. ~~Since the extreme NPF and growth events usually resembled the~~

764 ~~time evolution for regional events (well-developed banana curves) – sometimes with multiple~~

765 ~~onsets –, the missing atmospheric players in increased concentrations or their relevant processes~~

766 ~~are expected to appear on a larger horizontal spatial scale.~~

767

768 **Table 3.** Date (in a format of dd–MM–yyyy), new particle formation rate J_6 (in a unit of cm^{-3} s^{-1}),

769 particle diameter growth rate GR$_{10}$ (nm h^{-1}), starting time t_1 of nucleation (HH:mm UTC+1), duration

770 time interval $\Delta t=t_2-t_1$ of nucleation (HH:mm), mean condensation sink CS during the nucleation process

771 (10^{-3} s^{-1}), daily maximum gas-phase H$_2$SO$_4$ proxy (10^4 µg m^{-5} W s), daily mean air temperature T (°C),

772 daily mean relative humidity RH (%), daily median concentrations of SO$_2$, O$_3$, NO$_x$ (µg m^{-3}) and CO

773 (mg m^{-3}) gases, and the type of the onset for extreme quantifiable (class 1A) new particle formation and

774 growth events. The cells in yellow indicate the values which are above the 98% percentile of the

775 corresponding data sets. N.a.: not available.

776

Date/ property	15–09–2009	20–04–2014	19–05–2015	04–07–2015	28–05–2017	25–06–2017	02–08–2017	31–08–2017	09–09–2017
J_6	15.9	17.8	24	16.3	27	33	30	47	17.3
GR$_{10}$	17.4	19.0	12.2	18.0	9.2	17.0	11.8	21	19.8
t_1	10:20	08:52	08:52	09:38	06:34	10:18	07:39	10:06	11:38
Δt	01:23	01:42	03:57	02:06	07:15	02:46	06:58	06:19	02:06
Proxy	38	42	25	16	229	41	69	92	45
CS	13.4	8.9	13.7	11.9	6.9	10.5	23	18.2	15.5
T	20	13.0	22	26	20	24	29	23	19.1
RH	60	62	48	40	40	68	49	47	58
SO$_2$	6.1	2.5	4.4	2.3	3.4	3.1	5.6	8.1	6.6
O$_3$	16.3	43	n.a.	33	61	56	34	24	12.9
NO$_x$	69	34	174	70	44	66	n.a.	109	112
CO	0.42	n.a.	0.71	0.33	0.31	0.50	0.97	0.62	0.71
Onset	ordinary	double	broad	ordinary	broad	broad	broad	broad	ordinary

777

778

779 Each quantifiable NPF and growth event was labelled as ordinary or broad by visual inspection

780 of its beginning part. If the width of the beginning was smaller than approximately 2 h or there

781 was a determinant single growth curve (rib) on the size distribution surface plot then the onset

782 was labelled as ordinary, otherwise as broad (Fig. S1a and S1c for broad onsets). Broad onsets

783 can be generated by 1) long-lasting nucleation process, 2) disrupted and started over nucleation

784 due to changing atmospheric and meteorological conditions or 3) multiple nucleation processes

785 close to each other in time (Salma et al., 2016b). The broad onsets were specified as doublets

786 if the nucleation mode could be separated into 2 submodes by size distribution fitting.

787 Approximately 40% of all quantifiable events had a broad onset. This indicates that NPF and

788 growth events with broad/multiple onsets are abundant in the urban environment, which could

789 be an important difference from remote or clean atmospheres.

790

791 For 9% of all quantifiable days, it was feasible to calculate 2 sets of dynamic properties for

792 onsets 1 and 2 with a reasonable accuracy. In the near-city background, the medians of J_6 and

793 GR_{10} for the onset 1 were similar ~~or somewhat smaller~~ than the corresponding medians for the

794 whole near-city background data set, while for the onset 2, they were substantially larger,

795 namely 4.1 cm^{-3} s^{-1} and 10.0 nm h^{-1}, respectively (cf. Table 2). Actually, the latter values were

796 closer to the medians of the city centre than for the near-city background. ~~The dynamic~~

797 ~~properties for the city centre for both the onset 1 and onset 2 were somewhat larger than for the~~

798 ~~whole the city centre data set.~~ Approximately 75% of the doublets resulted in individual

799 onset2/onset1 ratios larger than unity. Their overall median ratios for J_6 and GR_{10} were similar

800 and approximately 1.4, while for the near-city background, they were about 2. The results are

801 in line with ~~and confirm~~ our earlier conclusion according to which the second onsets (if it is a

802 new formation process and not just a started over event) ~~often generate new particles more~~

803 ~~intensively~~ are more intensive than the first onsets (Salma et al., 2016b). These particles also

804 grow faster. This can be explained by the fact that the first event is ~~often or likely~~ of regional

805 scale since its dynamic properties resemble those of the regional background ~~process~~ (Yli-Juuti

806 et al., 2009), while the later event can be characterised by values typical for the city centre

807 (Salma et al., 2016b). The later event (or events) are mainly caused and governed by sub-

808 regional processes. These findings are also coherent with a previous observation of NPF and

809 growth events with multiple onsets in semi-clean savannah and industrial environments

810 (Hirsikko et al., 2013), and they also fit well into the existing ideas on mixing regional and

26

811 urban air parcels that exhibit different properties such as precursor concentrations, T and RH
812 (Kulmala et al., 2017).

813

814 **5 Conclusions**

815

816 Magnitude of the particle number concentration level produced solely by NPF and growth
817 (strength of the events) can roughly be estimated by considering the median J_6, median duration
818 of nucleation Δt (their distribution function is lognormal; Table 2) and the mean coagulation
819 loss of these particles F_{coag} (0.17; Sect. 3.1 and Table S1) as: $J_6 \times \Delta t \times (1 - F_{coag})$. In central
820 Budapest, it yields a concentration of 10^4 cm^{-3}. This is in line with another result achieved by
821 nucleation strength factor (Salma et al., 2017). More importantly, the estimated concentration
822 from NPF and growth process is comparable to the annual median atmospheric concentrations
823 (Sect. 4). This simple example indicates that the phenomenon is not only relevant for aerosol
824 load and climate issues on regional or global spatial scales – which were first recognised – but
825 it can affect the urban climate and the health risk of inhabitants of cities as well.

826

827 Similar recognitions have led to the emerge of urban atmospheric nucleation studies. As part of
828 this international progress, we presented here a considerable variety of contributions, which
829 became feasible thank to gradually generating, multi-year long, critically evaluated, complex
830 and coherent data sets. Dynamic and timing properties of 247 NPF and growth events were
831 studied together with supporting aerosol properties, meteorological data and pollutant gas
832 concentrations in near-city background and city centre of Budapest for 6 years. The results and
833 conclusions derived form in important component that is based on atmospheric observations.
834 The present study can also be considered as the first step toward a larger statistical evaluation
835 process. The results are to be combine with results from laboratory experiments and finally,
836 with theoretical models to further improve our understanding on the atmospheric processes in
837 cities. Specialities and features of the urban atmospheric NPF and growth phenomena are finally
838 to be also considered when assessing their potentials to increase UF and CCN concentrations
839 or their health implications.

840

841 The present research based on ambient atmospheric measurements provided evidence that some
842 important chemical players in the NPF and growth events are still missing. Considering the
843 results and conclusions of cloud chamber experiments, these factors are expected to be related
844 mainly to oxidation products of VOCs and/or their processes. Further dedicated research

845 including sophisticated measurements, data evaluations and modelling studies is required to

846 find and identify these species and their processes, and to account their multifactorial role in

847 more detail. Such measurement campaign focusing on chemical composition of molecular

848 clusters, precursors and nucleating vapours by applying recent expedient instruments in

849 Budapest over the months of the highest expected event occurrence has been just realised within

850 a frame of an international cooperation. Its perspective results can hopefully provide additional

851 valuable information for some of the conclusion base on indirect evidence for the time being

852 and can further clarify the overall picture on urban multicomponent nucleation and growth

853 phenomenon.

854

858

860

865

866 **References**

867 Alam, A., Shi, J. P., and Harrison, R. M.: Observations of new particle formation in urban air, J.

868   Geophys. Res., 108 (D3), 4093, doi:10.1029/2001JD001417, 2003.

869 Almeida, J., Schobesberger, S., Kurten, A., Ortega, I. K., Kupiainen-Maatta, O., Praplan, A. P.,

870   Adamov, A., Amorim, A., Bianchi, F., Breitenlechner, M., David, A., Dommen, J., Donahue, N.

871   M., Downard, A., Dunne, E., Duplissy, J., Ehrhart, S., Flagan, R. C., Franchin, A., Guida, R.,

872   Hakala, J., Hansel, A., Heinritzi, M., Henschel, H., Jokinen, T., Junninen, H., Kajos, M.,

873   Kangasluoma, J., Keskinen, H., Kupc, A., Kurten, T., Kvashin, A. N., Laaksonen, A., Lehtipalo,

874   K., Leiminger, M., Leppa, J., Loukonen, V., Makhmutov, V., Mathot, S., McGrath, M. J.,

875   Nieminen, T., Olenius, T., Onnela, A., Petäjä, T., Riccobono, F., Riipinen, I., Rissanen, M., Rondo,

876   L., Ruuskanen, T., Santos, F. D., Sarnela, N., Schallhart, S., Schnitzhofer, R., Seinfeld, J. H.,

877   Simon, M., Sipilä, M., Stozhkov, Y., Stratmann, F., Tome, A., Tröstl, J., Tsagkogeorgas, G.,

878   Vaattovaara, P., Viisanen, Y., Virtanen, A., Vrtala, A., Wagner, P. E., Weingartner, E., Wex, H.,

879   Williamson, C., Wimmer, D., Ye, P. L., Yli-Juuti, T., Carslaw, K. S., Kulmala, M., Curtius, J.,

880   Baltensperger, U., Worsnop, D. R., Vehkamäki, H., and Kirkby, J.: Molecular understanding of

881   sulphuric acid–amine particle nucleation in the atmosphere, Nature, 502, 359–363, 2013.

882   Baltensperger, U., Streit, N., Weingartner, E., Nyeki, S., Prévôt, A. S. H., Van Dingenen, R., Virkkula,

883   A., Putaud, J. P., Even, A., Brink, H., Blatter, A., Neftel, A., and Gaggeler, H. W.: Urban and rural

884   aerosol characterization of summer smog events during the PIPAPO field campaign in Milan, Italy,

885   J. Geophys. Res., 107(D22), 8193, doi:10.1029/2001JD001292, 2002.

886   Bianchi, F., Tröstl, J., Junninen, H., Frege, C., Henne, S., Hoyle, C. R., Molteni, U., Herrmann, E.,

887   Adamov, A., Bukowiecki, N., Chen, X., Duplissy, J., Gysel, M., Hutterli, M. Kangasluoma, J.,

888   Kontkanen, J., Kürten, A. Manninen, H. E., Münch, S., Peräkylä, O., Petäjä, T., Rondo, L.,

889   Williamson, C., Weingartner, E. Curtius, J., Worsnop, D. R., Kulmala, M., Dommen, J., and

890   Baltensperger, U.: New particle formation in the free troposphere: A question of chemistry and

891   timing, Science, 352, 1109–1112, https://doi.org/10.1126/science.aad5456, 2016.

892   Braakhuis, H. M., Park, M. V., Gosens, I., De Jong, W. H., and Cassee, F. R.: Physicochemical

893   characteristics of nanomaterials that affect pulmonary inflammation, Part. Fibre Toxicol., 11:18,

894   doi: 10.1186/1743-8977-11-18, 2014.

895   Cai, R. and Jiang, J.: A new balance formula to estimate new particle formation rate: reevaluating the

896   effect of coagulation scavenging, Atmos. Chem. Phys., 17, 12659–12675, 2017.

897   Carslaw, K. S., Lee, L. A., Reddington, C. L., Pringle, K. J., Rap, A., Forster, P. M., Mann, G. W.,

898   Spracklen, D. V., Woodhouse, M. T., Regayre, L. A., and Pierce, J. R: Large contribution of

899   natural aerosols to uncertainty in indirect forcing, Nature, 503, 67–71, 2013.

900   Crounse, J. D., Nielsen, L. B., Jørgensen, S., Kjaergaard, H. G., and Wennberg, P. O.: Autoxidation of

901   organic compounds in the atmosphere, J. Phys. Chem. Lett., 4, 20, 3513–3520, 2013.

902   Dal Maso, M., Kulmala, M., Lehtinen, K. E. J., Mäkelä, J. M., Aalto, P. P., and O'Dowd, C.:

903   Condensation and coagulation sinks and formation of nucleation mode particles in coastal and

904   boreal forest boundary layers, J. Geophys. Res., 107(19D), 8097, 10.1029/2001jd001053, 2002.

905   Dal Maso, M., Kulmala, M., Riipinen, I., Wagner, R., Hussein, T., Aalto, P. P., and Lehtinen, K. E. J.:

906   Formation and growth of fresh atmospheric aerosols: eight years of aerosol size distribution data

907   from SMEAR II, Hyytiälä, Finland, Boreal Environ. Res., 10, 323–336, 2005.

908   Dall'Osto, M., Querol, X., Alastuey, A., O'Dowd, C., Harrison, R. M., Wenger, J., and Gómez-

909   Moreno, F. J.: On the spatial distribution and evolution of ultrafine particles in Barcelona, Atmos.

910   Chem. Phys., 13, 741–759, 2013.

911   Ehn, M., Thornton, J. A., Kleist, E., Sipilä, M., Junninen, H., Pullinen, I., Springer, M., Rubach, F.,

912   Tillmann, R., Lee, B., Lopez-Hilfiker, F., Andres, S., Acir, I. H., Rissanen, M., Jokinen, T.,

913   Schobesberger, S., Kangasluoma, J., Kontkanen, J., Nieminen, T., Kurten, T., Nielsen, L. B.,

914   Jorgensen, S., Kjaergaard, H. G., Canagaratna, M., Dal Maso, M., Berndt, T., Petäjä, T., Wahner,

915   A., Kerminen, V. M., Kulmala, M., Worsnop, D. R., Wildt, J., and Mentel, T. F.: A large source of

916   low-volatility secondary organic aerosol, Nature, 506, 476–479, 2014.

917 Gordon, H., Sengupta, K., Rap, A., Duplissy, J., Frege, C., Williamson, C., Heinritzi, M., Simon, M.,

918 Yan, C., Almeida, J., Tröstl, J., Nieminen, T., Ortega, I. K., Wagner, R., Dunne, E. M., Adamov,

919 A., Amorim, A., Bernhammer, A. K., Bianchi, F., Breitenlechner, M., Brilke, S., Chen, X., Craven,

920 J. S., Dias, A., Ehrhart, S., Fischer, L., Flagan, R. C., Franchin, A., Fuchs, C., Guida, R., Hakala, J.,

921 Hoyle, C. R., Jokinen, T., Junninen, H., Kangasluoma, J., Kim, J., Kirkby, J., Krapf, M., Kürten,

922 A., Laaksonen, A., Lehtipalo, K., Makhmutov, V., Mathot, S., Molteni, U., Monks, S. A., Onnela,

923 A., Peräkylä, O., Piel, F., Petäjä, T., Praplan, A. P., Pringle, K. J., Richards, N. A. D., Rissanen, M.

924 P., Rondo, L., Sarnela, N., Schobesberger, S., Scott, C. E., Seinfeld, J. H., Sharma, S., Sipilä, M.,

925 Steiner, G., Stozhkov, Y., Stratmann, F., Tomé, A., Virtanen, A., Vogel, A. L., Wagner, A. C.,

926 Wagner, P. E., Weingartner, E., Wimmer, D., Winkler, P. M., Ye, P., Zhang, X., Hansel, A.,

927 Dommen, J., Donahue, N. M., Worsnop, D. R., Baltensperger, U., Kulmala, M., Curtius, J., and

928 Carslaw, K. S.: Reduced anthropogenic aerosol radiative forcing caused by biogenic new particle

929 formation, Proc. Natl. Acad. Sci. U.S.A., 113, 12053–12058,

930 https://doi.org/10.1073/pnas.1602360113, 2016.

931 Hirsikko, A., Vakkari, V., Tiitta, P., Hatakka, J., Kerminen, V.-M., Sundström, A.-M., Beukes, J. P.,

932 Manninen, H. E., Kulmala, M., and Laakso, L.: Multiple daytime nucleation events in semi-clean

933 savannah and industrial environments in South Africa: analysis based on observations, Atmos.

934 Chem. Phys., 13, 5523–5532, 2013.

935 Hussein, T., Puustinen, A., Aalto, P. P., Mäkelä, J. M., Hämeri, K., and Kulmala, M.: Urban aerosol

936 number size distributions, Atmos. Chem. Phys., 4, 391–411, 2004.

937 Hussein, T., Martikainen, J., Junninen, H., Sogacheva, L., Wagner, R., Dal Maso, M., Riipinen, I.,

938 Aalto, P. P., and Kulmala, M.: Observation of regional new particle formation in the urban

939 atmosphere, Tellus 60B, 509–521, 2008.

940 Jokinen, T., Berndt, T., Makkonen, R., Kerminen, V.-M., Junninen, H., Paasonen, P., Stratmann, F.,

941 Herrmann, H., Guenther, A. B., Worsnop, D. R., Kulmala, M., Ehn, M. and Sipilä, M.: Production

942 of extremely low volatile organic compounds from biogenic emissions: Measured yields and

943 atmospheric implications, Proc. Natl. Acad. Sci. U.S.A., 112, 7123–7128, 2015.

944 Kerminen, V.-M., Paramonov, M., Anttila, T., Riipinen, I., Fountoukis, C., Korhonen, H., Asmi, E.,

945 Laakso, L., Lihavainen, H., Swietlicki, E., Svenningsson, B., Asmi, A., Pandis, S. N., Kulmala, M.,

946 and Petäjä, T.: Cloud condensation nuclei production associated with atmospheric nucleation: a

947 synthesis based on existing literature and new results, Atmos. Chem. Phys., 12, 12037–12059,

948 2012.

949 Kerminen, V.-M., Chen, X., Vakkari, V., Petäjä, T., Kulmala, M., and Bianchi, F.: Atmospheric new

950 particle formation and growth: review of field observations, Environ. Res. Lett., 13 (2018) 103003,

951 2018.

952 Kirkby, J., Curtius, J., Almeida, J., Dunne, E., Duplissy, J., Ehrhart, S., Franchin, A., Gagné, S., Ickes,

953 L., Kürten, A., Kupc, A., Metzger, A., Riccobono, F., Rondo, L., Schobesberger, S.,

954 Tsagkogeorgas, G., Wimmer, D., Amorim, A., Bianchi, F., Breitenlechner, M., David, A.,

955   Dommen, J., Downard, A., Ehn, M., Flagan, R. C., Haider, S., Hansel, A., Hauser, D., Jud, W.,
956   Junninen, H., Kreissl, F., Kvashin, A., Laaksonen, A., Lehtipalo, K., Lima, J., Lovejoy, E. R.,
957   Makhutov, V., Mathot, S., Mikkilä, J., Minginette, P., Mogo, S., Nieminen, T., Onnela, A., Pereira,
958   A., Petäjä, T., Schnitzhofer, R., Seinfeld, J. H., Sipilä, M., Stozhkov, Y., Stratmann, F., Tome, A.,
959   Vanhanen, J., Viisanen Y., Vrtala, A., Wagner, P.E., Walther, H., Weingartner, E., Wex, H.,
960   Winkler, P.M., Carslaw, K. S., Worsnop, D. R., Baltensperger, U., and Kulmala, M.: The role of
961   sulfuric acid, ammonia and galactic cosmic rays in atmospheric aerosol nucleation, Nature, 476,
962   429–433, 2011.

963 Kirkby, J., Duplissy, J., Sengupta, K., Frege, C., Gordon, H., Williamson, C., Heinritzi, M., Simon,
964   M., Yan, C., Almeida, J., Tröstl, J., Nieminen, T., Ortega, I. K., Wagner, R., Adamov, A., Amorim,
965   A., Bernhammer, A.-K., Bianchi, F., Breitenlechner, M., Brilke, S., Chen, X., Craven, J., Dias, A.,
966   Ehrhart, S., Flagan, R. C., Franchin, A., Fuchs, C., Guida, R., Hakala, J., Hoyle, C. R., Jokinen, T.,
967   Junninen, H., Kangasluoma, J., Kim, J., Krapf, M., Kürten, A., Laaksonen, A., Lehtipalo, K.,
968   Makhmutov, V., Mathot, S., Molteni, U., Onnela, A., Peräkylä, O., Piel, F., Petäjä, T., Praplan, A.
969   P., Pringle, K., Rap, A., Richards, N. A. D., Riipinen, I., Rissanen, M. P., Rondo, L., Sarnela, N.,
970   Schobesberger, S., Scott, C. E., Seinfeld, J. H., Sipilä, M., Steiner, G., Stozhkov, Y., Stratmann, F.,
971   Tomé, A., Virtanen, A., Vogel, A. L., Wagner, A., Wagner, P. E., Weingartner, E., Wimmer, D.,
972   Winkler, P. M., Ye, P., Zhang, X., Hansel, A., Dommen, J., Donahue, N. M., Worsnop, D. R.,
973   Baltensperger, U., Kulmala, M., Carslaw, K. S., and Curtius, J.: Ion-induced nucleation of pure
974   biogenic particles, Nature, 533, 521–526, https://doi.org/10.1038/nature17953, 2016.

975 Kulmala, M., Dal Maso, M., Mäkelä, J. M., Pirjola, L., Väkevä, M., Aalto, P., Miikkulainen, P.,
976   Hämeri, K., and O'Dowd, C. D.: On the formation, growth and composition of nucleation mode
977   particles, Tellus B53, 479–490, 2001.

978 Kulmala, M., Vehkamäki, H., Petäjä, T., Dal Maso, M., Lauri, A., Kerminen, V.-M., Birmili, W., and
979   McMurry, P.: Formation and growth rates of ultrafine atmospheric particles: a review of
980   observations, J. Aerosol Sci., 35, 143–176, 2004.

981 Kulmala, M., Petäjä, T., Nieminen, T., Sipilä, M., Manninen, H. E., Lehtipalo, K., Dal Maso, M.,
982   Aalto, P. P., Junninen, H., Paasonen, P., Riipinen, I., Lehtinen, K. E. J., Laaksonen, A., and
983   Kerminen, V.-M.: Measurement of the nucleation of atmospheric aerosol particles, Nat. Protoc., 7,
984   1651–1667, doi:10.1038/nprot.2012.091, 2012.

985 Kulmala, M., Kontkanen, J., Junninen, H., Lehtipalo, K., Manninen, H. E., Nieminen, T., Petäjä, T.,
986   Sipilä, M., Schobesberger, S., Rantala, P., Franchin, A., Jokinen, T., Järvinen, E., Äijälä, M.,
987   Kangasluoma, J., Hakala, J., Aalto, P.P., Paasonen, P., Mikkilä, J., Vanhanen, J., Aalto, J., Hakola,
988   H., Makkonen, U., Ruuskanen, T., Mauldin, R. L. III, Duplissy, J., Vehkamäki, H., Bäck, J.,
989   Kortelainen, A., Riipinen, I., Kurtén, T., Johnston, M. V., Smith, J. N., Ehn, M., Mentel, T. F.,
990   Lehtinen, K. E. J., Laaksonen, A., Kerminen, V.-M., and Worsnop, D. R.: Direct observations of
991   atmospheric aerosol nucleation, Science, 339, 943–946, 2013.

992   Kulmala, M., Petäjä, T., Ehn, M., Thornton, J., Sipilä, M., Worsnop, D. R., and Kerminen, V.-M.:
993   Chemistry of atmospheric nucleation: On the recent advances on precursor characterization and
994   atmospheric cluster composition in connection with atmospheric new particle formation, Annu.
995   Rev. Phys. Chem., 65, 21−37, 2014.

996   Kulmala, M., Kerminen, V. M., Petäjä, T., Ding, A. J., and Wang, L.: Atmospheric gas-to-particle
997   conversion: why NPF events are observed in megacities, Faraday Discuss.,
998   doi:10.1039/C6FD00257A, 2017.

999   Makkonen, R., Asmi, A., Korhonen, H., Kokkola, H., Järvenoja, S., Räisänen, P., Lehtinen, K. E. J.,
1000   Laaksonen, A., Kerminen, V.-M., Järvinen, H., Lohmann, U., Bennartz, R., Feichter, J., and
1001   Kulmala, M.: Sensitivity of aerosol concentrations and cloud properties to nucleation and
1002   secondary organic distribution in ECHAM5-HAM global circulation model, Atmos. Chem. Phys.,
1003   9, 1747–1766, 2009.

1004   Makkonen, R., Asmi, A., Kerminen, V.-M., Boy, M., Arneth, A., Hari, P., and Kulmala, M.: Air
1005   pollution control and decreasing new particle formation lead to strong climate warming, Atmos.
1006   Chem. Phys., 12, 1515–1524, 2012.

1007   Merikanto, J., Spracklen, D. V., Mann, G. W., Pickering, S. J., and Carslaw, K. S.: Impact of
1008   nucleation on global CCN, Atmos. Chem. Phys., 9, 8601–8616, 2009.

1009   Metzger, A., Verheggen, B., Dommen, J., Duplissy, J., Prévôt, A. S. H., Weingartner, E., Riipinen, I.,
1010   Kulmala, M., Spracklen, D. V., Carslaw, K. S., and Baltensperger, U.: Evidence for the role of
1011   organics in aerosol particle formation under atmospheric conditions, Proc. Natl. Acad. Sci. U. S.
1012   A., 107, 6646–6651, 2010.

1013   Németh, Z. and Salma, I.: Spatial extension of nucleating air masses in the Carpathian Basin, Atmos.
1014   Chem. Phys., 14, 8841–8848, 2014.

1015   Németh, Z., Rosati, B., Zíková, N., Salma, I., Bozó, L., Dameto de España, C., Schwarz, J., Ždímal,
1016   V., and Wonaschütz, A.: Comparison of atmospheric new particle formation and growth events in
1017   three Central European cities, Atmos. Environ., 178, 191–197, 2018.

1018   Nieminen, T., Kerminen, V.-M., Petäjä, T., Aalto, P. P., Arshinov, M., Asmi, E., Baltensperger, U.,
1019   Beddows, D. C. S., Beukes, J. P., Collins, D., Ding, A., Harrison, R. M., Henzing, B., Hooda, R.,
1020   Hu, M., Hõrrak, U., Kivekäs, N., Komsaare, K., Krejčí, R., Kristensson, A., Laakso, L., Laaksonen,
1021   A., Leaitch, W. R., Lihavainen, H., Mihalopoulos, N., Németh, Z., Nie, W., O'Dowd, C., Salma, I.,
1022   Sellegri, K., Svenningsson, B., Swietlicki, E., Tunved, P., Ulevicius, V., Vakkari, V., Vana, M.,
1023   Wiedensohler, A., Wu, Z., Virtanen, A., and Kulmala, M.: Global analysis of continental boundary
1024   layer new particle formation based on long-term measurements, Atmos. Chem. Phys., 18, 14737–
1025   14756, 2018.

1026   Oberdörster, G., Oberdörster, E., and Oberdörster, J.: Nanotoxicology: an emerging discipline
1027   evolving from studies of ultrafine particles, Environ. Health Perspect., 113, 823–839, 2005.

1028   O'Dowd, C. D., Jimenez, J. L., Bahreini, R. Flagan, R. C., Seinfeld, J. H., Hämeri, K., Pirjola, L.,

1029   Kulmala, M., Jennings, S. G., and Hoffmann, Th.: Marine aerosol formation from biogenic iodine

1030   emissions, Nature 417, 632–636, 2002.

1031   Paasonen, P., Kupiainen, K., Klimont, Z., Visschedijk, A., Denier van der Gon, H. A. C., and Amann,

1032   M.: Continental anthropogenic primary particle number emissions, Atmos. Chem. Phys., 16, 6823–

1033   6840, 2016.

1034   Paasonen, P., Peltola, M., Kontkanen, J., Junninen, H., Kerminen, V.-M., and Kulmala, M.:

1035   Comprehensive analysis of particle growth rates from nucleation mode to cloud condensation

1036   nuclei in Boreal forest, Atmos. Chem. Phys. Discuss., https://doi.org/10.5194/acp-2018-169, in

1037   review, 2018.

1038   Petäjä, T., Mauldin, III, R. L., Kosciuch, E., McGrath, J., Nieminen, T., Paasonen, P., Boy, M.,

1039   Adamov, A., Kotiaho, T., and Kulmala, M.: Sulfuric acid and OH concentrations in a boreal forest

1040   site, Atmos. Chem. Phys., 9, 7435–7448, 2009.

1041   Putaud, J.-P., Van Dingenen, R., Alastuey, A., Bauer, H., Birmili, W., Cyrys, J., Flentje, H., Fuzzi, S.,

1042   Gehrig, R., Hansson, H. C., Harrison, R. M., Herrmann, H., Hitzenberger, R., Hüglin, C., Jones,

1043   A.M., Kasper-Giebl, A., Kiss, G., Kousa, A., Kuhlbusch, T. A. J., Löschau, G., Maenhaut, W.,

1044   Molnár, A., Moreno, T., Pekkanen, J., Perrino, C., Pitz, M., Puxbaum, H., Querol, X., Rodriguez,

1045   S., Salma, I., Schwarz, J., Smolík, J., Schneider, J., Spindler, G., ten Brink, H., Turšič, J., Viana,

1046   M., Wiedensohler, and A., Raes, F.: A European Aerosol Phenomenology - 3: physical and

1047   chemical characteristics of particulate matter from 60 rural, urban, and kerbside sites across

1048   Europe, Atmos. Environ., 44, 1308–1320, 2010.

1049   Riccobono, F., Schobesberger, S., Scott, C., Dommen, J., Ortega, I., Rondo, L., Almeida, J., Amorim,

1050   A., Bianchi, F., Breitenlechner, M., David, A., Downard, A., Dunne, E., Duplissy, J., Ehrhart, S.,

1051   Flagan, R., Franchin, A., Hansel, A., Junninen, H., Kajos, M., Keskinen, H., Kupc, A., Kurten, A.,

1052   Kvashin, A., Laaksonen, A., Lehtipalo, K., Makhmutov, V., Mathot, S., Nieminen, T., Onnela, A.,

1053   Petäjä, T., Praplan, A., Santos, F., Schallhart, S., Seinfeld, J., Sipila, M., Spracklen, D., Stozhkov,

1054   Y., Stratmann, F., Tome, A., Tsagkogeorgas, G., Vaattovaara, P., Viisanen, Y., Vrtala, A., Wagner,

1055   P., Weingartner, E., Wex, H., Wimmer, D., Carslaw, K., Curtius, J., Donahue, N., Kirkby, J.,

1056   Kulmala, M., Worsnop, D., and Baltensperger, U.: Oxidation products of biogenic emissions

1057   contribute to nucleation of atmospheric particles, Science, 344, 717–721, 2014.

1058   Riipinen, I., Pierce, J. R., Yli-Juuti, T., Nieminen, T., Häkkinen, S., Ehn, M., Junninen, H., Lehtipalo,

1059   K., Petäjä, T., Slowik, J., Chang, R., Shantz, N. C., Abbatt, J., Leaitch, W. R., Kerminen, V.-M.,

1060   Worsnop, D. R., Pandis, S. N., Donahue, N. M., and Kulmala, M.: Organic condensation: a vital

1061   link connecting aerosol formation to cloud condensation nuclei (CCN) concentrations, Atmos.

1062   Chem. Phys., 11, 3865–3878, 2011.

1063   Salma, I., Borsós, T., Weidinger, T., Aalto, P., Hussein, T., Dal Maso, M., and Kulmala, M.:

1064   Production, growth and properties of ultrafine atmospheric aerosol particles in an urban

1065   environment, Atmos. Chem. Phys., 11, 1339–1353, 2011.

1066 Salma, I., Borsós, T., Németh, Z., Weidinger, T., Aalto, T., and Kulmala, M.: Comparative study of
1067   ultrafine atmospheric aerosol within a city, Atmos. Environ., 92, 154–161, 2014.

1068 Salma, I., Füri, P., Németh, Z., Farkas, Á., Balásházy, I., Hofmann, W., and Farkas, Á.: Lung burden
1069   and deposition distribution of inhaled atmospheric urban ultrafine particles as the first step in their
1070   health risk assessment, Atmos. Environ., 104, 39–49, 2015.

1071 Salma, I., Németh, Z., Weidinger, T., Kovács, B., and Kristóf, G.: Measurement, growth types and
1072   shrinkage of newly formed aerosol particles at an urban research platform, Atmos. Chem. Phys.,
1073   16, 7837–7851, 2016a.

1074 Salma, I., Németh, Z., Kerminen, V. M., Aalto, P., Nieminen, T., Weidinger, T., Molnár, Á., Imre, K.,
1075   and Kulmala, M.: Regional effect on urban atmospheric nucleation, Atmos. Chem. Phys., 16,
1076   8715–8728, 2016b.

1077 Salma, I., Varga, V., and Németh, Z.: Quantification of an atmospheric nucleation and growth process
1078   as a single source of aerosol particles in a city, Atmos. Chem. Phys., 17, 15007–15017, 2017.

1079 Schobesberger, S., Junninen, H., Bianchi, F., Lonn, G., Ehn, M., Lehtipalo, K., Dommen, J., Ehrhart,
1080   S., Ortega, I. K., Franchin, A., Nieminen, T., Riccobono, F., Hutterli, M., Duplissy, J., Almeida, J.,
1081   Amorim, A., Breitenlechner, M., Downard, A. J., Dunne, E. M., Flagan, R. C., Kajos, M.,
1082   Keskinen, H., Kirkby, J., Kupc, A., Kurten, A., Kurten, T., Laaksonen, A., Mathot, S., Onnela, A.,
1083   Praplan, A. P., Rondo, L., Santos, F. D., Schallhart, S., Schnitzhofer, R., Sipilä, M., Tome, A.,
1084   Tsagkogeorgas, G., Vehkamäki, H., Wimmer, D., Baltensperger, U., Carslaw, K. S., Curtius, J.,
1085   Hansel, A., Petäjä, T., Kulmala, M., Donahue, N. M., and Worsnop, D. R.: Molecular
1086   understanding of atmospheric particle formation from sulfuric acid and large oxidized organic
1087   molecules, Proc. Natl. Acad. Sci. U.S.A., 110, 17223–17228, 10.1073/pnas.1306973110, 2013.

1088 Sihto, S.-L., Mikkilä, J., Vanhanen, J., Ehn, M., Liao, L., Lehtipalo, K., Aalto, P. P., Duplissy, J.,
1089   Petäjä, T., Kerminen, V.-M., Boy, M., and Kulmala, M.: Seasonal variation of CCN concentrations
1090   and aerosol activation properties in boreal forest, Atmos. Chem. Phys., 11, 13269–13285, 2011.

1091 Sipilä, M., Berndt, T., Petäjä, T., Brus, D., Vanhanen, J., Stratmann, F., Patokoski, J., Mauldin, R. L.
1092   3rd, Hyvärinen, A. P., Lihavainen, H., and Kulmala, M.: The role of sulfuric acid in atmospheric
1093   nucleation, Science, 327(5970), 1243-6. doi: 10.1126/science.1180315, 2010.

1094 Spracklen, D. V., Carslaw, K. S., Merikanto, J., Mann, G. W., Reddington, C. L., Pickering, S., Ogren,
1095   J. A., Andrews, E., Baltensperger, U., Weingartner, E., Boy, M., Kulmala. M., Laakso, L.,
1096   Lihavainen, H., Kivekäs, N., Komppula, M., Mihalopoulos, N., Kouvarakis, G., Jennings, S. G.,
1097   O'Dowd, C., Birmili, W., Wiedensohler, A., Weller, R., Gras, J., Laj, P., Sellegri, K., Bonn, B.,
1098   Krejčí, R., Laaksonen, A., Hamed, A., Minikin, A., Harrison, R. M., Talbot, R., and Sun, J.: The
1099   contribution of boundary layer nucleation events to total particle concentrations on regional and
1100   global scales, Atmos. Chem. Phys., 6, 5631–5648, 2006.

1101 Tröstl, J., Chuang, W. K., Gordon, H., Heinritzi, M., Yan, C., Molteni, U., Ahlm, L., Frege, C.,
1102   Bianchi, F., Wagner, R., Simon, M., Lehtipalo, K., Williamson, C., Craven, J. S., Duplissy, J.,
1103   Adamov, A., Almeida, J., Bernhammer, A. K., Breitenlechner, M., Brilke, S., Dias, A., Ehrhart, S.,

Flagan, R. C., Franchin, A., Fuchs, C., Guida, R., Gysel, M., Hansel, A., Hoyle, C. R., Jokinen, T., Junninen, H., Kangasluoma, J., Keskinen, H., Kim, J., Krapf, M., Kürten, A., Laaksonen, A., Lawler, M., Leiminger, M., Mathot, S., Möhler, O., Nieminen, T., Onnela, A., Petäjä, T., Piel, F. M., Miettinen, P., Rissanen, M. P., Rondo, L., Sarnela, N., Schobesberger, S., Sengupta, K., Sipilä, M., Smith, J. N., Steiner, G., Tomè, A., Virtanen, A., Wagner, A. C., Weingartner, E., Wimmer, D., Winkler, P. M., Ye, P. L., Carslaw, K. S., Curtius, J., Dommen, J., Kirkby, J., Kulmala, M., Riipinen, I., Worsnop, D. R., Donahue, N. M., and Baltensperger, U.: The role of low-volatility organic compounds in initial particle growth in the atmosphere, Nature, 533, 527, 10.1038/nature18271, 2016.

Vakkari, V., Tiitta, P., Jaars, K., Croteau, P., Beukes, J. P., Josipovic, M., Kerminen, V.-M., Kulmala, M., Venter, A. D., van Zyl, P. G., Worsnop, D. R., and Laakso, L.: Reevaluating the contribution of sulfuric acid and the origin of organic compounds in atmospheric nanoparticle growth, Geophys. Res. Lett., 42, 10486−10493, 2015.

Vuollekoski, H., Sihto, S.-L., Kerminen, V.-M., Kulmala, M., and Lehtinen, K. E. J.: A numerical comparison of different methods for determining the particle formation rate, Atmos. Chem. Phys., 12, 2289–2295, 2012.

Wehner, B., Wiedensohler, A., Tuch, T. M., Wu, Z. J., Hu, M., Slanina, J., and Kiang, C. S.: Variability of the aerosol number size distribution in Beijing, China: new particle formation, dust storms, and high continental background, Geophys. Res. Lett., 31, L22108, 2004.

Wiedensohler, A., Cheng, Y. F., Nowak, A., Wehner, B., Achtert, P., Berghof, M., Birmili, W., Wu, Z. J., Hu, M., Zhu, T., Takegawa, N., Kita, K., Kondo, Y., Lou, S. R., Hofzumahaus, A., Holland, F., Wahner, A., Gunthe, S. S., Rose, D., Su, H., and Pöschl, U.: Mobility particle size spectrometers: harmonization of technical standards and data structure to facilitate high quality long-term observations of atmospheric particle number size distributions, Atmos. Meas. Tech., 5, 657–685, 2012.

Woo, K. S., Chen, D. R., Pui, D. Y. H., and McMurry, P. H.: Measurement of Atlanta aerosol size distributions: observations of ultrafine particle events, Aerosol Sci. Technol., 34, 75–87, 2001.

Xiao, S., Wang, M. Y., Yao, L., Kulmala, M., Zhou, B., Yang, X., Chen, J. M., Wang, D. F., Fu, Q. Y., Worsnop, D. R., and Wang, L.: Strong atmospheric new particle formation in winter in urban Shanghai, China, Atmos. Chem. Phys., 15, 1769–1781, 2015.

Yli-Juuti, T., Riipinen, I., Aalto, P. P., Nieminen, T., Maenhaut, W., Janssens, I. A., Claeys, M., Salma, I., Ocskay, R., Hoffer, A., Imre, K., and Kulmala, M.: Characteristics of new particle formation events and cluster ions at K-puszta, Hungary. Boreal Environ. Res., 14, 683–698, 2009.

Zhang, R., Wang, G., Guo, S., Zamora, M. L., Ying, Q., Lin, Y., Wang, W., Hu, M., and Wang, Y.: Formation of urban fine particulate matter, Chem. Rev., 115, 3803−3855, 2015.